

國立臺灣大學地理環境資源學系暨研究所

博士論文

Department of Geography

College of Science

National Taiwan University

Doctor of Philosophy Dissertation



不同尺度台灣森林生物量與枯落物動態之分析

Patterns of forest biomass and litterfall at different scales in
Taiwan

王雪卿

Hsueh-Ching Wang


指導教授：黃倬英 博士

Advisor: Dr. Cho-ying Huang

中華民國 104 年 08 月

August 2015

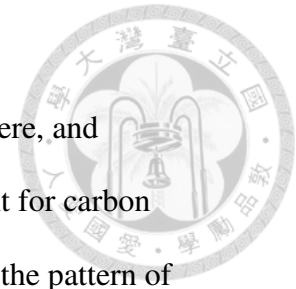
摘要



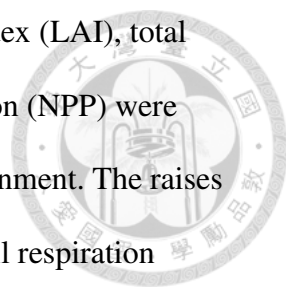
森林生態系是陸域生物圈主要的碳庫，而森林碳儲藏量與流動則是瞭解碳收支的關鍵。此論文利用遙測影像評估熱帶與亞熱帶生物量與枯落物之動態，也利用動態全球植被模式模擬颱風干擾所產生的落葉，以及颱風強度與頻率的改變對森林碳循環之影響。在第二章的研究中，此論文利用高空間解析度的 QuickBird 衛星影像獲取林冠面積，並利用林冠面積計算生態系碳儲藏量，以瞭解碳儲藏量在棲蘭山地形與邊際效應影響下的空間異質性情形。研究結果顯示，棲蘭山扁柏雲霧林平均每棵樹的碳儲藏量為 $138 \pm 118 \text{ kgC}$ ，密度為 $119.3 \text{ MgC ha}^{-1}$ 。在空間分佈上，溫度與太陽輻射隨著海拔上升而遞減，而坡度則是影響扁柏林冠面積變異的重要因子。顯示地形異質性的存在，改變營養與生物氣候環境，進而影響植被結構的空間分佈情形。在第三章的研究中，此論文利用時間序列的 MODIS 遙測影像，萃取地表溫度(land surface temperature, LST)與可行光合作用植被覆蓋指數(photosynthetically active vegetation cover)來估算森林枯落物量。研究結果顯示，台灣森林平均年枯落物量為 $5.1 \pm 1.2 \text{ Mg ha}^{-1} \text{ yr}^{-1}$ 。在枯落物的年變異上，可能受到颱風與乾旱干擾因子影響，而海拔與坡向則是影響枯落物空間變異的重要因子。在第四章的研究中，此論文利用動態全球植被模式 Hybrid v4.2，並加入風速、溫度、雨量參數，以模擬福山森林生態系受到颱風干擾所產生的落葉情形。研究結果顯示，模擬與實地觀測的落葉量有顯著的關係($r^2 = 0.33, p < 0.001$)，但模擬結果有些微的低估現象(15.6%)。在颱風干擾的環境下，落葉量、葉面積指數、總生物量、總初級生產力、淨初級生產力皆比非颱風干擾的環境低。在提升颱風強度與頻率的模擬下，將產生更高的落葉量與土壤呼吸，使得葉面積指數、總生物量、總初級生產力、淨初級生產力減少，可能影響森林長期的碳收支能力。整體而言，利用遙測影像與動態全球植被模式監測森林生物量、枯落物、碳循環的時間與空間分佈情形，有助於瞭解與預測森林生態系在干擾環境下的碳收支動態。

關鍵字：碳循環、生物量、枯落物、落葉、遙測、模式、颱風、干擾

ABSTRACT



Forest ecosystem is the major carbon pool in terrestrial biosphere, and understanding dynamics of forest carbon stock and flux is important for carbon budget. This dissertation used remotely sensed imagery to evaluate the pattern of biomass and litterfall in subtropical/tropical forests. The dynamic global vegetation model was also included to model typhoon-induced defoliation and carbon cycle under scenarios of typhoon intensity and frequency. Firstly, this dissertation extracts canopy areas from a high spatial resolution QuickBird image to assess the patterns of carbon stock across topographical gradients and the edge effect in a Chilan montane cloud forest. Mean (\pm s.d.) carbon per individual was 138 ± 118 kgC with an estimated site carbon density of $119.3 \text{ MgC ha}^{-1}$ in a false cypress (*Chamaecyparis obtusa* var. *formosana*, CHFO) cloud forest. The negative trends of temperature and solar radiation along the elevation gradient were observed, and slope played a crucial role in varying CHFO canopy area. The findings suggest that topographical heterogeneity may alter the spatial patterns of nutrients and bioclimate that influence the structure of the vegetation. Secondly, time-series MODIS LST- (land surface temperature) and PV-derived (photosynthetically active vegetation cover) metrics were used to derive litterfall. The mean annual litterfall was $5.1 \pm 1.2 \text{ Mg ha}^{-1} \text{ yr}^{-1}$ in Taiwan montane forests. The temporal dynamics of the litterfall revealed that typhoons and consecutive drought events might be important for temporal variability of litterfall. The elevation gradient and aspects were critical to dominate spatial patterns of litterfall. Thirdly, a wind built-in function with wind speed, temperature and precipitation variables was developed in a dynamic global vegetation model Hybrid v4.2 to simulate typhoon-induced leaf litter in the Fushan experimental forest. The modeled and observed leaf litter was significant correlation ($r^2 = 0.33$, $p < 0.001$)



with moderate underestimation (15.6%). The leaf litter, leaf area index (LAI), total biomass, gross primary production (GPP) and net primary production (NPP) were higher in non-typhoon environment than in typhoon-affected environment. The raises of typhoon intensity and frequency would increase leaf litter and soil respiration resulting in the decreases of LAI, biomass, GPP and NPP. If the substantial defoliation from more intense or frequent typhoon might affect regional carbon budget at long-term time scale. Overall, using satellite images and a dynamic global vegetation model to monitor spatial and temporal patterns of living biomass, litterfall and carbon flux may facilitate monitoring and predicting of carbon budget and perturbations in forest ecosystems.

Keywords: carbon cycle, biomass, litterfall, defoliation, remote sensing, model, typhoon, disturbance

致謝

時光飛逝，終於走到撰寫致謝的階段了，再過幾天也終將與長久的學生身份告別，心情總是五味雜陳。這本論文的完成要感謝的人實在太多，首先要感謝指導教授黃偉英老師這幾年來的細心指導，不論是論文寫作、畫圖技巧、或是研究分析能力，都使得這幾年來的收穫不勝枚舉。再來要感謝口試委員關秉宗老師、莊振義老師、林登秋老師、張世杰老師給予的各種建議，雖然是個震撼教育的體驗，但卻也使自己反省不足的地方，以及未來有待努力的方向，相信這終將使研究之路走的更長與更遠。此外也要感謝英國劍橋大學 Andrew Friend 教授，在我待在英國一年的期間裡提供模式使用，並持續與我討論模式的改善與論文的内容。感謝林國銓老師提供多年心血的枯落物資料。在這些年中，研究室的人員來來去去，感謝我在裡面遇到的每位學弟妹與同學，在無數個研究室討論會議中，所提供的各種建議與經驗分享。一個人的博士班路途是孤單寂寞的，感謝世彬、紫翎、智昕在學術路途上的討論與分享。最後，我想謝謝我最愛的家人，感謝他們這幾年來的體諒與支持，讓我走到今日。未來的日子，是挑戰的開始，也是學術漫漫長路的起點，僅以此論文，感謝旅程中所有遇到的人事物。



TABLE OF CONTENTS



CHAPTER

I.	Introduction.....	1
II.	<i>Investigating the spatial heterogeneity of subtropical montane cloud forest plantation with a QuickBird image</i>	
	1. Abstract.....	6
	2. Introduction.....	7
	3. Methods.....	9
	4. Results.....	20
	5. Discussion.....	28
III.	<i>Temporal and spatial patterns of remotely sensed litterfall in subtropical forests of Taiwan</i>	
	1. Abstract.....	34
	2. Introduction.....	35
	3. Methods.....	38
	4. Results.....	53
	5. Discussion.....	64
	6. Conclusions.....	69
IV.	<i>Using a dynamic global vegetation Hybrid v4.2 model to simulate typhoon-induced leaf litter under different typhoon intensity and frequency in a subtropical forest</i>	
	1. Abstract.....	71
	2. Introduction.....	72
	3. Methods.....	75
	4. Results.....	83
	5. Discussion.....	100
V.	Conclusions.....	105
VI.	References.....	108

LIST OF TABLE

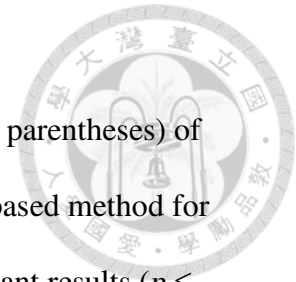


Table 1. The vegetation characteristics (\pm standard deviation [sd] in parentheses) of *Chamaecyparis obtusa* var. *formosana* extracted by an object-based method for different elevation and slope classes. Asterisks indicate significant results ($p \leq 0.05$) according to analysis of variance. Note that canopies touched by the boundaries of topographical groups (high vs. low elevation, steep vs. flat slope) are included in the analysis. Therefore, values of mean carbon, density, carbon density and cover would be slightly higher than the overall estimates.....23

Table 2. The vegetation characteristics (\pm standard deviation [s.d.] in parentheses) of broadleaf plant patches extracted by an object-based method for different classes of elevation and slope. Asterisks indicate significant results ($p \leq 0.05$) according to analysis of variance. Note that patches touched by the boundaries of topographical groups are included in the analysis. Therefore, the values of patch density would be slightly higher than the overall estimate.....24

Table 3. Site characteristics for model simulation and validation; CF and EBF correspond to coniferous forest and evergreen broadleaf forest, respectively.....42

Table 4. Models ($Y = b_0 + b_1T + b_2R + b_3PV-CV$) to estimate litterfall ($Mg\ ha^{-1}\ yr^{-1}$) using the Moderate Resolution Imaging Spectroradiometer (MODIS) land surface temperature, the Tropical Rainfall Measuring Mission (TRMM) precipitation data, and photosynthetically active vegetation cover fraction (PV) derived from the 500 m MODIS surface reflectance data. T is the annual accumulated temperature ($^{\circ}C$), R is annual precipitation (ap, mm) or coefficient of variation of monthly precipitation (CV, %), and the PV-CV is CV of monthly PV (%). All these models are statistically significant ($p < 0.001$).....57

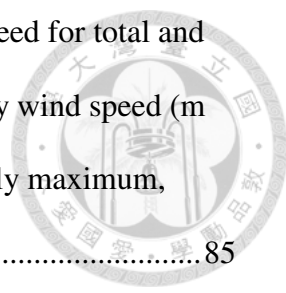


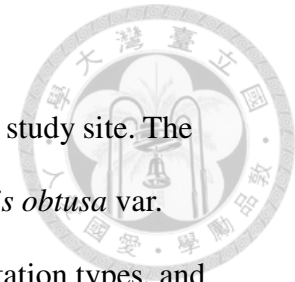
Table 5. The relationships between leaf litter (kgC m^{-2}) and wind speed for total and typhoon months by the linear regression model. Maximum daily wind speed (m s^{-1}) and turbulence kinetic energy were used to calculate monthly maximum, mean and variance of wind speed.85

Table 6. The statistics results of leaf litter productions and wind speeds among four seasons by one-way ANOVA analysis. Spring is from March to May, summer is from June to August, autumn is from September to November, and winter is from December to February.....87

Table 7. The statistics results of different typhoon intensities and frequency for leaf litter (kgC m^{-2}) by one-way ANOVA analysis. Typhoon intensity was classified as mild, moderate and severe typhoons, and typhoon frequency was classified as occurrence of typhoon per month and per year.....88

Table 8. Validation of mean (\pm s.d.) of field observed and modeled data for leaf litter, LAI and total biomass. The first observed LAI was the direct measurement of foliage in the field, while the second one was indirect LAI measurement from LAI-2000 Plant Canopy Analyzer. The modeled data represent the Hybrid model with wind built-in function, while baseline modeled data represent the primitive Hybrid model.91

LIST OF FIGURES



- Figure 1. A panchromatic QuickBird image of the Chilan Mountain study site. The dark-coloured polygon outlines the boundary of *Chamaecyparis obtusa* var. *formosana* (CHFO) plantation forest surrounded by other vegetation types, and the bright-coloured irregular line within the site is an unpaved dirt road. The location of the study site (the star) with the background of a digital elevation model is displayed in the lower right corner. 11
- Figure 2. An object-based canopy extraction process. The contrasted QuickBird panchromatic and multispectral images were fused to enhance the edges of tree crowns in order to delineate canopy area..... 13
- Figure 3. (a) Elevation (solid lines) and slope (background) of the study area; (b) broadleaf plant patches extracted from the 0.7 m sharpened QuickBird image; and (c) the Enhanced Vegetation Index (EVI) of study area estimated by the QuickBird 2.8 m multispectral image. 17
- Figure 4. Thirty metre equal path distance (solid lines) (first eight intervals) away from (a) the road (the solid thick line) and (b) natural vegetation (*Cryptomeria japonica*, mature, mixed forests) edges (all but the interior core area) in the study area (Figure 1). Dotted lines in (a) indicate the intervals of 60 m, 100 m and 412 m (in order) away from the road. 19
- Figure 5. Proportions (%) of plants and covered areas of different size classes of *Chamaecyparis obtusa* var. *formosana* in the study site. 21
- Figure 6. The edge effect of unpaved road on the *Chamaecyparis obtusa* var. *formosana* plantation within each interval (Figure 4(a)). Bars indicate ranges of 95% confidence interval; proportions (%) of intervals to the study area are given

in parentheses under the x-axis. (a) Mean CHFO canopy area and tree density. (b) Mean carbon and carbon density for each individual tree and interval, respectively. (c) Mean patch area and patch density of broadleaf vegetation.26

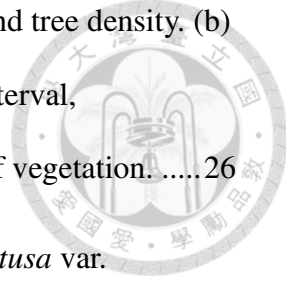


Figure 7. The edge effect of natural edges on the *Chamaecyparis obtusa* var. *formosana* plantation within each interval (Figure 4(b)). The data analysis and presentation are identical to Figure 6.27

Figure 8. (a) The model (triangles) and validation (circles) sites used to establish and verify the litterfall model, respectively. A full name and short description for each site can be found in Table 3. The green monochromatic layer is a long-term (2000–2011) average of the photosynthetically active vegetation (PV) fractional cover (%) of the forests. (b) The geographic map of Taiwan.39

Figure 9. The anomalies of temperature (°C) (dashed line) and precipitation (mm month⁻¹) (above mean: light-colored bars; below mean: dark-colored bars) were calculated from monthly temperature and precipitation minus long-term (1993–2011) mean values. Positive temperature and precipitation indicates hotter and wetter conditions than the long-term median value. The black arrow indicates a typhoon in which the central wind velocity of the typhoon is over 32.7 m s⁻¹.40

Figure 10. Data from the MODIS land surface temperature (T_{LST}, x-axis) were compared to field temperature records (T_f) derived from local weather stations in the model sites during 2001–2011. There was a significant correlation between the satellite and field measurements ($r^2 = 0.722$, $p < 0.001$). The weather stations were at the Taiwan Forestry Research Institute (for FS, Figure 8), National Taiwan University (CLM), and Taiwan Central Weather Bureau (the remaining sites).46

Figure 11. Spectral profiles of the endmember library of (a) photosynthetically active vegetation (PV), (b) nonphotosynthetically active vegetation (NPV), and (c) bare soil (BS). The spectra were convoluted to match with the MODIS wavelengths (d-f for PV, NPV and BS, respectively). The PV hyperspectral endmembers were extracted from Hyperion images, whereas those of the NPV and BS were acquired from a portable field spectroradiometer. The solid, dashed and dotted lines indicate one standard deviation on each side of mean and the minimum and maximum reflectance values, respectively.....50

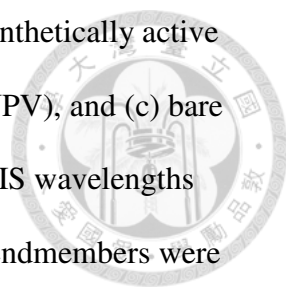


Figure 12. Spatial patterns of the mean (2001–2011) MODIS (a) MODIS PV-CV (annual coefficient of variation of PV), (b) LST (Land surface temperature) and (c) TRMM (Tropical Rainfall Measuring Mission) precipitation data at the spatial resolutions of 500 m, 1000 m and 0.25° (~ 27.5 km), respectively.....55

Figure 13. The relationship between the field litterfall (LF_f , from the validation sites in Taiwan, Figure 8, the x-axis) and estimated litterfall (LF_m , the y-axis) ($p < 0.05$, $n = 11$). The circles are evergreen broadleaf forests and triangles are coniferous forests. The black colors represent validated sites in Taiwan and remaining colors represent other subtropical forests. The solid line is the fit line and the dashed line depicts the 1:1 relationship.58

Figure 14. The mean litterfall (2001–2011) estimated by a multiple regression model using MODIS (Moderate Resolution Imaging Spectroradiometer) PV-CV (annual coefficient of variation of PV) and LST (Land Surface Temperature) as explanatory variables (Table 4).....60

Figure 15. The temporal variations of annual litterfall during 2001–2011. The 11-year LST (Land Surface Temperature) and PV-CV (annual coefficient of variation of

PV) were calculated as explanatory parameters to estimate the LF with a multiple regression model. 61

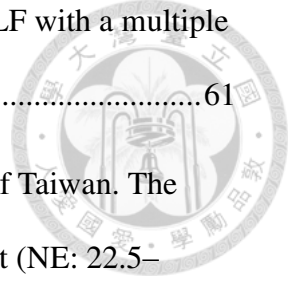


Figure 16. The topography ((a) elevation, (b) slope and (c) aspect) of Taiwan. The aspect classes are: north (N: 0–22.5° and 337.5–360°), northeast (NE: 22.5–67.5°), east (E: 67.5–112.5°), southeast (SE: 112.5–157.5°), south (S: 157.5–202.5°), southwest (SW: 202.5–247.5°), west (W: 247.5–292.5°) and northwest (NW: 292.5–337.5°)..... 62

Figure 17. (a) The significant ($r^2 = 0.284, p < 0.05$) relationship between 11-year (2001–2011) modeled (Table 4) mean annual litterfall (LF) and elevation. (b) The insignificant ($r^2 = 0.065, p > 0.05$) correlation between mean LF and slope. (c) The mean LF and standard error (bars) of different aspect classes (north [N: 0–22.5° and 337.5–360°], northeast [NE: 22.5–67.5°], east [E: 67.5–112.5°], southeast [SE: 112.5–157.5°], south [S: 157.5–202.5°], southwest [SW: 202.5–247.5°], west [W: 247.5–292.5°], northwest [NW: 292.5–337.5°]) (One-way ANOVA F -test, $p < 0.05$). Different letters indicate significant differences between groups based upon a significant level (α) of 0.05 of the Tukey-Kramer multiple comparison. 63

Figure 18. The daily mean temperature from 1993 to 2013 was fitted by a polynomial formula (Temperature = $15.44 - 5.15\text{day} + 2.44\text{day}^2 - 0.28\text{day}^3 + 0.00959\text{day}^4$). 80

Figure 19. The patterns of monthly maximum daily precipitation and wind speed in typhoon and non-typhoon months. 81

Figure 20. Plot of maximum wind speed and observed leaf litter. Wind speed represents maximum daily wind speed in a month, while observed leaf litter

represents monthly litter. The relationships between wind speed and leaf litter for (a) typhoon and non-typhoon months, (b) spring, summer, autumn and winter seasons, (c) different typhoon intensities and (d) typhoon occurrence per month, respectively. The gray lines are linear regression. 86

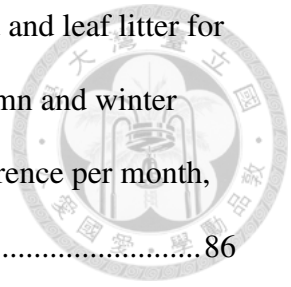


Figure 21. The plots of modeled against observed leaf litter for baseline Hybrid model and the Hybrid model with wind built-in function. The dark circle symbol represents non-typhoon impacted months, while the dark square symbol means typhoon months. The dark line represents linear regression and gray line represents 1:1 line. 90

Figure 22. The frequency distribution of maximum daily wind speed in typhoon and non-typhoon events from 1993 to 2013. 93

Figure 23. The frequency distribution of maximum daily wind speed in typhoon events was fitted by a normal distribution. (a) the fitted function of normal distribution ($\mu= 19.39, \sigma = 5.985$), (b) normal quantile-quantile plot, (c) patterns of empirical and theoretical CDFs, (d) normal probability plot. 94

Figure 24. Frequency distribution of typhoon events per year. (a) The Poisson probability density function ($\lambda = 2.0, p = 0.636$) and (b) the Poisson cumulative distribution function. 95

Figure 25. Frequency distribution of typhoon events per month in typhoon season. (a) The Poisson probability density function ($\lambda = 8.8$) and (b) the Poisson cumulative distribution function. The distribution did not follow Poisson distribution ($p < 0.001$). 95

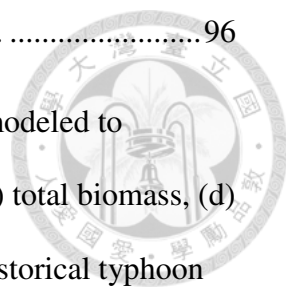
Figure 26. The historical climate dataset with typhoon and non-typhoon from 1993 to 2013 were modeled to evaluate the influences of typhoon on (a) leaf litter, (b)

LAI, (c) total biomass, (d) soil respiration, (e) GPP and (f) NPP. 96

Figure 27. The increases of typhoon intensity on wind speed were modeled to evaluate the influences of intensity on (a) leaf litter, (b) LAI, (c) total biomass, (d) soil respiration, (e) GPP and (f) NPP. The zero represents the historical typhoon intensity with the mean wind speed at 19.39 (m s⁻¹). 97

Figure 28. The increases of typhoon frequency per year were modeled to evaluate the influences of frequency on (a) leaf litter, (b) LAI, (c) total biomass, (d) soil respiration, (e) GPP and (f) NPP. The zero represents the historical typhoon frequency. 98

Figure 29. The changes of ratio of leaf litter to total biomass (%) in typhoon intensity and frequency simulations. 99



CHAPTER I

Introduction



The carbon stock of the forest ecosystem is the quantity of carbon in a system and it determines the capacity of the forest ecosystem to accumulate or release the carbon (Field et al. 2014). The annual carbon fluxes between vegetation-soil system and the atmosphere via photosynthesis and respiration is 12 times larger ($\approx 123 \text{ GtC yr}^{-1}$ and $118.7 \text{ GtC yr}^{-1}$) than the anthropogenic carbon emission ($\approx 9.5 \text{ GtC yr}^{-1}$ in 2011) (Ciais et al. 2013). Forest ecosystems storing more than 80% of all terrestrial aboveground carbon and more than 70% of all soil organic carbon represent the largest component of terrestrial stocks for atmospheric CO_2 (Ciais et al. 2013; Jandl et al. 2007). Therefore, evaluating carbon stock and flux of forest ecosystem is critical in understanding global carbon budget.

The terrestrial ecosystem contains 450-650 GtC carbon in living vegetation biomass (Ciais et al. 2013), and estimating living biomass is a critical step to quantify carbon stock in forest ecosystem. Litterfall, which is the shedding of plant tissues and dead plants, is the major transfer of carbon and nutrients from aboveground living biomass to the soil (Leff et al. 2012; Ostertag et al. 2008). The carbon loss from litterfall and roots via decomposition is an important flow to maintain the balance of an ecosystem carbon budget (Ostertag et al. 2008; Sayer et al. 2007). Disturbance is a factor to alter forest regeneration, composition, structure and function within a short period, and it can sometimes remove large amounts of biomass or derive substantial litterfall to change forest carbon stocks and flux (Dale et al. 2001). Tropical cyclone ('typhoon' or 'hurricane', depending on the geographic region; this dissertation uses 'typhoon') is one of the most active natural disturbances in Western North Pacific

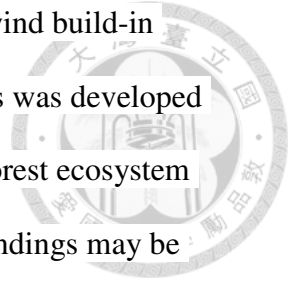
ocean (Lin et al. 2011). Strong wind and heavy precipitation may cause massive litterfall, which will increase soil respiration and alter ecosystem carbon cycle (Brokaw and Walker 1991; Chambers et al. 2007a; Lin et al. 2011; Vargas and Allen 2008). Global warming may have contributed to the increasing of sea surface temperature in typhoon formation regions, and might affect typhoon activity by altering typhoon intensity or frequency (Emanuel 2005; Knutson et al. 2010). Therefore, estimating living biomass and litterfall and considering typhoon effects on carbon stock and flux may be important to evaluate responses and feedbacks of forest carbon cycle under perturbed events.

Forest inventory is the conventional method to estimate aboveground living biomass by measuring the diameter at breast height of trees, which can be converted to biomass using empirical allometry for each tree species (Gibbs et al. 2007). Forest inventory is also the major way to observe litterfall by collecting litter from litter traps. However, field inventory is labour-intensive and just a few of them have repeated, long-term inventories, which may not capture seasonal and interannual dynamics. Remote sensing has been widely used for the systematic observation of Earth for over 40 years at regional scale (DeFries 2008). Remote sensing methods are generating new regional perspectives for ecology on phenology, canopy nutrients, species identification, biomass, forest structure attributes, land-use and land-cover change (Chambers et al. 2007b). For instance, vegetation greenness time-series (e.g., the Normalized Difference Vegetation Index, NDVI) derived from optical (350–2500 nm) remotely sensed data can be treated as a surrogate to determine the vegetation dynamics and ecosystem productivity of different settings (Chambers et al. 2007b; Frohling et al. 2009; Ostertag et al. 2008). Hyperspatial remote sensing provided a way to quickly and effectively measure the canopy area over a vast region (Wang et al.

2004), which is probably the only structural parameter that is highly correlated to carbon stocks (Brown et al. 2005). These parameters are pivotal to observe and model the forest structure and biogeochemistry (Huang et al. 2008). Furthermore, a simulation model is the process of creating and analyzing of a physical model to predict Earth system operate and interact with each other. When the ecosystem is disturbed by typhoons, changes of biogeochemical cycles and ecological process might constrain the system's structure and function (Beard et al. 2005; Chambers et al. 2007a; Lin et al. 2011). A simulation model tries to represent these biogeochemical linkages and ecological process, and make reliable predictions of future ecosystem behavior and responses under simulated conditions (Friend 2010; Hurtt et al. 2010).

Although using remote sensing or a simulation model to evaluate the carbon cycle in forest ecosystems are important, it was still absent to estimate litterfall by satellite images at regional scale in tropical/subtropical forests. There was also bare to use a process-based simulation model to evaluate the effects of typhoons on the carbon cycle of forest ecosystems. Therefore, the objectivities of this dissertation were: (1) In Chapter 2, *Investigating the spatial heterogeneity of subtropical montane cloud forest plantation with a QuickBird image*, canopy areas from a high spatial resolution QuickBird image were extracted to estimate living biomass and to observe vegetation characteristics across topographical gradients in a montane cloud forest. (2) In Chapter 3, *Temporal and spatial patterns of remotely sensed litterfall in subtropical forests of Taiwan*, time-series vegetation and climate indices were utilized from the Moderate Resolution Imaging Spectroradiometer (MODIS) satellite imagery to derive litterfall. The results would be useful to understand long-term temporal and spatial patterns of litterfall across subtropical forests. (3) In Chapter 4, *Using a dynamic global vegetation Hybrid v4.2 model to simulate typhoon-induced leaf litter under*

different typhoon intensity and frequency in a subtropical forest, a wind build-in function with wind speed, temperature and precipitation as variables was developed into the Hybrid model to simulate defoliation and carbon cycle of forest ecosystem under different scenarios of typhoon intensity and frequency. The findings may be useful to evaluate the biomass and litterfall at regional scale and understand the patterns of carbon cycle under typhoon disturbances.



CHAPTER II



Investigating the spatial heterogeneity of subtropical montane cloud forest plantation with a QuickBird image

This chapter has been published in the International Journal of Remote Sensing.

Wang HC, & Huang CY (2012). Investigating the spatial heterogeneity of a subtropical montane cloud forest plantation with a QuickBird image. *International Journal of Remote Sensing*, 33(24): 7868-7885.

Investigating the spatial heterogeneity of subtropical montane cloud forest plantation with a QuickBird image



Abstract

Forest plantations, consisting of a single, even-age species, have long been recognized as homogeneous landscapes. However, the heterogeneity of the system may be amplified by bioclimate, which in turn can be modified by physical environments. This study attempted to assess the ramifications of two major factors, topography and the edge effect, on the subtropical montane cloud forest false cypress (*Chamaecyparis obtusa* var. *formosana*, CHFO) plantation in Taiwan by integrating field observations, a high spatial resolution QuickBird satellite image and spatial layers of topography. Our regional analysis indicated that there was a negative relationship between slope and the size of CHFO. Surprisingly, this study also observed a significant amount of natural broadleaf plant patches within the site, and large size patches were frequently encountered at low elevation. For the edge effect analysis, the area along (0-30 m) the road and natural edges yielded low canopy area and carbon (kgC stem^{-1}) for each individual CHFO plant as well as low CHFO population (stems ha^{-1}) and carbon (MgC ha^{-1}) densities. Contrarily, large broadleaf plant patches were found along the road edges. Our findings suggest that topography and the edge effect may alter the spatial patterns of nutrients and bioclimate that vary the structure of the vegetation; the heterogeneity of forest plantation may be underestimated. This study also demonstrates the feasibility of integrating field, remote sensing and Geographic Information System techniques to quantify forest structure at the landscape scale. The derived structure parameters can be further utilized to model ecosystem carbon dynamics over a vast region.

Keywords: carbon stock, crown area, edge effect, Taiwan, topography



1. Introduction

Plantation forests occupy about 3.8% (140 million ha) of the world's forests and have increased rapidly (2.8 million ha y^{-1}) in recent years (FAO 2005). Most plantation forests consist of short-rotation and fast-growing trees, which contribute significantly to carbon (C) sequestration in terrestrial environments. Plantation forests are often even-age, pure and uniform stands. It is often assumed in plantation research (e.g., carbon stock estimation) that heterogeneity is negligible in this type of ecosystem (Lodhiyal and Lodhiyal 1997; Montagnini 2000; Specht and West 2003) and many others).

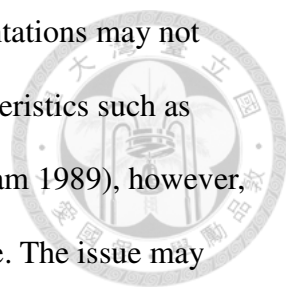
Montane cloud forests (MCF) are commonly found in tropical and subtropical regions of the world (Foster 2001) and are frequently immersed in heavy fog and high humidity that would greatly reduce solar radiation (Hamilton et al. 1995). Plantations are commonly planted in this foggy zone and are habitat for several species of high economic value such as *Chamaecyparis* spp. (Klemm et al. 2006). Previous studies revealed that fog may represent about half of the annual precipitation in MCF; the water cycle of the system could be affected significantly due to the swift cloudbank (the source of fog) height caused by climate change (Cavelier and Goldstein 1989). Pounds et al. (1999) found that global warming has raised the height of the orographic cloudbank resulting in less cloud immersion and increasing dryness. These micrometeorological changes may influence the abundance of epiphytes and tree ferns that play critical roles in maintaining the health of MCF (Foster 2001). The increased height of the cloudbank may also affect the rate of photosynthesis and respiration and reduce the capacity of carbon sequestration in MCF (Chang et al. 2008; Foster 2001;

Mildenberger et al. 2009).

There is a close relationship between topography, bioclimate (precipitation, surface temperature and solar radiation), and soil nutrient and water contents, which are the determinants of plant growth (Briggs and Knapp 1995; Chen et al. 2007). Previous studies showed that stem size and stand density were sensitive to topography; patterns in above- (AGB) and below-ground biomass (BGB) and net primary production (NPP) allocation were also changed along the topographical gradients (Clark and Clark 2000). Substrate characteristics such as soil nutrients, texture and water availability vary greatly across landscapes, and these may influence vegetation structure substantially (Hook and Burke 2000).

The edge effect is another pivotal factor for modifying landscape patterns. Two types of edges are commonly found in forest plantations: (1) Man-made edges (e.g., roads) resulting from anthropogenic activities creating sharp boundaries (Reed et al. 1996); and (2) natural edges between two vegetation types which form relatively moderate transitions (Murcia 1995). The magnitude of the edge effect declines with the increment of distance from the edge and may form its own microenvironment and biota (Malcolm 1994). Edges often have higher incident light, air and soil temperature, wind speed, and lower relative humidity and soil moisture relative to the forest interior (Baker and Dillon 2000). Edges with higher incident light facilitate plant growth as a result of higher stem densities and basal areas in tropical and warm temperate forests (Williams-Linera 1990; Young and Mitchell 1994). However, plants may also be vulnerable to the edge effect resulting in high tree mortality due to low tolerance to edge-related perturbations such as strong winds (Aguilar and Tabarelli 2010).

Based upon the aforementioned physical and biological drivers that may alter



landscape patterns, this study suspect that the structure of MCF plantations may not be as homogeneous as previously recognise. Plant structural characteristics such as canopy area can be precisely measured using a field method (Bonham 1989), however, the variation of forest structure is difficult to assess at the local scale. The issue may be resolved by utilizing high spatial resolution optical images (hyperspatial remote sensing) and object-based image segmentation tools (Wang et al. 2004) to delineate tree canopies over a large area at low cost. Consequently, biomass and carbon stocks of the region may be estimated with the knowledge of an allometric equation and biomass-carbon conversion coefficient of the site (Fuchs et al. 2009), respectively. Stem and carbon densities and cover can also be computed after taking the area into account (Huang et al. 2009). Following this approach, regional assessment of forest structure variations across environmental gradients can be conducted by integrating the remote sensing estimates with topographical data (e.g., a digital elevation model [DEM]). Therefore, the objective of this study is to investigate the spatial heterogeneity of a MCF plantation by coupling field, remote sensing and Geographical Information System (GIS) techniques. The specific questions we sought to answer were the following: (1) how do vegetation characteristics change across topographical gradients; (2) how do the road and natural boundary edges influence vegetation structure of a forest plantation?

2. Methods

2.1 *Site description*

The 61-ha MCF plantation is located on the Chilan Mountain in northern Taiwan (24°35'N, 121°25'E) (Figure 1) across a wide elevation range (1400-1800 m asl). The climate is temperate and humid, and the mean annual temperature and precipitation

are 13°C and 4005 mm, respectively. The occurrence of fog events caused by air masses lifting from the valley is about 300 days y⁻¹ and occupies 38% of the total time. The high frequency and long duration of fog events reduces solar radiation and adds about 330 mm y⁻¹ of water deposition to the system. In addition, many nutrient inputs (e.g., ammonia) carried by fog may also have pronounced contribution and account for 35-55% of total depositions (Klemm et al. 2006). *Chamaecyparis obtusa* var. *formosana* (CHFO) is the predominant tree species of the site and was planted after clear-cutting in the 1960s. The surroundings are natural, old-growth *Chamaecyparis* forests that have existed for at least 2000 years (Figure 1). The major management objective of CHFO plantations at Chilan Mountain is to restore the populations of CHFO, which is a habitat for many endemic flora and fauna. Because of the variation of topography and climate regime, the study site affords unique opportunities to study the spatial heterogeneity of subtropical montane cloud forest plantation. Broadleaf tree species were also recorded in the region such as *Dendropanax dentiger*, *Illicium anisatum*, *Machilus thunbergii* and *Lindera communis* (Chang et al. 2008).

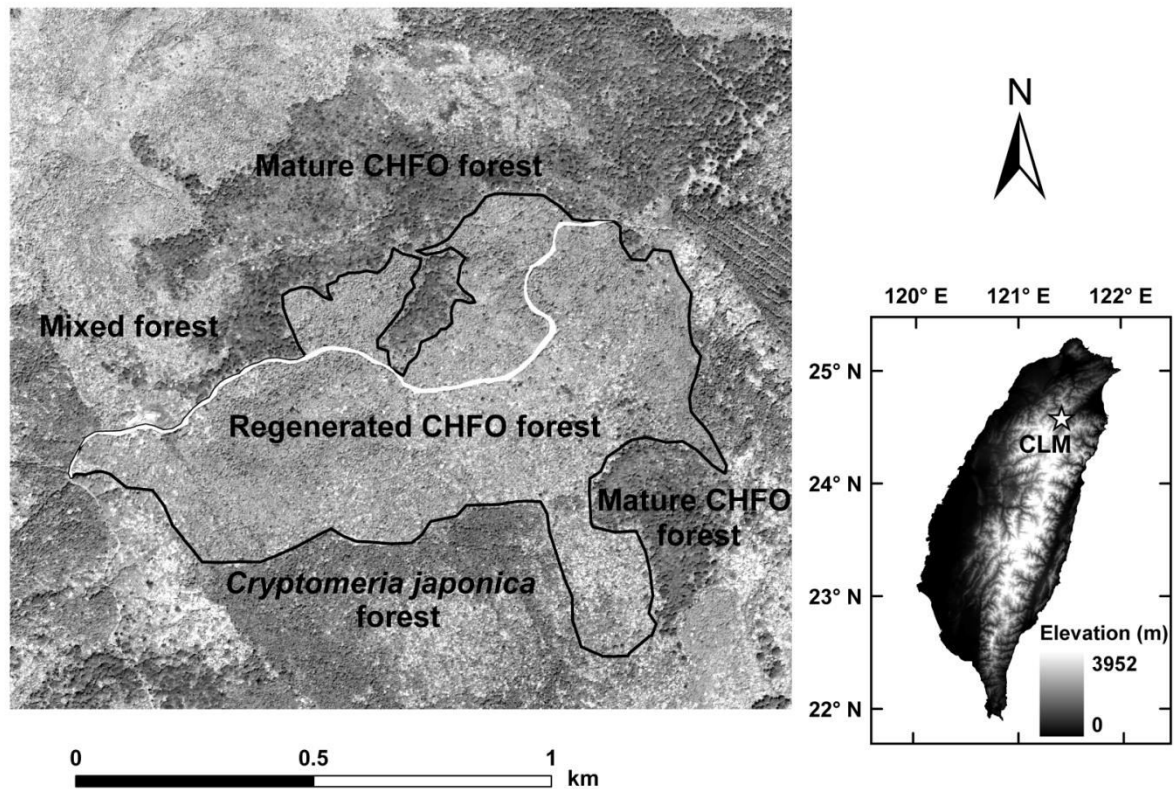


Figure 1. A panchromatic QuickBird image of the Chilan Mountain study site. The dark-coloured polygon outlines the boundary of *Chamaecyparis obtusa* var. *formosana* (CHFO) plantation forest surrounded by other vegetation types, and the bright-coloured irregular line within the site is an unpaved dirt road. The location of the study site (the star) with the background of a digital elevation model is displayed in the lower right corner.

2.2 Remotely sensed data acquisition and pre-processing

The biophysical properties of CHFO vegetation were characterized using a high spatial resolution cloud-free QuickBird image (Ozdemir 2008) (Figure 1). The sensor was launched in 2001 and collects one panchromatic (spectral range: 450-900 nm) and four multispectral images (blue, green, red and near-infrared [NIR] spectral ranges: 450-520 nm, 520-600 nm, 630-690 nm and 760-900 nm, respectively). The dynamic range of the image is 11-bit, and the spatial resolutions are 0.61-0.7 m and 2.44-2.8 m for the panchromatic and multispectral images, respectively, dependent on viewing angle. The image of this subtropical MCF was acquired at 10:12 (UTC) on 11 May 2009. A standard imagery product was obtained, with geo-registration applied by the provider.

Two types of remote sensing pre-processing procedures, image contrasting and atmospheric correction, were applied to the image. The image contrasting enhances the texture in an image, whereas atmospheric correction procedure removes the atmosphere profile (e.g., molecular and aerosol scattering, water vapour) from remotely sensed data so the retrieved signals would truly reflect the properties of the land surface. We first used reported standard conversion coefficients to compute at-sensor spectral radiance ($\text{W m}^{-2}\mu\text{m}^{-1}\text{sr}^{-1}$) from the raw data. For the image contrasting, we stretched the data by subtracting the lowest measured spectral radiance from each panchromatic and multispectral band, and normalized the data range to 0-1 (Figure 2). For the standard atmospheric correction, we used radiative transfer software, the Atmospheric CORrection Now (ACORN) v. 6b (ImSpec LLC, Palmdale, CA, USA), to remove the atmosphere profile from the image and convert at-sensor radiance to surface radiance (unitless). A tropic mode, atmosphere visibility and water vapour of 90 km and 20 mm, respectively, were set for ACORN by

referring to the user manual (ACORN 2008) and using an international network of precipitable water vapour estimation (SuomiNet 2012).

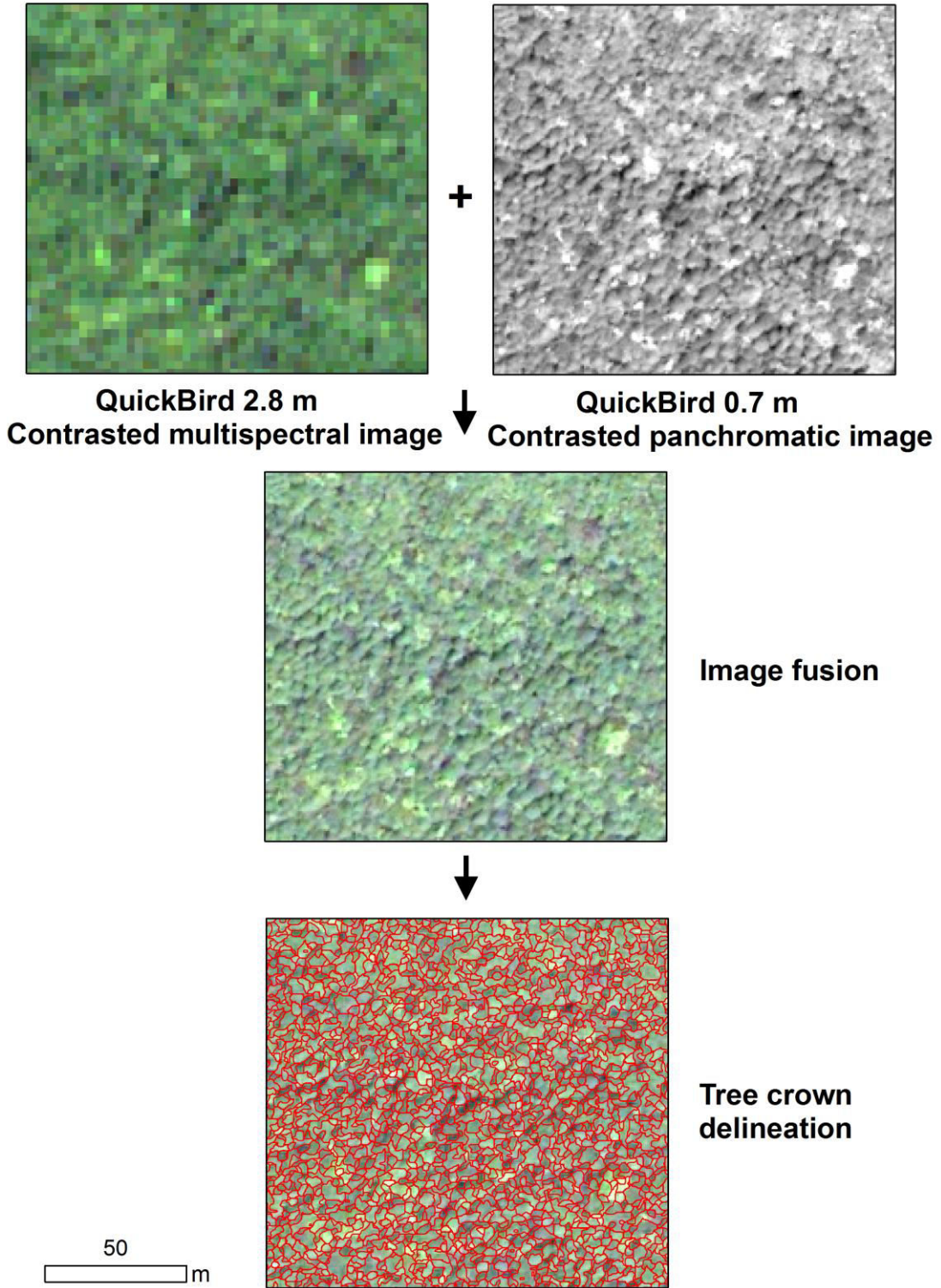


Figure 2. An object-based canopy extraction process. The contrasted QuickBird

panchromatic and multispectral images were fused to enhance the edges of tree crowns in order to delineate canopy area.



2.3 Field CHFO total carbon estimation

An *in-situ* CHFO allometric method was utilized to use canopy area as an independent variable to estimate total carbon (Yeh 2004). Aboveground biomass (AGB) of 15 top-layer trees of different sizes of canopy (mean \pm standard deviation [sd] = $6.6 \pm 3.5 \text{ m}^2$, range = 1.4-13.0 m^2) were harvested; the canopy area (A) was estimated by dividing it into eight equal-angle (45°) triangles (eq. 1), where L_n is the projected length of canopy area (A) from the main stem of CHFO.

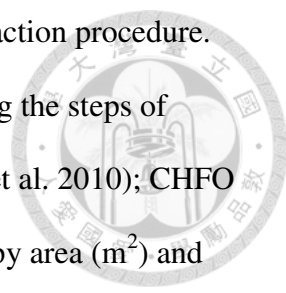
$$A = \sum_{n=1}^8 L_n \times L_{n+1} \times \sin 45^\circ \quad (1)$$

According to another study of this same area (Chu 2005), the ratio of AGB and BGB is 1.55 (AGB = $140.40 \text{ Mg ha}^{-1}$ and BGB = 76.60 Mg ha^{-1}) and the carbon content of CHFO biomass is approximately 50%. Therefore, by integrating these parameters, we estimated the total carbon storage of CHFO using canopy area (eq. 2).

$$\ln(C) = 1.01 + 1.58\ln(A), \quad r^2 = 0.96 \quad (2)$$

2.4 Regional vegetation structure delineation

To delineate tree canopy areas, an advanced image fusion algorithm, the Gram-Schmidt spectral sharpening method (Fuchs et al. 2009), was applied to the contrasted QuickBird image to generate a 0.7 m multispectral image (Figure 2) was used as an input for a Feature Extraction module (Canty 2006). The Feature Extraction module provides object-based algorithms to extract information from an image based on its spatial, spectral and texture characteristics. The feature extraction



workflow consists of a threshold setting and an optional object extraction procedure. The threshold setting is used to find objects from an image following the steps of segmentation, merging, refinement and attribute computation (Tan et al, 2010); CHFO canopy area can then be delineated and used to estimate mean canopy area (m^2) and carbon (kg stem^{-1}) using eq. 2. Moreover, the stem density (stems ha^{-1}), woody carbon density (Mg ha^{-1}) and cover of the study site can be computed after taking the area into account. An optional procedure of the Feature Extraction module is to extract an object of interest by implementing supervised or rule-based classification. These methods have been commonly found in remote sensing literature. Details of the classification algorithms are described in Jensen (2004). Rule-based classification was selected to delineate broadleaf plant attributes (patches and patch area) with less distinct crown shape in the image, and patch density can be computed using a GIS.

To validate the performance of image segmentation, we compared it with field CHFO cover measured using a hemispherical (fisheye) photography approach (Rich 1990) in spring 2010. Hemispherical photographs were taken from seven transects and canopy cover of each sampled area was derived by averaging 4-5 measures with a 5 m interval. Locations were geolocated using a sub-metre resolution Global Positioning System (Trimble GeoXH 3000, Trimble Navigation Limited, Sunnyvale, CA, USA) in order to precisely match field observations with the spatially corresponding remote sensing estimates. To maximise the contrast between gap openings and plant, we took photographs on an overcast day and utilised the HemiView 2.0 software (Delta-T 2000) to calculate canopy cover.

2.5 Vegetation greenness estimation

The atmospherically corrected QuickBird multispectral bands were used to

compute the Enhanced Vegetation Index (EVI), which was used to estimate the greenness of the site. The EVI enhances vegetation signals that would not saturate in a highly vegetated area. It is also not sensitive to background noise from the soil and atmosphere profile that would typically contaminate satellite signals (Huete et al. 2002). The model for the EVI is:

$$EVI = G \times \frac{(\rho_{NIR} - \rho_{Red})}{(\rho_{NIR} + C_1 \times \rho_{Red} - C_2 \times \rho_{Blue} + L)} \quad (3)$$

where ρ is surface reflectance (unitless) and the subscripts indicate NIR, red and blue bands. Note that G is a gain factor, C_1 and C_2 are atmosphere resistance correction coefficients, and L is the canopy background brightness correction factor. The coefficients adopted in eq. 3 were $G = 2.5$, $C_1 = 6$, $C_2 = 7.5$, and $L = 1$. EVI values of CHFO and broadleaf plant vegetation were compared using analysis of variance (ANOVA).

2.6 Topography analysis

A 30 m DEM was acquired from the Advanced Spaceborne Thermal Emission and Reflection Radiometer (ASTER) global DEM database (ASTER 2012) (Figure 3 (a)). We derived the topographic information (elevation, slope and aspect) from DEM using ArcGIS v. 9.3 (Ormsby et al. 2009). Elevation and slope were regrouped to low (1469-1629 m) and high (1630-1789 m), flat (1-16°) and steep (17-31°), respectively, following the rule of equal range. Aspect was discarded from the analysis due to the homogeneity of the slope facings (only south to southeast facing slopes on the site). To avoid the interaction between elevation and slope, we further partitioned the topography into four groups (low/high elevation \times flat/steep slope). ANOVA was used to test the differences between CHFO canopy area, carbon mass, and broadleaf plant

patch area in different terrains, and other attributes (CHFO stem density, carbon density, cover and broadleaf plant patch density) were directly compared.

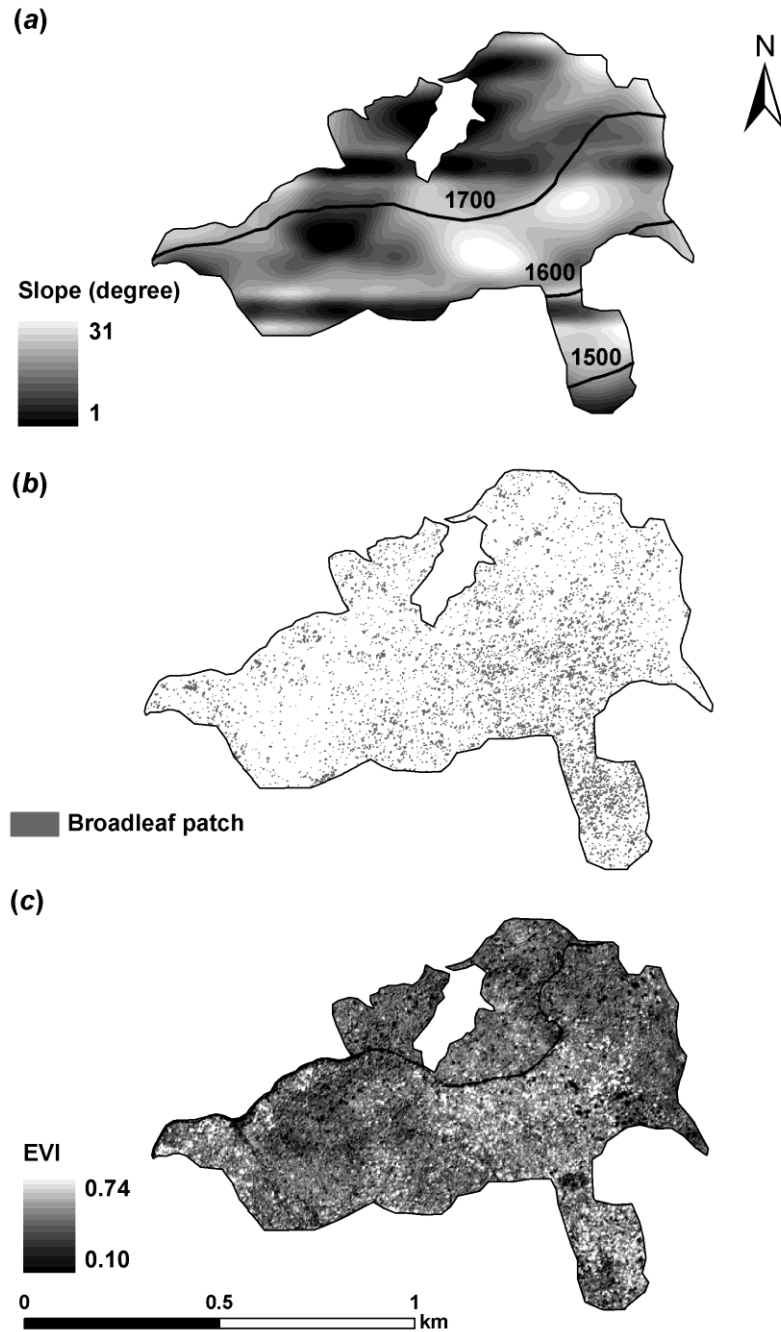
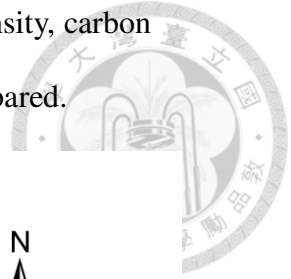


Figure 3. (a) Elevation (solid lines) and slope (background) of the study area; (b) broadleaf plant patches extracted from the 0.7 m sharpened QuickBird image; and (c) the Enhanced Vegetation Index (EVI) of study area estimated by the QuickBird 2.8 m multispectral image.

2.7 The edge effect analysis

In this study, two types of edges were studied: The edges between the study site and the unpaved dirt road (man-made edges) and natural vegetation (natural edges) (Figure 1). We used the 30 m DEM to compute path distance (distance taking terrain variation into account) away from the edges. According to more than 70 studies (see review by Baker and Dillon 2000), the influence of edge effects was evident at distances less than 240 m in most cases. Hence, we set the distance for the first eight intervals away from the 4 m wide road to 30 m and increased the length gradually to 60 m, 100 m and 412 m intervals (Figure 4 (a)). For the natural vegetation edges, we used a 30 m interval toward the core of the study area except for the last one at the centre of the site (Figure 4 (b)). The remote sensing estimates of CHFO canopy area, carbon, stem density, carbon density, broadleaf plant patch areas and broadleaf plant patch density within each interval were compared.

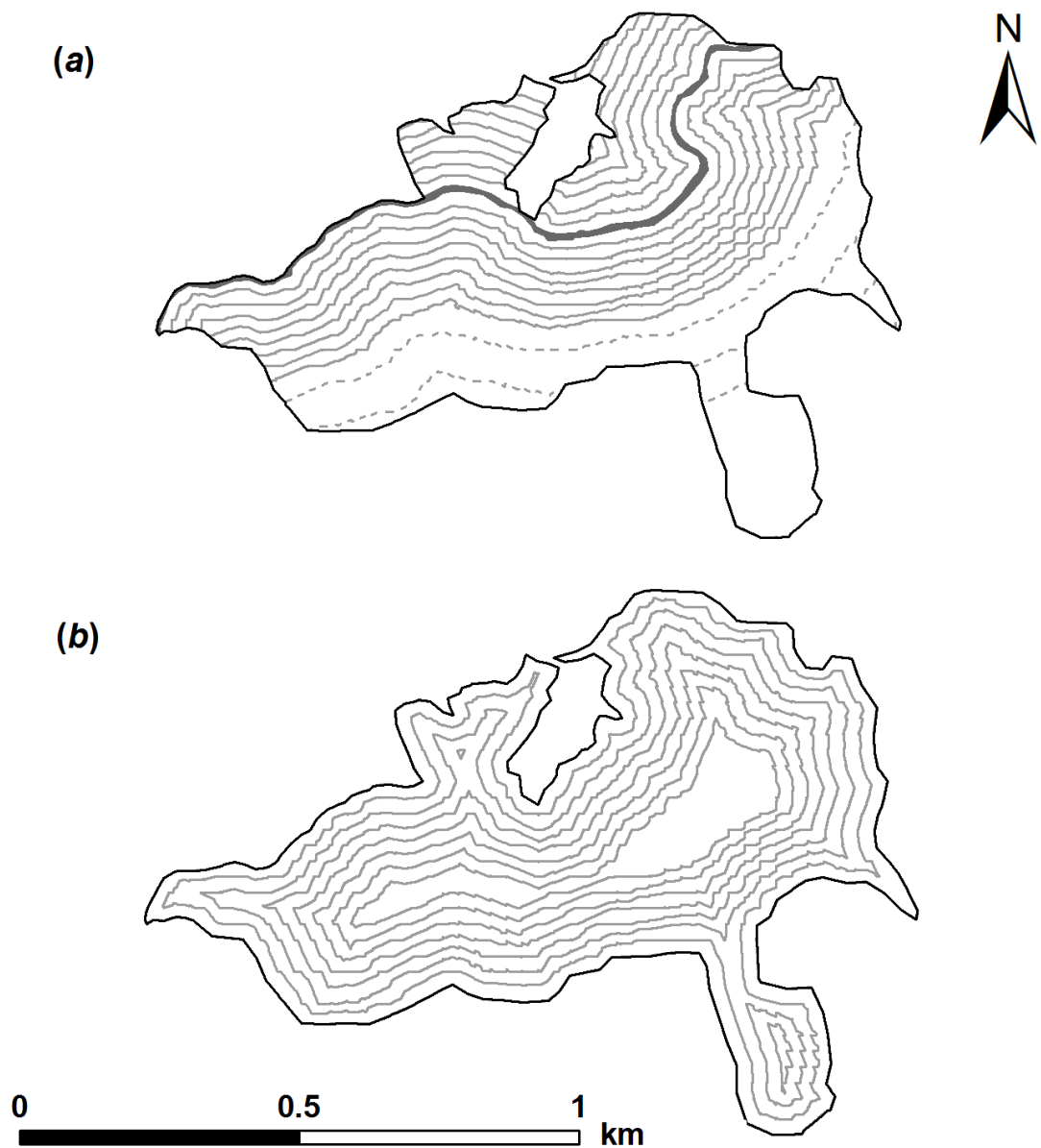


Figure 4. Thirty metre equal path distance (solid lines) (first eight intervals) away from (a) the road (the solid thick line) and (b) natural vegetation (*Cryptomeria japonica*, mature, mixed forests) edges (all but the interior core area) in the study area (Figure 1). Dotted lines in (a) indicate the intervals of 60 m, 100 m and 412 m (in order) away from the road.

2.8 Sampling strategy

Remotely sensed data usually generates a tremendous amount of samples, which would be an issue for a statistical test; the difference among groups may become negligible after taking the sample size into account. In addition, the spatial dependence of these data may prevent the use of regular statistical tests (Isaaks and Srivastava 1989). Therefore, it is necessary to sample the data in a random fashion (Brus and DeGrujter 1993). Yamane (1967) provided a simple model (eq. 4) to select a proper sample size:

$$n = N / (1 + N \times e^2) \quad (4)$$

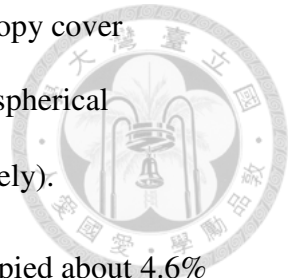
where n , N and e are the sample size, the population size and the uncertainty respectively. In this study, we set $e = 0.05$ for statistical tests. The model was applied to the topographic and greenness analyses with large samples.

3. Results

3.1 The structure of regenerated CHFO forest

In this study, we utilized high spatial resolution remote sensing coupled with object-based algorithms to delineate tree crowns in a regenerated CHFO forest. A total of 39,785 CHFO trees were delineated in the study site. The mean (\pm s.d.) canopy area of this study site was $12.4 \pm 9.6 \text{ m}^2$. Mean (\pm sd) carbon per individual was $138 \pm 118 \text{ kgC}$ with an estimated site C density of $119.3 \text{ MgC ha}^{-1}$. The CHFO sizes ranged from $34\text{-}992 \text{ kgC stem}^{-1}$ (Figure 5). The majority (78%) of CHFO plants was less than $200 \text{ kgC stem}^{-1}$, but the remaining small portion of large trees occupied about 43% of total carbon. In general, the performance of object-based tree crown delineation was satisfactory in successfully outlining the texture of image based upon the visual

inspection (Figure 2). There was a minor discrepancy (7.9%) of canopy cover estimates by the remote sensing image segmentation and field hemispherical photography (mean \pm s.d. = $83.3 \pm 4.0\%$ and $91.2 \pm 1.2\%$, respectively).



Fractional cover of CHFO was 81%, and broadleaf plants occupied about 4.6% of the site (Figure 3(b)). The mean broadleaf plant patch area was $6.4 \pm 9.5 \text{ m}^2$. The patch density of broadleaf species was 72 patches ha^{-1} (total 4,376 patches). The mean EVI of broadleaf plant patches (0.56 ± 0.05) was significantly higher than that of CHFO (0.50 ± 0.05) ($p < 0.001$; n for CHFO and broadleaf plants were 399 and 387, respectively) (Figure 3(c)).

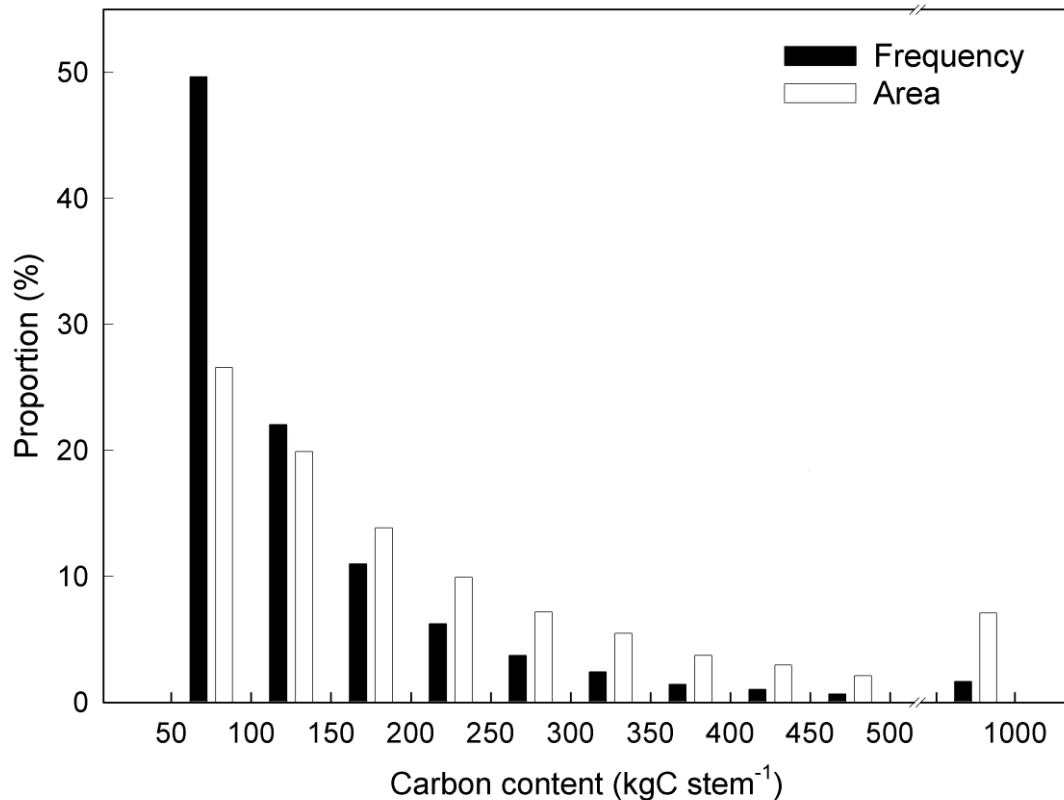


Figure 5. Proportions (%) of plants and covered areas of different size classes of *Chamaecyparis obtusa* var. *formosana* in the study site.

3.2 *Vegetation characteristics across topographic variations*

Elevation plays an important role in modifying bioclimate, which can have significant influence on plant growth. However, this topographic effect was not pronounced ($p \geq 0.2$; n for high and low elevations were 780 and 733, respectively) in this study for CHFO canopy area and carbon (Table 1). Stem and carbon densities, and cover were all slightly lower at high elevation. Unlike elevation, slope was a pivotal factor affecting plant growth. Canopy area was significantly higher ($p = 0.04$; n for steep and flat terrains were 766 and 747, respectively) and mean carbon per tree was relatively higher ($p = 0.06$) on flat terrain; very slight differences were found between steep and flat terrains for CHFO stem and carbon densities, and cover.

In contrast to the CHFO plantation, elevation had crucial impacts on broadleaf plant patches ($p < 0.001$; n for high and low elevation were 625 and 492, respectively). Smaller patches with lower patch density were located at high elevation compared to those at low elevation (Table 2). There was no significant difference in broadleaf plant patch area between steep and flat terrains ($p \geq 0.2$; n for steep and flat terrains were 604 and 513, respectively), but areas with a steep slope had slightly higher patch density. Note that no interactions between elevation and slope were found ($p \geq 0.08$) in the aforementioned statistical tests, which justified the analysis using only one topographic attribute.

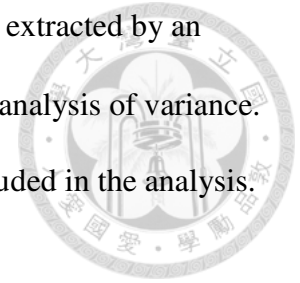
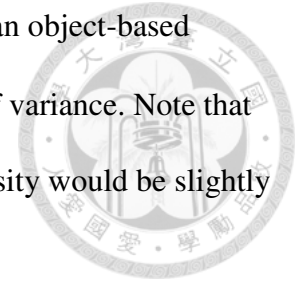


Table 1. The vegetation characteristics (\pm standard deviation [sd] in parentheses) of *Chamaecyparis obtusa* var. *formosana* extracted by an object-based method for different elevation and slope classes. Asterisks indicate significant results ($p \leq 0.05$) according to analysis of variance. Note that canopies touched by the boundaries of topographical groups (high vs. low elevation, steep vs. flat slope) are included in the analysis. Therefore, values of mean carbon, density, carbon density and cover would be slightly higher than the overall estimates.


Topography		Proportion	Mean canopy (\pm sd)	Mean carbon (\pm sd)	Density	Carbon density	Cover
		(%)	(m ²)	(kgC stem ⁻¹)	(stems ha ⁻¹)	(MgC ha ⁻¹)	(%)
Elevation	High	78.8	12.9 (\pm 9.7)	194 (\pm 280)	689	132.8	88
	Low	21.2	12.3 (\pm 8.6)	176 (\pm 233)	750	134.5	93
Slope	Steep	60.5	12.1 (\pm 8.7)*	198 (\pm 285)	703	128.0	88
	Flat	39.5	13.1 (\pm 9.7)*	173 (\pm 230)	701	137.5	90

Table 2. The vegetation characteristics (\pm standard deviation [s.d.] in parentheses) of broadleaf plant patches extracted by an object-based method for different classes of elevation and slope. Asterisks indicate significant results ($p \leq 0.05$) according to analysis of variance. Note that patches touched by the boundaries of topographical groups are included in the analysis. Therefore, the values of patch density would be slightly higher than the overall estimate.



Topography		Occupation (%)	Mean patch area (\pm sd) (m ²)	Patch density (patches ha ⁻¹)
Elevation	High	4.0	5.4 (\pm 6.5)*	67
	Low	8.5	7.6 (\pm 9.6)*	106
Slope	Steep	5.5	6.7 (\pm 8.5)	80
	Flat	4.0	6.1 (\pm 7.6)	67

3.3 The edge effects



The area next to the main road (0-30 m) yielded the lowest amount of CHFO canopy area (mean \pm s.d. = $12.8 \pm 10.5 \text{ m}^2$), stem density ($762 \text{ stems ha}^{-1}$), carbon ($195 \pm 385 \text{ kgC stem}^{-1}$) and C density (149 MgC ha^{-1}) compared with other 30 m interval areas (30-240 m) (Figure 6(a) and (b)). The values of these CHFO structure attributes decrease gradually after the first eight intervals (240-912 m). Unlike CHFO vegetation, the mean broadleaf plant patch area within the first interval (0-30 m) was high ($7.7 \pm 17.1 \text{ m}^2$), and it stabilized with little fluctuation after the first interval ($5.3 \pm 7.8 - 7.1 \pm 9.5 \text{ m}^2$) between 30-400 m. The areas containing the highest mean (\pm sd) broadleaf plant patch areas were the farthest from the road (400-912 m) ($7.9 \pm 10.5 - 8.5 \pm 11.0 \text{ m}^2$) (Figure 6(c)). Broadleaf plant patch density was the lowest within the first interval ($62 \text{ patches ha}^{-1}$), no apparent trend was observed with the increment of distance away from the road, and the area within the farthest interval (500-912 m) having the highest density ($125 \text{ patches ha}^{-1}$).

For the natural vegetation edge analysis, the areas close to the edges yielded low mean CHFO canopy area ($12.6 \pm 10.3 \text{ m}^2$), stem density ($712 \text{ stems ha}^{-1}$), carbon ($190 \pm 380 \text{ kgC stem}^{-1}$) and carbon density (93 MgC ha^{-1}) (Figure 7(a) and (b)). The trends of CHFO structural attributes were stable after the first seven intervals (30-210 m) and then dropped rapidly in the core (210-302 m). The mean area and density of broadleaf plant patches were relatively constant across intervals ($6.5 \pm 9.5 \text{ m}^2 - 7.5 \pm 12.5 \text{ m}^2$ and $74 - 86 \text{ patches ha}^{-1}$, respectively). However, low broadleaf plant path area (mean = $5.6 \pm 6.1 \text{ m}^2$) and high patch density ($93.5 \text{ patches ha}^{-1}$) points were observed within the core of the

study area (Figure 7(c)).

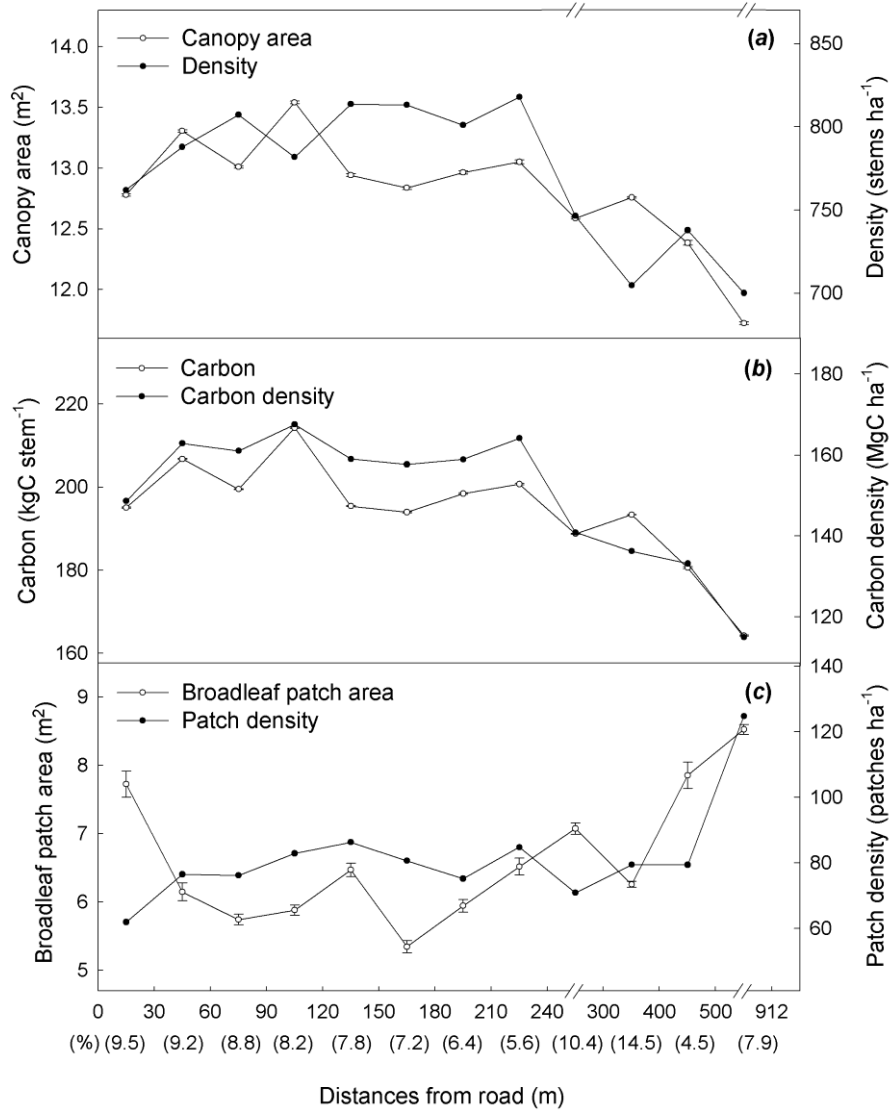
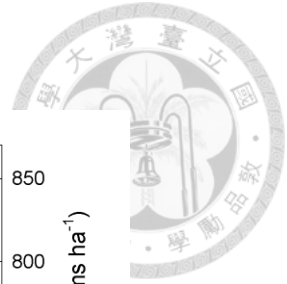


Figure 6. The edge effect of unpaved road on the *Chamaecyparis obtusa* var. *formosana* plantation within each interval (Figure 4(a)). Bars indicate ranges of 95% confidence interval; proportions (%) of intervals to the study area are given in parentheses under the x-axis. (a) Mean CHFO canopy area and tree density. (b) Mean carbon and carbon density for each individual tree and interval, respectively. (c) Mean patch area and patch density of broadleaf vegetation.

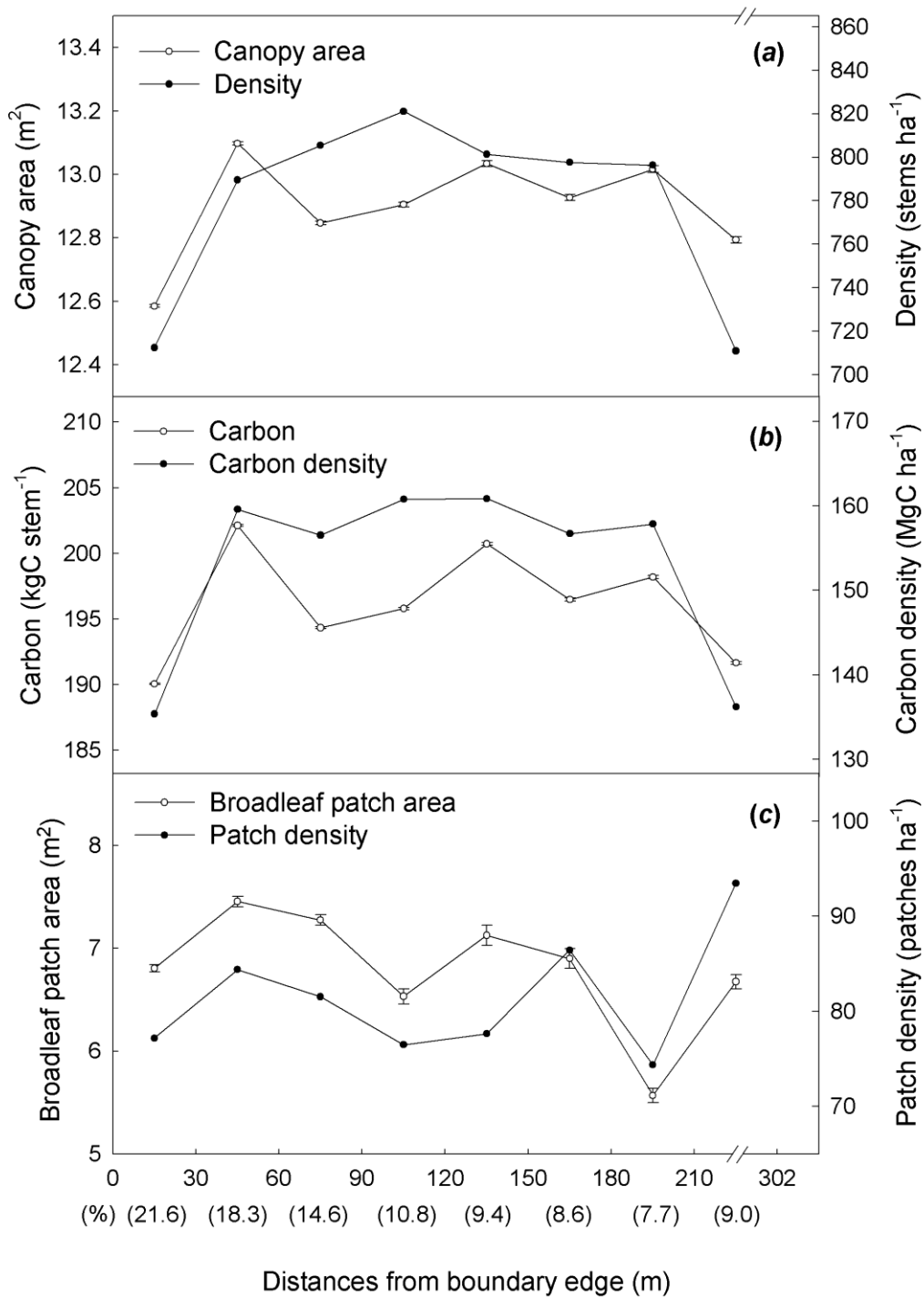


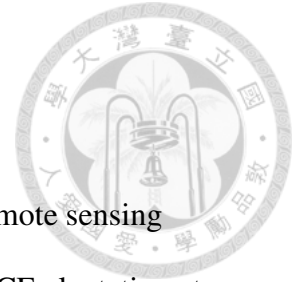
Figure 7. The edge effect of natural edges on the *Chamaecyparis obtusa* var. *formosana* plantation within each interval (Figure 4(b)). The data analysis and presentation are identical to Figure 6.

4. Discussion

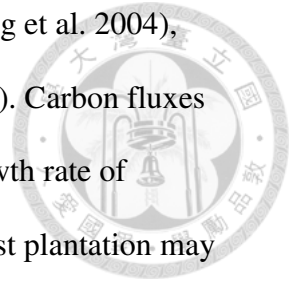
4.1 *Vegetation characteristics of the subtropical MCF plantation*

This study demonstrated the feasibility of utilising hyperspatial remote sensing techniques to characterise the vegetation structure of the subtropical MCF plantation at the landscape scale. The object-based approach can precisely outline the edge of a canopy from a sharpened high spatial resolution QuickBird image, which allowed us to estimate CHFO structure efficiently. In the study site, plants smaller than $100 \text{ kgC stem}^{-1}$ occupied about half of the CHFO population (Figure 5). The plantation activity after clear-cutting in the 1960s resulted in the high proportion of young growth at the site. However, a considerable number (12.9%) of trees contained more than $300 \text{ kgC stem}^{-1}$ and up to almost $1000 \text{ kgC stem}^{-1}$, which was 21.6% of total carbon of the site. Trees with large canopies are particularly important in terms of carbon storage because of the nature of the log-log relationship between biomass (C) and canopy area (Jenkins et al. 2003). This reveals that conventional field measurements with the assumption of homogeneity in estimating forest plantation C budgets may not be valid to quantify the structure of MCF plantations and possibly other plantations especially in mountainous terrain due to the variation of canopies amplified by physical environments.

The study area is designated for a CHFO plantation; however, we found that only 81% of the site was covered by CHFO canopies based upon the large-scale remote sensing observation. The remaining natural area was mainly occupied by broadleaf plant patches. In terms of the greenness of the vegetation, the EVI values for broadleaf plant patches were significantly higher than those for CHFO plantation (Figure 3(b) and 3(c)). Broadleaf plant canopies can reflect 50% more energy in the NIR region than that of



conifer trees due to foliar abundance (e.g., leaf area index [LAI]) (Zheng et al. 2004), which is positively related to ecosystem productivity (Huete et al. 2008). Carbon fluxes of the CHFO plantation could be underestimated if taking only the growth rate of plantation species into account. In summation the heterogeneity of forest plantation may be underestimated at the landscape scale, which is difficult to assess at the local scale.



4.2 Topographic effects

Topographic effects on plant growth were not due to topography per se but were due to bioclimate and substrate contents, which are indirectly influenced by variations of elevation, slope and/or aspect. In the study region, there is a positive relationship between precipitation and elevation. However, negative trends of temperature and solar radiation along the elevation gradient are commonly observed. CHFO adapts very well in this unique narrow “belt” of foggy zone, and the effects of elevation on CHFO were negligible (Table 1). However, fog can influence the bioclimate substantially, especially the reduction of the amount of solar radiation received by plants (Mildenberger et al. 2009), which is pivotal for plant growth (Chen et al. 2007). In the study area, larger broadleaf plant patches were more frequently encountered at lower elevation (Figure 3(a) and 3(b); Table 2), and the intensity of solar radiation could be the main driver altering the spatial arrangement of broadleaf plant patches. The topographic attribute that affected the growth of CHFO in the region was the declination of land surface (Table 1). Several studies have shown that high concentrations of organic matter and soil nutrients can be found in flat terrain, which may facilitate plant growth (Hook and Burke 2000). Our finding indicated that slope played a crucial role in varying CHFO canopy area and possibly C storage producing larger CHFO plants on flatter terrain, which might be the

effect of topography-induced substrate enrichment.



4.3 The edge effect

For the road edges, the interval nearest the main road (0-30 m) yielded the lowest canopy area and carbon (kgC stem^{-1}) for each individual CHFO plant, and population (stems ha^{-1}) and carbon (MgC ha^{-1}) densities for a given area than those CHFO attributes within other intervals (30-210 m) (Figure 6(a) and 6(b)). Edges close to an open space received relatively higher light intensity, air and surface temperature, and wind speed but lower humidity and soil moisture than these bioclimatic and biophysical attributes away from edges (Baker and Dillon 2000). Mildenerger et al. (2009) found that the rate of photosynthesis of CHFO was hardly reduced during very foggy conditions, and they concluded that CHFO was well adapted to low solar radiation. Therefore, the reduction of growth and population of CHFO along the road may be influenced by factors other than light intensity (e.g., soil nutrients and competition with broadleaf plants).

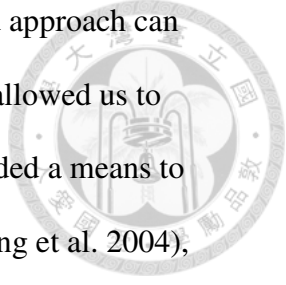
For the broadleaf vegetation analysis, we found relatively large patches in the image near the road edges (Figure 6(c)). Flat leaves can be less effective than cylindrical conifer needles at photon absorption, especially under diffuse light conditions that predominate under cloud cover. This may explain the predominance of conifers in temperate forests where conditions are often cloudy (Chapin III et al. 2011). High light intensity near the edges may facilitate the growth of broadleaf plants resulting in large broadleaf plant patches near the road. The main road in the study site was narrow (4 m), and the influence of the edge effect was rarely beyond 240 m (Baker and Dillon 2000). Therefore, large, high density broadleaf plant patches observed 500+ m away from the road may be

influenced by other physical environments but not by edges. Note that there is a negative relationship between the distance from the road and the elevation (Figure 1 and 3(a)). Therefore, the bioclimate at lower elevation may benefit the growth of broadleaf plants (Table 2) and enhance their ability to compete for resources with the dominant CHFO plants.

The data patterns for CHFO size and abundance at the natural vegetation edges were very similar to those at the road edges yielding low values for canopy area (m^2) and carbon ($kgC\ stem^{-1}$) for individuals, and population ($stems\ ha^{-1}$) and carbon ($MgC\ ha^{-1}$) densities for the study site (Figure 7(a) and 7(b)). High wind turbulence and possibly other factors such as competition with other species near the natural vegetation can limit CHFO growth resulting in low tree density and crown area near the edges (Baker and Dillon 2000). Lower CHFO tree density and crown area in the core region could be due to the slope effect; there was a higher slope (21°) in the core (210-302 m) compared to the other region (17°). On the other hand, the data pattern between the broadleaf plant patch area and the distance from the natural edges was erratic, and the interaction was difficult to decipher. Based on the aforementioned findings, we conclude that the edge effect is an important factor for modifying plantation landscape patterns.

4.4 Potentials and limitations

Forest is defined by high biological diversity and complex vegetation structure. Conducting a conventional field-based inventory to collect canopy information over a large region is labour intensive and costly. This study demonstrated the feasibility of utilising advanced spatial analysis techniques to characterise the vegetation structure of



the subtropical MCF plantation at the landscape scale. The object-based approach can precisely outline the edge of a canopy from a QuickBird image, which allowed us to estimate CHFO structure efficiently. Hyperspatial remote sensing provided a means to quickly and effectively measure the canopy area over a vast region (Wang et al. 2004), which is probably the only structural parameter that is highly correlated to carbon stocks and can be directly measured by optical remote sensing (Brown et al. 2005). In addition, canopy cover can be utilized to estimate the gap fraction in a forest (Asner et al. 2005), which is highly related to other important biophysical parameters such as the fraction of photosynthetically active radiation absorbed by green vegetation and LAI (Campbell and Norman 1998). These parameters are pivotal for modeling carbon flux dynamics of an ecosystem (Huang et al. 2008).

In this study, we showed that remote sensing techniques (image fusion + object-based delineation) can be used to quantify the vegetation structure of a subtropical MCF. However, we found that it may be difficult to detect small attached tree canopies and these will likely be mislabelled as one large tree. This two-dimensional remote sensing limitation was commonly observed regardless of the vegetation types (Huang et al. 2007; Huang et al. 2008), and the carbon overestimation could be substantial. For example, errors can be from 4.3-86.5 kgC stem⁻¹ by mis-identifying a group of clustered small trees (the category of the smallest tree size in Figure 5) as larger canopies (other categories). This technical issue may be resolved by combining the outcomes of the study with Light Detection And Ranging (LiDAR) data measuring tree height, which would provide a unique 3-D perspective of a forest ecosystem (Asner 2009). This image-fusion technique may help us further decipher the complexity of vegetation structure.

CHAPTER III



Temporal and spatial patterns of remotely sensed litterfall in subtropical forests of Taiwan

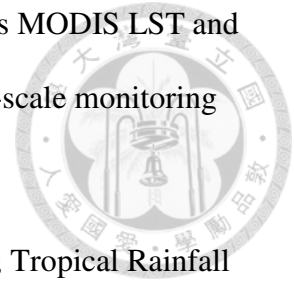
Temporal and spatial patterns of remotely sensed litterfall in subtropical forests of Taiwan



Abstract

Litterfall is important for returning nutrients and carbon to the forest floor, and microbes decompose the litterfall into CO₂ releasing into the atmosphere. Litterfall is a pivotal component in the biogeochemical cycle in forests. Field litterfall data were collected to develop a model and validate the estimates in tropical/subtropical forests in Taiwan. Time-series (2001–2011) climate (the Moderate Resolution Imaging Spectroradiometer [MODIS] land surface temperature [LST] and Tropical Rainfall Measuring Mission [TRMM] precipitation) and green vegetation (MODIS photosynthetically active vegetation cover [PV]) variables were utilized to estimate regional annual litterfall based on a multiple regression model. This study found that time-series MODIS LST- and PV-derived metrics, the annual accumulated MODIS LST and coefficient of variation of PV, respectively, but not the TRMM precipitation variables were salient factors for the estimation ($r^2 = 0.548$, $p < 0.001$). The mean (\pm s.d.) annual litterfall was 5.1 ± 1.2 Mg ha⁻¹ yr⁻¹ during the observed period. The temporal dynamics of the litterfall revealed that typhoons and consecutive drought events might affect the litterfall temporal variation. The annual litterfall decreased along the elevation gradient, which may reflect a change in the vegetation type. The northeast and northwest facing slopes yielded the highest amount of annual litterfall (≥ 5.9 Mg ha⁻¹ yr⁻¹), which was in contrast with the southern aspect (5.1 Mg ha⁻¹ yr⁻¹). This variation may be associated with differences in plant growth from the dryness of the microclimate influenced by solar

radiation. This study demonstrates the feasibility of utilizing time-series MODIS LST and PV data to predict large-scale field litterfall, which may facilitate large-scale monitoring of biogeochemical cycles in forest ecosystems.



Keywords: Moderate Resolution Imaging Spectroradiometer (MODIS); Tropical Rainfall Measuring Mission (TRMM); spectral mixture analysis; typhoon; drought; topography

1. Introduction

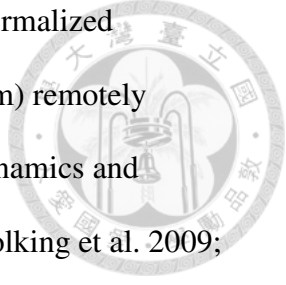
Litterfall is the major pathway to return dead organic matter and nutrients from aboveground biomass to forest floor, which plays an important role on the maintenance of soil fertility and is a pivotal component in terrestrial biogeochemical cycles (Brown and Lugo 1982; Vitousek 1984). Litterfall is decomposed by microbes, which convert dead organic matter to either inorganic nutrients utilized by plants or carbon dioxide (CO₂) into the atmosphere (Chapin III et al. 2011). The decomposition of litterfall is also a major source for global soil organic carbon, which is 2–3 times greater than the carbon stores in the biomass and atmosphere (Cou[^]teaux et al. 1995; Jha and Prasad Mohapatra 2010). The mineralization of the annual litterfall contributes to approximately half the CO₂ output from the soil, and the balance between the rates of litter decomposition and net primary production (NPP) is closely related to carbon cycling, which makes litterfall a pivotal parameter for modeling ecosystem productivity (Friend et al. 1997; Running and Hunt 1993). Litterfall is also a critical indicator for assessing the impacts of disturbances on forest ecosystems, such as tropical cyclones (typhoons or hurricanes, depending on the geographic regions), drought and insect infestation (Brando et al. 2008; Lin et al. 2003a; Lovett et al. 2002). Because of the critical roles of litterfall production in the global

carbon cycle, it is important to understand the temporal and spatial patterns of litterfall (Cou^{teaux} et al. 1995; Davidson and Janssens 2006).



A commonly utilized approach to determine litterfall production is to collect leaves, twigs, branches, flowers and/or fruits from the canopy and sub-canopy over a period of time using randomly placed litter traps. The samples are then brought back to a laboratory to measure the dry weights and nutrient content, and the amount of litterfall for a site during the observation period can be estimated based on the size of the trap (Lin et al. 2003a; Whigham et al. 1991). To estimate the spatial pattern of litterfall, some studies used large numbers of *in-situ* litter traps to develop interpolation models, such as a distance-weighted averaging method (Hirabuki 1991), kriging (Joffre et al. 1996) or regression (Rothe 1997; Staelens et al. 2004). However, these field approaches are extremely labor intensive, which makes them difficult for large-scale monitoring. Some studies utilized statistical modeling techniques to acquire litterfall and found that temperature, precipitation, evapotranspiration, latitude, basal area and/or *diameter at breast height* (DBH) are salient variables to assess the annual litterfall of a site (Berg and Meentemeyer 2001; Bray and Gorham 1964; Lonsdale 1988; Matala et al. 2008). Although it is possible to use these climatic and/or forest stand characteristics to estimate the litterfall, these approaches are often region specific, which makes them challenging for temporal dynamics and regional gradient estimation.

Spaceborne remote sensing has been widely used for the systematic observation of Earth for over 40 years (DeFries 2008). Climatic variables, such as the land surface temperature (LST) and precipitation can also be retrieved from thermal infrared (3.5 – 13 μ m, Wan and Dozier (1996)), microwave or radar (0.1 – 100 cm, Stephens and



Kummerow (2007)) data. Vegetation greenness time-series (e.g., the Normalized Difference Vegetation Index, NDVI) derived from optical (350–2500 nm) remotely sensed data can be treated as a surrogate to determine the vegetation dynamics and ecosystem productivity of different settings (Chambers et al. 2007b; Frohking et al. 2009; Ostertag et al. 2008). According to the aforementioned field studies, litterfall may be related to climatic and canopy dynamics (Berg and Meentemeyer 2001; Starr et al. 2005; Wang et al. 2013), it may be able to utilize these data to map the patterns of litterfall over a large region. In former studies, Taskinsu-Meydan et al. (2010) used a fractional tree-cover to model Mediterranean litterfall based on a linear regression, and da Costa et al. (2014) combined field LAI, climatic variables and remotely sensed NDVI to model leaf production. Although few studies combined field variables and remotely sensed data to estimate litterfall, they simulated litterfall dynamics with thirteen months or less. Therefore, the objective of this study is to utilize time-series remotely sensed climate and vegetation data to estimate the long-term temporal dynamics of litterfall at the regional scale, which is important to observe patterns of leaf senescence and litter nutrients output in response to disturbance or climate changes. A large-scale analysis of the spatial patterns of the annual litterfall in different topographical settings was also conducted to describe the characteristics of the derived litterfall maps.

2. Methods

2.1 Study area

This study focused on the forest ecosystems of Taiwan (23°N, 121°E, Figure 8), which is a 36,000 km² island located between the world's largest continent (Eurasian) and largest ocean (Pacific). Forests cover approximately 60% (20,300 km²) of the territory. The terrain is generally rugged except for the western coastal plain and tableland. Taiwan has remarkable elevation, ranging from sea level to near 4000 m a.s.l. within a horizontal distance of 40 km. This abrupt change in altitude results in a variety of bioclimates, which govern the composition of plant communities and present a wide spectrum of vegetation types along the gradient. From low to high elevation, this vegetation includes an evergreen broadleaf forest, coniferous and broadleaf mixed forest, coniferous forest and grassland/dwarf bamboo forest including natural and plantation forests. Taiwan's climate is generally warm and humid. The mean air temperature varies from 5–25 °C along the elevation gradient, and the annual mean temperature during 2001–2011 range from 20–22 °C (Figure 9). The mean annual precipitation is approximately 1500–3400 mm yr⁻¹, and approximately 80% of the rainfall occurred from May–October due to the plum rain, summer monsoon and typhoons (Taiwan Data Bank for Atmospheric Research [<http://dbar.ttfri.narl.org.tw>]; Taiwan Central Weather Bureau [<http://www.cwb.gov.tw>]).



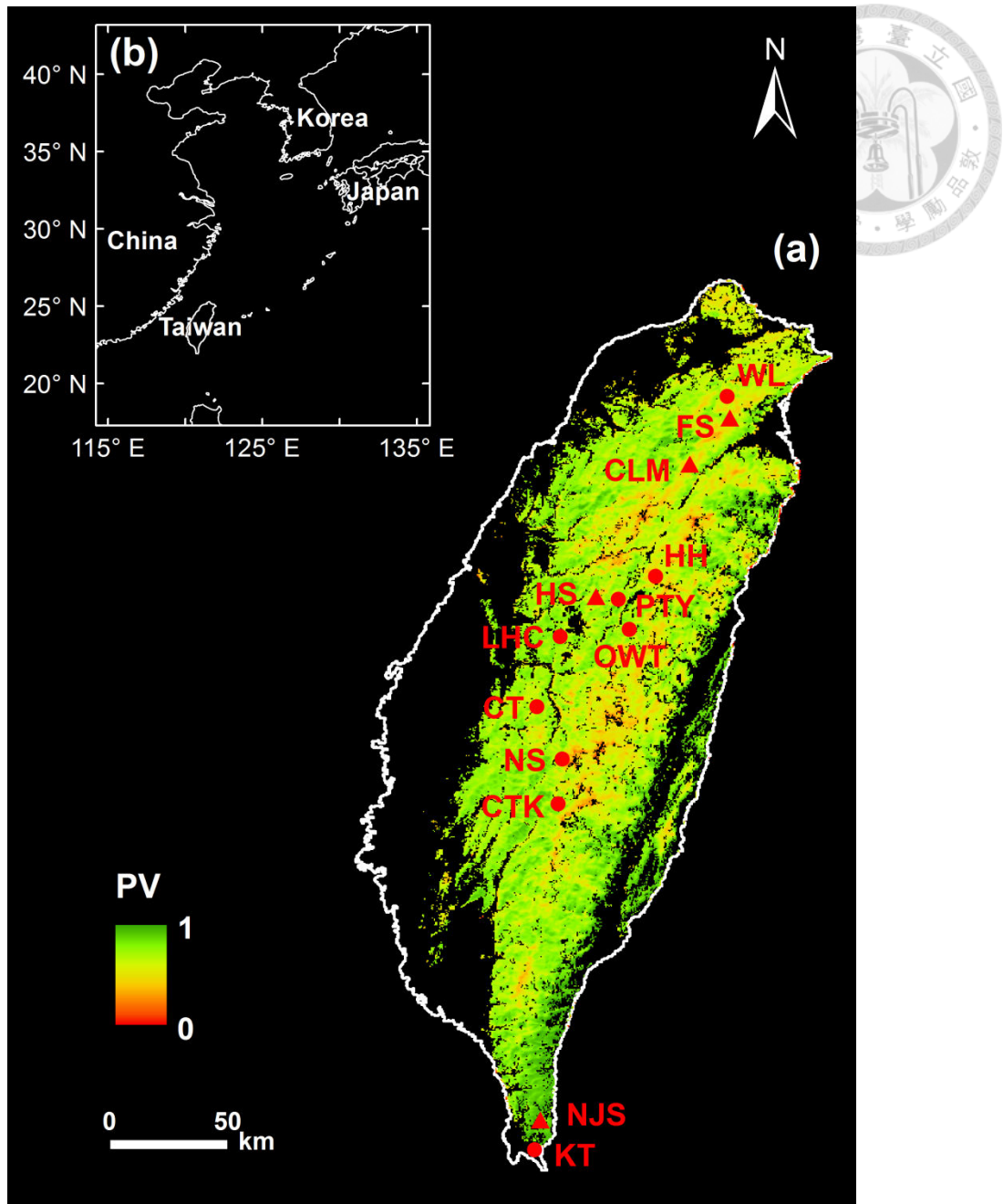


Figure 8. (a) The model (triangles) and validation (circles) sites used to establish and verify the litterfall model, respectively. A full name and short description for each site can be found in Table 3. The green monochromatic layer is a long-term (2000–2011) average of the photosynthetically active vegetation (PV) fractional cover (%) of the forests. (b) The geographic map of Taiwan.

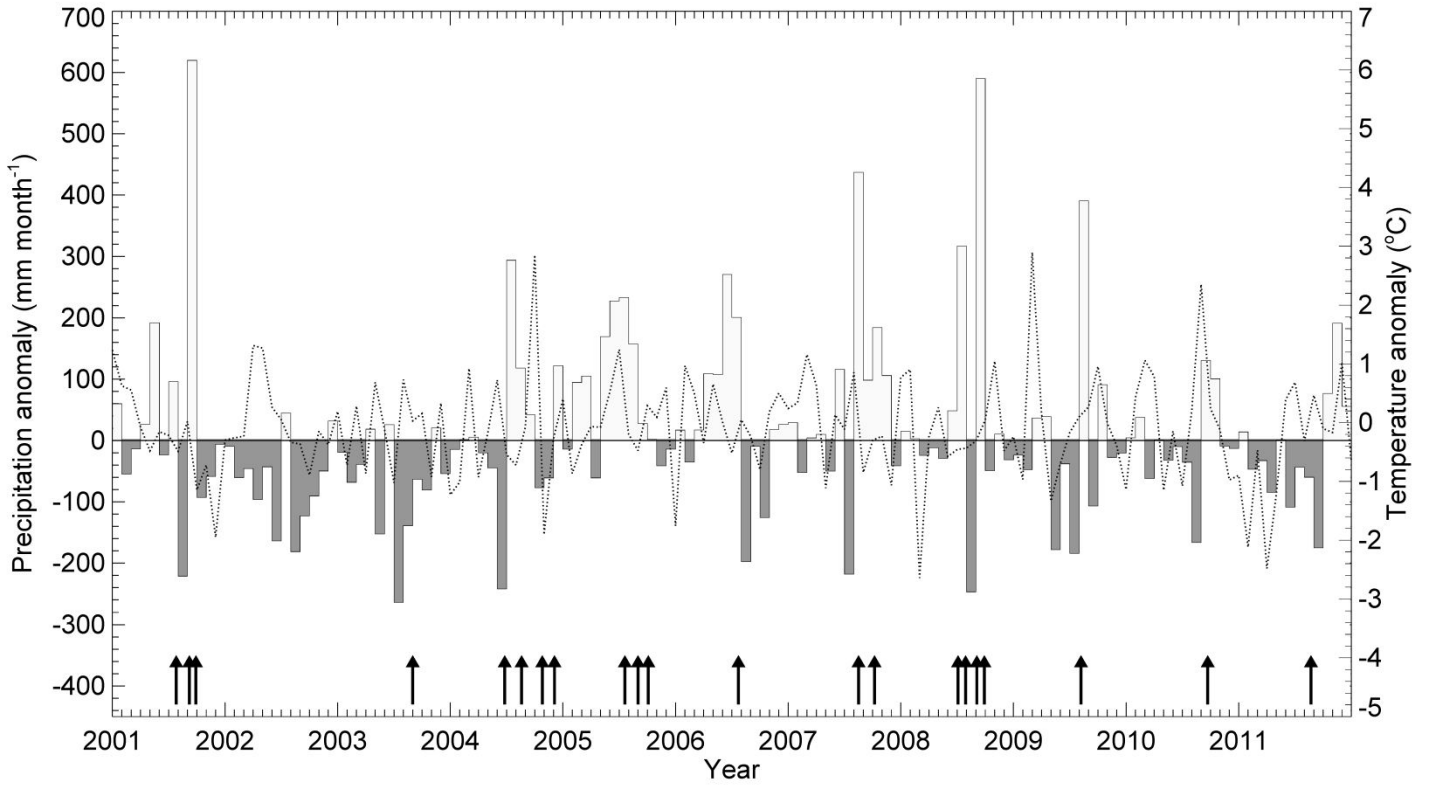


Figure 9. The anomalies of temperature ($^{\circ}\text{C}$) (dashed line) and precipitation (mm month^{-1}) (above mean: light-colored bars; below mean: dark-colored bars) were calculated from monthly temperature and precipitation minus long-term (1993–2011) mean values. Positive temperature and precipitation indicates hotter and wetter conditions than the long-term median value. The black arrow indicates a typhoon in which the central wind velocity of the typhoon is over 32.7 m s^{-1} .

2.2 Field data

We acquired monthly litterfall from our own field observations and intensive literature review using on-line search engines (Google Scholar [<http://scholar.google.com.tw/>], Taiwan Periodical Literature System [<http://readopac.ncl.edu.tw/>], and National Digital Library of Theses and Dissertations in Taiwan [<http://ndltd.ncl.edu.tw/>]) with the key words “litterfall” and “litter production” in traditional Chinese. The time of data acquisition was at least one full year (12 months) and the initiation time was not the spring (March–May) or summer (June–September), covering more than two growing seasons in different years. Thirteen sites in the tropical/subtropical evergreen broadleaf and coniferous forests across a wide elevation range (150–3000 m a.s.l.) were selected for this study (Figure 8 and Table 3). Four subtropical sites were also collected across the Northern Tropic to evaluate our model (Table 3). Protocols for the collection of field litterfall data were slightly different from site to site, but in general, 9–50 litter traps 0.25–1 m² in size were installed with a mesh size of 1–1.2 mm under canopies at 1–1.5 m above ground to avoid microbe decomposition. The traps were periodically visited (two weeks–one month), and the collected litterfall was oven dried at 60–70 °C for 48–72 h to constant weight. To match with the satellite data acquisition time, we only selected the data collected after 2001.





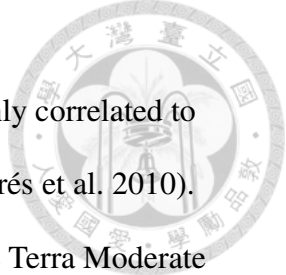
Table 3. Site characteristics for model simulation and validation; CF and EBF correspond to coniferous forest and evergreen broadleaf forest, respectively.

Sites	Vegetation [*]	Periods	Elevation (m)	Trap number	Litterfall (Mg ha ⁻¹ yr ⁻¹) (mean ± sd)	References
Model sites						
Chilan (CL)	CF	2004/01-2010/12	1500-1800	10	3.4 ± 0.8	(Wang 2011)
Fushan (FS)	EBF	2001/01-2011/12	650-800	10	6.2 ± 1.0	[Lin (unpublished data)]
Huisun (HS)	EBF	2001/01-2004/12	700-1300	12	6.3 ± 1.3	(Chang 2005; Chou 2003)
Nanjenshan (NJS)	EBF	2004/01-2010/12	150-350	35	4.2 ± 0.8	(Chin 2008; Kuo 2012)
Validation sites						
Chitou (CT)	SEBF	2006/02-2007/01	1500-1780	40	6.4	(Yang 2007)
Chungtzekuan (CTK)	SEBF	2004/01-2005/12	1876	40	4.2 ± 1.2	(Lee 2006)
Hehuan (HH)	CF	2011/01-2011/12	3000	24	3.1	(Lin 2012)
Kenting (KT)	TEBF	2004/02-2006/01	200-300	18	8.2 ± 0.7	(Liao 2006)



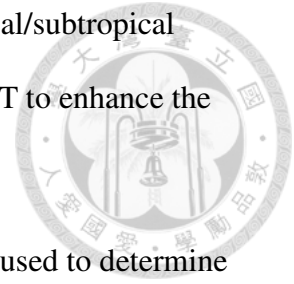
Sites	Vegetation *	Periods	Elevation (m)	Trap number	Litterfall (Mg ha ⁻¹ yr ⁻¹) (mean ± sd)	References
Lienhuachi (LHC)	SEBF	2009/03-2010/02	728-797	9	9.2	(Lu 2010)
Nansi (NS)	SEBF	2007/11-2008/10	1955-2065	50	4.8	(Weng 2009)
Ouwanta (OWT)	SEBF	2002/01-2002/12	1200-1600	18	8.9	(Hung 2003)
Peitungyen (PTY)	SEBF	2009/03-2010/02	2098	9	6.6	(Lu 2010)
Wulai (WL)	SEBF	2002/02-2003/01	210-230	12	7.1	(Hsiao 2005)
International sites						
China (Fujian)	CF	2012/02-2013/01	205-500	10	4.9	(Zhou et al. 2014)
Puerto Rico	EBF	2002/12-2003/12	300-600	36	7.5	(Zalamea and González 2008)
Thailand	EBF	2010/04-2011/03	700-860	36	4.2	(Podong et al. 2013)
USA (Hawaii)	EBF	2002/02-2003/01	20-100	10	7.1	(Hughes and Denslow 2005)

2.3 Remotely sensed climate data



Previous studies suggested that the dynamics of litterfall were highly correlated to air temperature and precipitation (Brown and Lugo 1982; Sánchez-Andrés et al. 2010). To produce time-series spatial coverage of the monthly temperature, the Terra Moderate Resolution Imaging Spectroradiometer (MODIS) LST (MOD11A2) v. 5 was utilized. This study realized that the spatial resolution of MODIS imagery was relatively coarser (1 km) compared to other public domain satellite data (e.g., Landsat [30–120 m]). However, the availability of high quality imagery with no or low cloud cover was key to delineate the temporal dynamics of litterfall ($n = 20+$ per year for MODIS vs. 4 for Landsat imagery to cover the study site). This should justify the use of the MODIS data. Although there is a discrepancy between the satellite (LST) and field measurements (air temperature) of the litterfall sites during the observation period, but a high correlation was observed (Figure 10). This warrants the use of the satellite measurements for further statistical analysis. The MODIS LST obtains ground temperature using the generalized split-window algorithm based on the bands 31 (10.780-11.280 μm) and 32 (11.770-12.270 μm) (Wan and Dozier 1996), and the uncertainty is only within the range of 1 K (Wan 2008). The majority of atmospheric effects and cloud pixels were removed, and the geographical coordinates were aligned by the data provider before data acquisition. The 8-day composites comprising daytime (10:30 am local time) LST with a 1 km spatial resolution from 2001 to 2011 were obtained. The nighttime LST composites were not combined due to higher missing values with signal noise and cloud contamination in the study site. The maximum LST in the late morning of a month was selected to represent the monthly mean temperature to minimize the sub-pixel cloud

contamination. Due to the relative stability of temperature in this tropical/subtropical region, this study accumulated monthly LST to annual accumulated LST to enhance the range of the variable.



The Tropical Rainfall Measuring Mission (TRMM) V7 3B43 was used to determine the monthly precipitation. The satellite was launched in 1997 to monitor the three-dimensional (3-D) distribution of precipitation and energy exchange in the tropics. The TRMM has the following five onboard sensors: a passive microwave radiometer (TMI), the first active spaceborne Precipitation Radar (PR), a Visible-Infrared Scanner (VIRS), Clouds and the Earth's Radiant Energy System (CERES) and Lighting Imaging Sensor (LIS). The TRMM V7 3B43 contains information on the multi-satellite precipitation rate (mm h^{-1}) at a spatial resolution of 0.25° between 50°N and 50°S (~ 27.5 km for the studied region). The global monthly precipitation combined the TRMM 3-hourly integrated high-quality data (3B-42) and the global gridded rain gauge products from the monthly accumulated Climate Assessment and Monitoring System (CAMS) and/or Global Precipitation Climatology Center (GPCC) to produce the best estimates of the precipitation rate (Huffman et al. 1995). Annual precipitation was used to present the inter-annual variances of precipitation and the coefficient of variation (CV) of monthly precipitation reflected the intra-annual variance of precipitation, respectively. The predictabilities of both variables to annual litterfall were investigated.

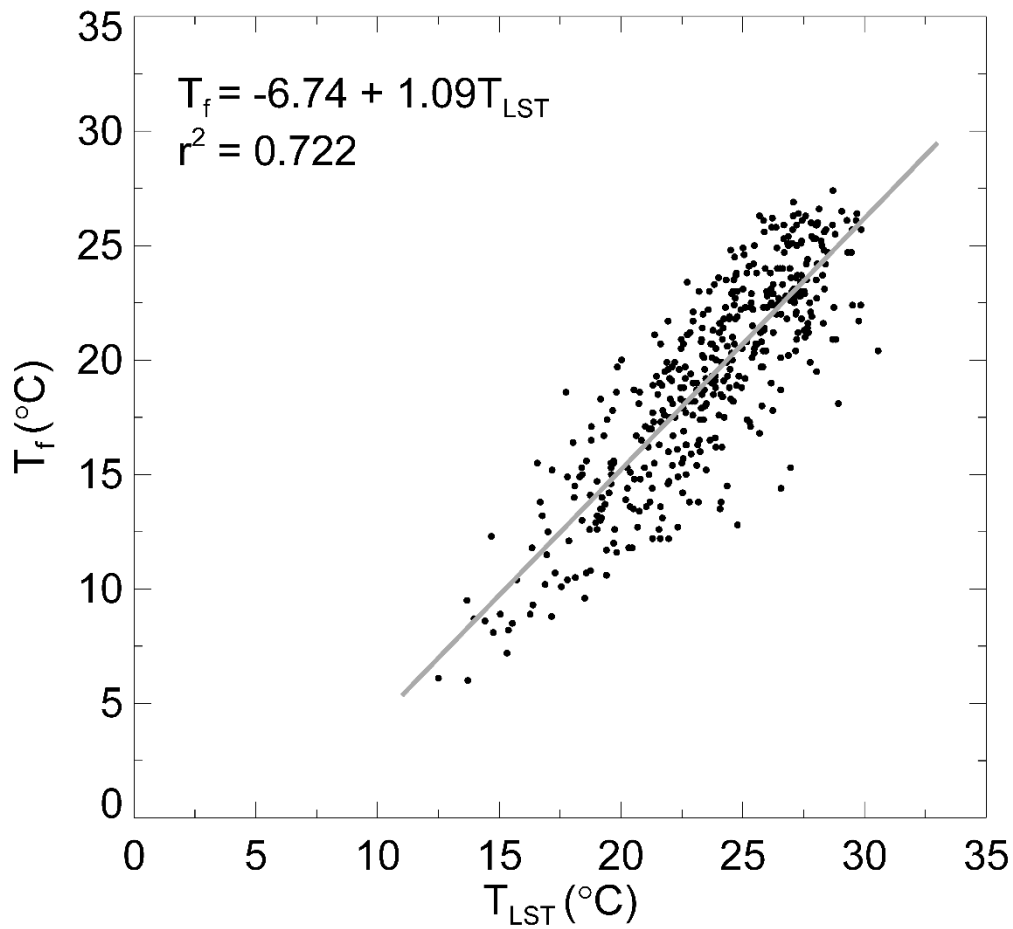
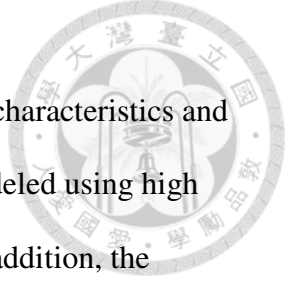


Figure 10. Data from the MODIS land surface temperature (T_{LST} , x-axis) were compared to field temperature records (T_f) derived from local weather stations in the model sites during 2001–2011. There was a significant correlation between the satellite and field measurements ($r^2 = 0.722$, $p < 0.001$). The weather stations were at the Taiwan Forestry Research Institute (for FS, Figure 8), National Taiwan University (CLM), and Taiwan Central Weather Bureau (the remaining sites).

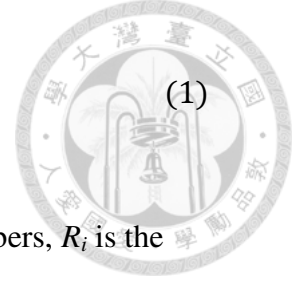
2.4 Green vegetation cover



The litterfall spatial and temporal variations are sensitive to stand characteristics and phenology (Bray and Gorham 1964; Lonsdale 1988), which can be modeled using high temporal resolution time-series satellite images (Zhang et al. 2003). In addition, the dynamics of litterfall may influence canopy closure or gap fraction over time. Therefore, the fractional photosynthetically active vegetation cover (PV) could capture canopy patterns and the coefficient of variation of PV (PV-CV) over a year reflect temporal dynamics of monthly PV. The PV-CV was calculated as one of the independent variables to estimate the annual litterfall from 2001 to 2011. The high temporal resolution data, the MODIS 8-day composites surface reflectance (MOD09A1 V5), contain seven optical bands with the spectral ranges of 0.620–0.670 μm , 0.841–0.876 μm , 0.459–0.479 μm , 0.545–0.565 μm , 1.230–1.250 μm , 1.628–1.652 μm , and 2.105–2.155 μm from band 1 to band 7, respectively, at 500 m spatial resolution. The majority of atmospheric effects were removed and the geographical coordinates were aligned by the data provider before data acquisition. Cloud-contaminated pixels were excluded by setting a threshold (surface reflectance > 28.29%, 40.38%, 28.62%, 29.48%, 38.60%, 28.93% and 17.67% in the band order) by referring to cloud endmembers ($n = 1271$) extract from 25 sets of 30-m atmospherically corrected (by Atmospheric CORrection Now [ACORN, ImSpec, Palmdale, CA, USA]) hyperspectral Hyperion images (Huang et al. 2013).

Time-series of MODIS PV were calculated by spectral mixture analysis, which is used to derive sub-pixel proportions of components in a pixel (Adams et al. 1995). Each endmember component contributes to pixel-level spectral reflectance (R) as a linear combination of endmember spectra:

$$R_i = \sum_{k=1}^n f_k R_{ik} + \varepsilon_i \quad \text{and} \quad \sum_{k=1}^n f_k = 1 \quad (1)$$



where i is the number of the spectral band, k is the number of endmembers, R_i is the spectral reflectance in band i for each pixel, f_k is the fraction of endmember k within a pixel, R_{ik} is the spectral reflectance of endmember k in band I , and ε is the error term for band i . In natural environments, land surfaces are dominated by PV, non-PV (NPV) and bare soil (BS). There are models to take natural variability, such as biochemical components, structures and water contents of endmembers into account by randomly selecting endmembers from a set of spectral libraries (Bateson et al. 2000). This study used a Monte Carlo simulation based spectral mixture analysis model to find the most possible combination of PV, NPV and BS for each pixel through iterative random selection of endmembers (details see Asner and Lobell 2000). A set of spectral libraries ($n_{PV} = 580$, $n_{NPV} = 267$, $n_{BS} = 256$) was established specifically for Taiwan's forest ecosystems (Huang et al. 2013). Endmember bundles for NPV and BS were directly sampled using a field spectroradiometer (FiedSpec 3, ASD Inc., CO, USA) at a 1 nm spectral resolution. However, due to the high stature of vegetation canopy in Taiwan, the PV endmembers were extracted from 25 widely distributed, atmospherically corrected (by ACORN) Hyperion images with high canopy closure by referring to high spatial resolution (≤ 5 m to sub-meter) remotely sensed images. High resolution spectra were convolved to match the spectral profiles of the MODIS surface reflectance data (Figure 11). According to Asner et al. (2003) and Huang et al. (2007), a 250 time repetition for each pixel should be sufficient for multispectral data. Histograms of PV, NPV and BS

abundance were produced to examine the accuracy of cover estimation, which should be a normal distribution with high kurtosis (a measure of peakedness), or the model would reject the process and request another round of unmixing. For each pixel, this study select the one that yielded the highest PV value within a month (3–4 images per month) to represent the mean monthly PV because the atmosphere induced noises would obscure the greenness signals. The PV-CV for each year per pixel can then be derived.

The Enhanced Vegetation Index (EVI) was selected for the greenness variable, which is suitable for assessing the greenness of dense vegetation in the mountainous region of Taiwan. The EVI was calculated as (Huete et al. 2002):

$$EVI = G \times \frac{(\rho_{NIR} - \rho_R)}{(\rho_{NIR} + C_1 \times \rho_R - C_2 \times \rho_B + L)} \quad (2)$$

where ρ_B (blue), ρ_R (red), and ρ_{NIR} (near infrared) are MODIS 8-day 500 m surface reflectance (MOD09A1) bands 3, 1 and 2, respectively. This study noted that G (= 2.5) is gain factor, and L (= 1) is the canopy background brightness correction factor. The C_1 (= 6) and C_2 (= 7.5) are atmosphere resistance correction coefficients for the red and blue bands, respectively. A greenness index may be obscured by cloud contamination, and we used the maximum value of EVI in a month to represent the monthly EVI assuming the clearest sky conditions. The elevation was acquired from the 30 m Advanced Spaceborne Thermal Emission and Reflection Radiometer (ASTER) digital elevation model (DEM). The spatial resolution of the EVI and DEM were coarsened to 1 km for the statistical analysis.

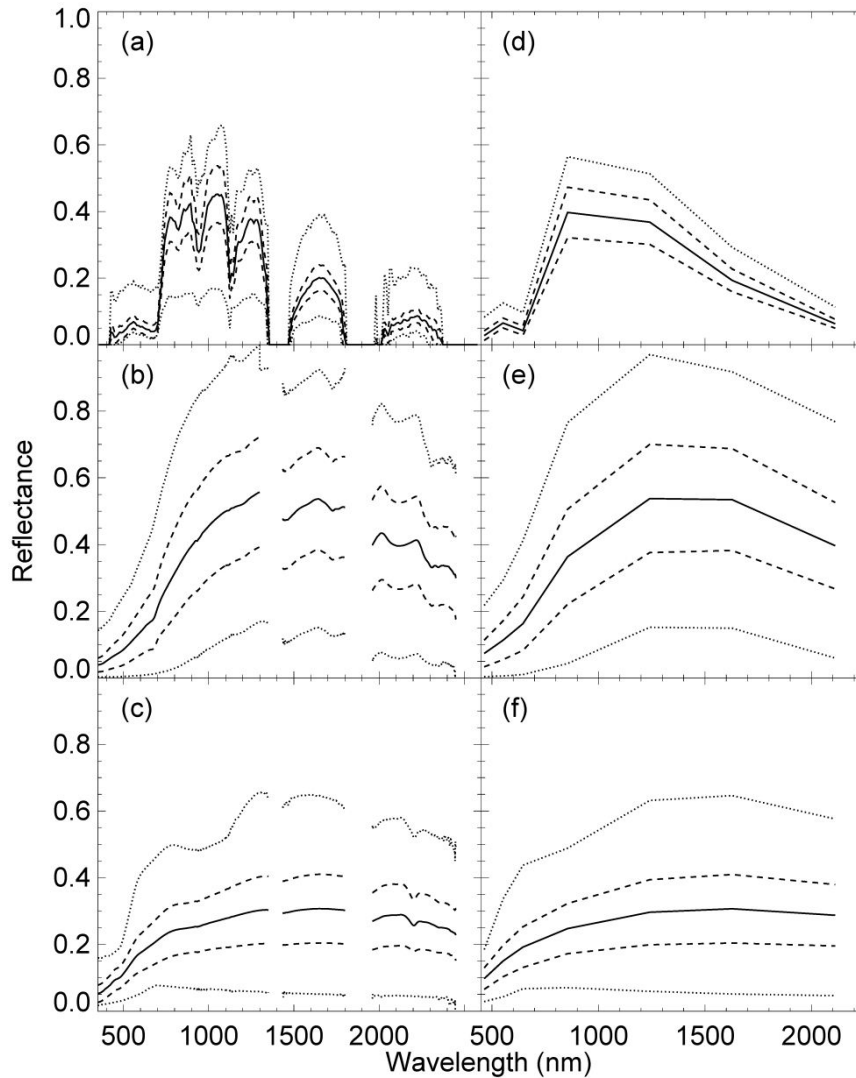


Figure 11. Spectral profiles of the endmember library of (a) photosynthetically active vegetation (PV), (b) nonphotosynthetically active vegetation (NPV), and (c) bare soil (BS). The spectra were convoluted to match with the MODIS wavelengths (d-f for PV, NPV and BS, respectively). The PV hyperspectral endmembers were extracted from Hyperion images, whereas those of the NPV and BS were acquired from a portable field spectroradiometer. The solid, dashed and dotted lines indicate one standard deviation on each side of mean and the minimum and maximum reflectance values, respectively.

2.5 Litterfall modeling and validation

Time-series temperature, precipitation and PV-CV during 2001–2011 were applied to estimate the annual litterfall using a simple multiple linear regression:

$$LF = b_0 + b_1 T + b_2 R + b_3 PV-CV \quad (3)$$

where LF is field annual litterfall ($\text{Mg ha}^{-1} \text{ yr}^{-1}$) from four model sites (Fushan, Chilan, Huisun, Nanjenshan, see Figure 8 for the locations and Table 3 for the site descriptions), and T , R and $PV-CV$ are the annual accumulated monthly mean temperature ($^{\circ}\text{C yr}^{-1}$), annual precipitation (mm yr^{-1}) or the CV of monthly precipitation (%), and the CV of PV (%) acquired/derived from the MODIS LST, TRMM, and MODIS reflectance data, respectively, for the corresponding locations. Only sites that consistently collected data for at least three years were selected for establishing the model (Table 3). The assumption was made based on our local knowledge and this study expected that long-term field litterfall monitoring may indicate more reliable and consistent measurements. Instead of averaging the temperature data for a year, this study accumulated them to enhance the dynamic range of the variable. Because the MODIS LST and PV-CV and TRMM are generated at different spatial resolutions (1 km, 0.5 km and 0.25° [~ 27.5 km], respectively), these data must be unified before performing a statistical analysis. A minimum sampling unit of 1 km was arbitrarily set based on the impacts of data collinearity (pixel refinement) and spatial complexity (pixel coarsening). A nearest neighbor method was applied to combine the PV-CV data. This study enhanced the spatial resolution of the TRMM precipitation data using a regression model with the



spatially corresponding *greenness* and elevation information (Immerzeel et al. 2009; Jia et al. 2011). Moreover, this study acquired the monthly air temperature and precipitation data from local weather stations of the model sites and substituted them for the MODIS LST and TRMM to justify the use of meteorological data for estimating the litterfall production of the region.

Performance of the remote sensing model was assessed using another independent set of field data (Figure 8 and Table 3, n [one site-12 months] = 11). The field litterfall data were collected monthly for 12 or 24 months. The coefficient of determination (r^2) between the modeled and ground truth was calculated. The bias (B) (eq. 4) and root mean square error (RMSE) (eq. 5) were computed to assess the accuracy of the estimation (eq. 5):

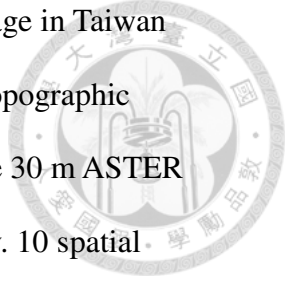
$$B = \frac{\sum_{i=1}^n \hat{y}_i}{\sum_{i=1}^n y_i} - 1 \quad (4)$$

$$\text{RMSE} = \left(\sum_{i=1}^n (y_i - \hat{y}_i)^2 / n \right)^{1/2} \quad (5)$$

where \hat{y}_i is the estimated litterfall extracted from the multiple regression model, y_i is the corresponding field litterfall data retrieved from validation sites, i is the index of field litterfall number, and n is the total number of field litterfall data.

2.6 Topographical analysis

Topography (mainly elevation, slope and aspect) plays an important role in governing microclimate and has tremendous influences to regional biogeochemical cycles



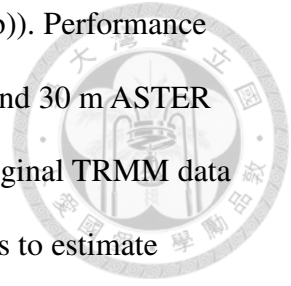
(Chen et al. 2007; Hook and Burke 2000). Remarkable elevation coverage in Taiwan makes it an ideal region to study the spatial patterns of litterfall along topographic (elevation, slope and aspect) gradients. Elevation was acquired from the 30 m ASTER DEM. Slope ($^{\circ}$) and aspect were derived from the DEM using ArcGIS v. 10 spatial analyst tools (Environmental Systems Research Institute, Redlands, CA, USA). This study regressed elevation and slope with litterfall to investigate the influences of these topographic metrics to the annual production. Aspect is not incremental, therefore, this study evenly divided it into eight nominal classes: north ($0\text{--}22.5^{\circ}$ and $337.5\text{--}360^{\circ}$), northeast ($22.5\text{--}67.5^{\circ}$), east ($67.5\text{--}112.5^{\circ}$), southeast ($112.5\text{--}157.5^{\circ}$), south ($157.5\text{--}202.5^{\circ}$), southwest ($202.5\text{--}247.5^{\circ}$), west ($247.5\text{--}292.5^{\circ}$) and northwest ($292.5\text{--}337.5^{\circ}$). The Tukey-Kramer multiple comparison, which is a statistical model utilizing the unique structure of the multiple comparisons by selecting a specific multiplier from the studentized range distributions rather than from the t -distributions to control for the family-wise error (Ramsey and Schafer 1997), was applied to test the differences of litterfall among these aspect classes based on a 0.05 significant level (α).

3. Results

3.1 Explanatory variables

In general, the mean (2001–2011) PV was higher in the lowlands and decreased with increasing elevation ($r^2 = 0.237$, $p < 0.001$) (Figure 8). The mean PV-CV increased along the elevation gradient ($r^2 = 0.067$, $p < 0.001$), and the spatial heterogeneity of the PV-CV was higher in the central and northern regions than the southern region (Figure 12(a)). As expected, a negative relationship was found between the LST and elevation ($r^2 = 0.511$, p

< 0.001), and the mean annual LST ranged from 13–34 °C (Figure 12(b)). Performance of the TRMM spatial resolution refinement using 500 m MODIS EVI and 30 m ASTER DEM was poor ($r^2 = 0.012$, $p > 0.05$). Therefore, this study used the original TRMM data with 0.25° spatial resolution as one of the explanatory climatic variables to estimate litterfall. The annual precipitation derived from the TRMM ranged from 1500–2300 mm yr⁻¹. The central to southern regions yielded the highest amount of mean annual precipitation, and there was slightly higher precipitation in the northern region compared to the southern region (Figure 12(c)).



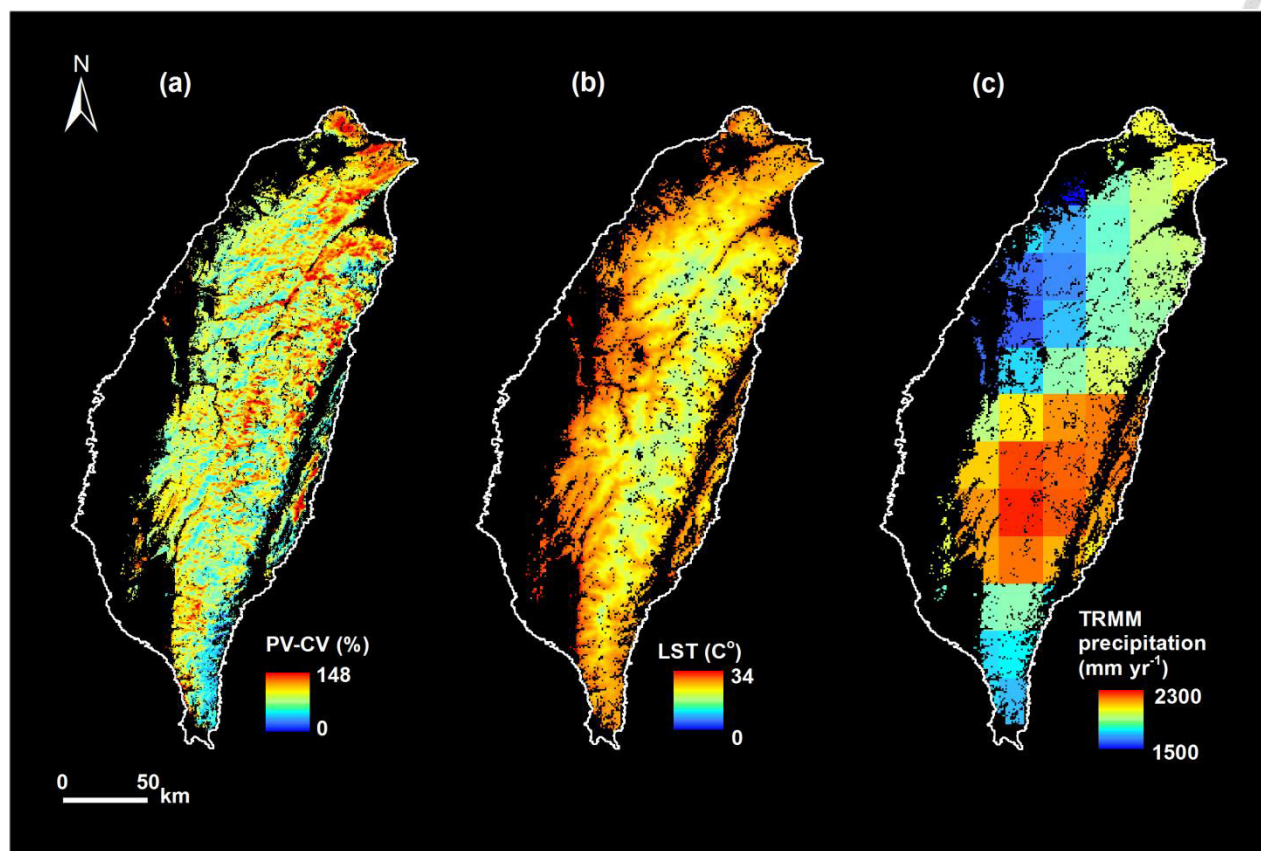


Figure 12. Spatial patterns of the mean (2001–2011) MODIS (a) MODIS PV-CV (annual coefficient of variation of PV), (b) LST (Land surface temperature) and (c) TRMM (Tropical Rainfall Measuring Mission) precipitation data at the spatial resolutions of 500 m, 1000 m and 0.25° (~ 27.5 km), respectively.

3.2 The litterfall model and validation

A multiple regression model for annual litterfall estimation was derived using the annual accumulated MODIS LST and PV-CV as explanatory variables (Table 4), and the predictivity was satisfactory ($r^2 = 0.548$, $p < 0.001$). The TRMM annual and monthly CV precipitation data were excluded from the analysis because the coefficients were insignificant ($p > 0.05$). This study also noted that there were no significant correlations ($p > 0.05$) among these explanatory variables. A significant correlation ($r^2 = 0.608$, $p = 0.003$) was found between the modeled annual litterfall productions and those acquired from the validation sites (Figure 13 and Table 3). The multiple regression model slightly underestimated the litterfall (bias = -0.158) with moderate RMSE ($1.6 \text{ Mg ha}^{-1} \text{ yr}^{-1}$) and an offset ($1.23 \text{ Mg ha}^{-1} \text{ yr}^{-1}$), and the slope was 0.95 (Figure 13).

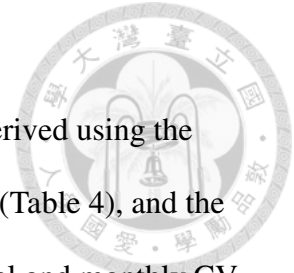


Table 4. Models ($Y = b_0 + b_1T + b_2R + b_3PV-CV$) to estimate litterfall ($Mg\ ha^{-1}\ yr^{-1}$) using the Moderate Resolution Imaging Spectroradiometer (MODIS) land surface temperature, the Tropical Rainfall Measuring Mission (TRMM) precipitation data, and photosynthetically active vegetation cover fraction (PV) derived from the 500 m MODIS surface reflectance data. T is the annual accumulated temperature ($^{\circ}C$), R is annual precipitation (ap, mm) or coefficient of variation of monthly precipitation (CV, %), and the PV-CV is CV of monthly PV (%). All these models are statistically significant ($p < 0.001$).

b_0	b_1	b_2^{ap}	b_2^{CV}	b_3	Adjusted r^2
-5.42	0.024	0.000306*		0.165	0.537
-4.53	0.026		-0.0038*	0.149	0.507
-4.45	0.023			0.166	0.548

* The regression coefficient was not significant ($p > 0.05$)

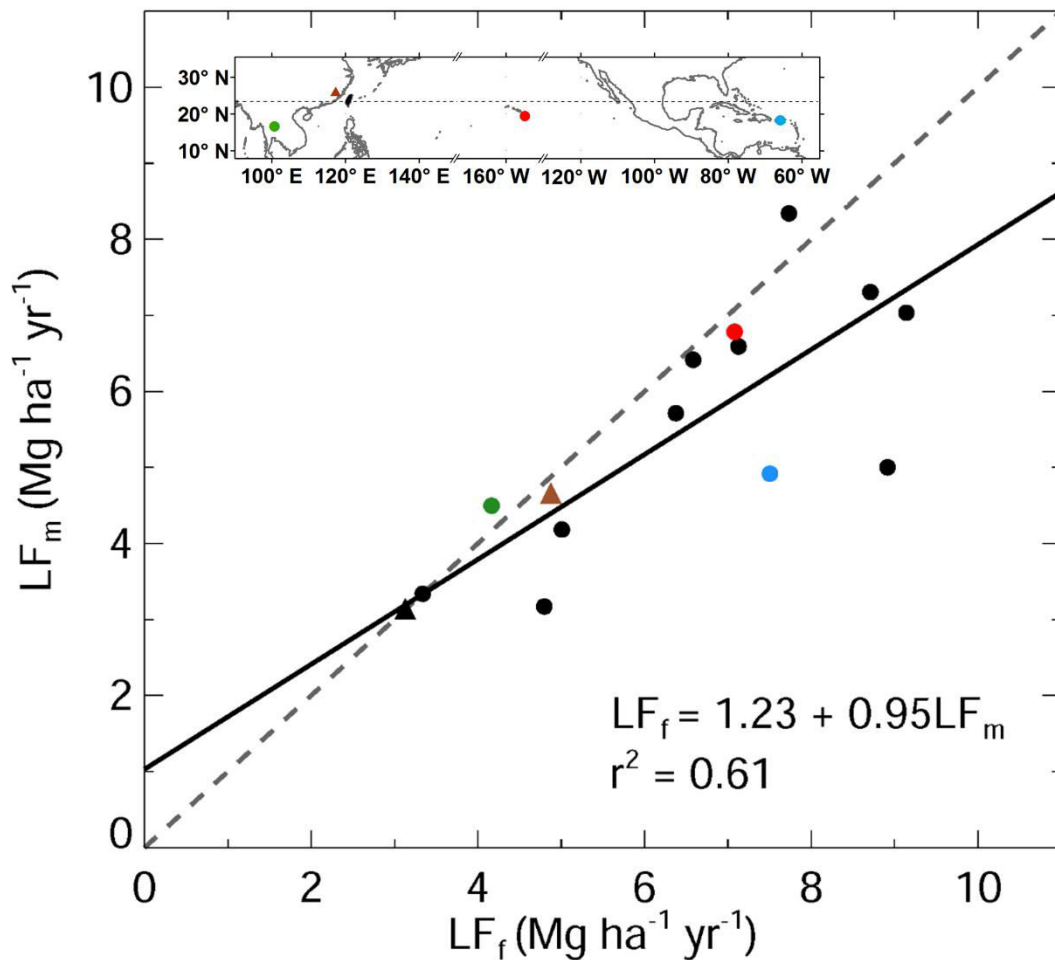
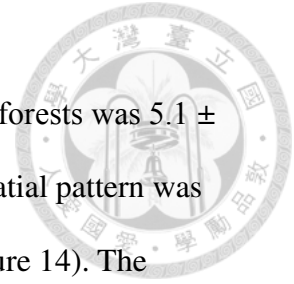


Figure 13. The relationship between the field litterfall (LF_f , from the validation sites in Taiwan, Figure 8, the x-axis) and estimated litterfall (LF_m , the y-axis) ($p < 0.05$, $n = 11$). The circles are evergreen broadleaf forests and triangles are coniferous forests. The black colors represent validated sites in Taiwan and remaining colors represent other subtropical forests. The solid line is the fit line and the dashed line depicts the 1:1 relationship.

3.3 Litterfall patterns and topographic analysis

The mean (\pm standard deviation, s.d.) annual litterfall in Taiwan's forests was $5.1 \pm 1.2 \text{ Mg ha}^{-1} \text{ yr}^{-1}$ during the observation period (2001–2011), and the spatial pattern was highly variable, ranging from $1.4 \text{ Mg ha}^{-1} \text{ yr}^{-1}$ to $10.2 \text{ Mg ha}^{-1} \text{ yr}^{-1}$ (Figure 14). The temporal variations of litterfall were 4.7 ± 1.4 (year 2009) – 5.6 ± 1.7 (year 2001) $\text{Mg ha}^{-1} \text{ yr}^{-1}$ (Figure 15). The litterfall patterns revealed a pronounced ($p < 0.05$) tendency of the litterfall to decrease along the elevation gradient (Figure 16(a) and 17(a)). By contrast, the slope (Figure 16(b)) was not a salient variable ($p > 0.05$) for estimating the variation of litterfall across regions (Figure 17(b)). The proportions of the aspects for each group were quite even (north: 11.3%, northeast: 10.2%, east: 12.5%, southeast: 16.0%, south: 12.3%, southwest: 11.2%, west: 12.6%, northwest: 13.9%). There were significant differences among the aspect classes (one-way ANOVA F -test, $p < 0.001$) (Figure 16(c) and 17(c)). The northeast ($6.0 \pm 1.0 \text{ Mg ha}^{-1} \text{ yr}^{-1}$) and northwest facing ($5.9 \pm 1.1 \text{ Mg ha}^{-1} \text{ yr}^{-1}$) classes yielded the largest amount of litterfall, which was in contrast to the south facing slope ($5.1 \pm 1.2 \text{ Mg ha}^{-1} \text{ yr}^{-1}$) based upon Tukey-Kramer multiple comparisons ($\alpha \leq 0.05$) (Figure 16(c) and 17(c)).



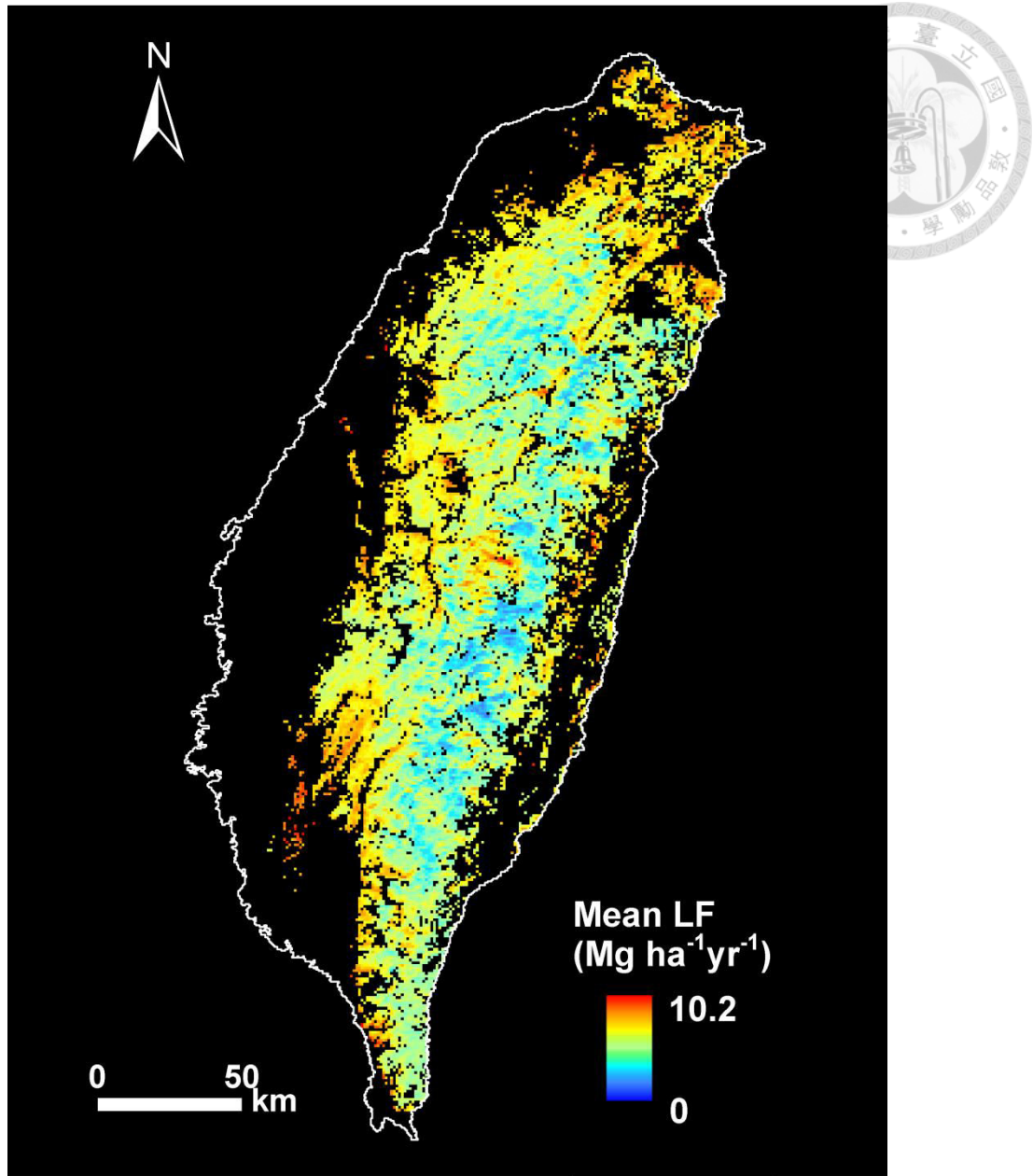


Figure 14. The mean litterfall (2001–2011) estimated by a multiple regression model using MODIS (Moderate Resolution Imaging Spectroradiometer) PV-CV (annual coefficient of variation of PV) and LST (Land Surface Temperature) as explanatory variables (Table 4).

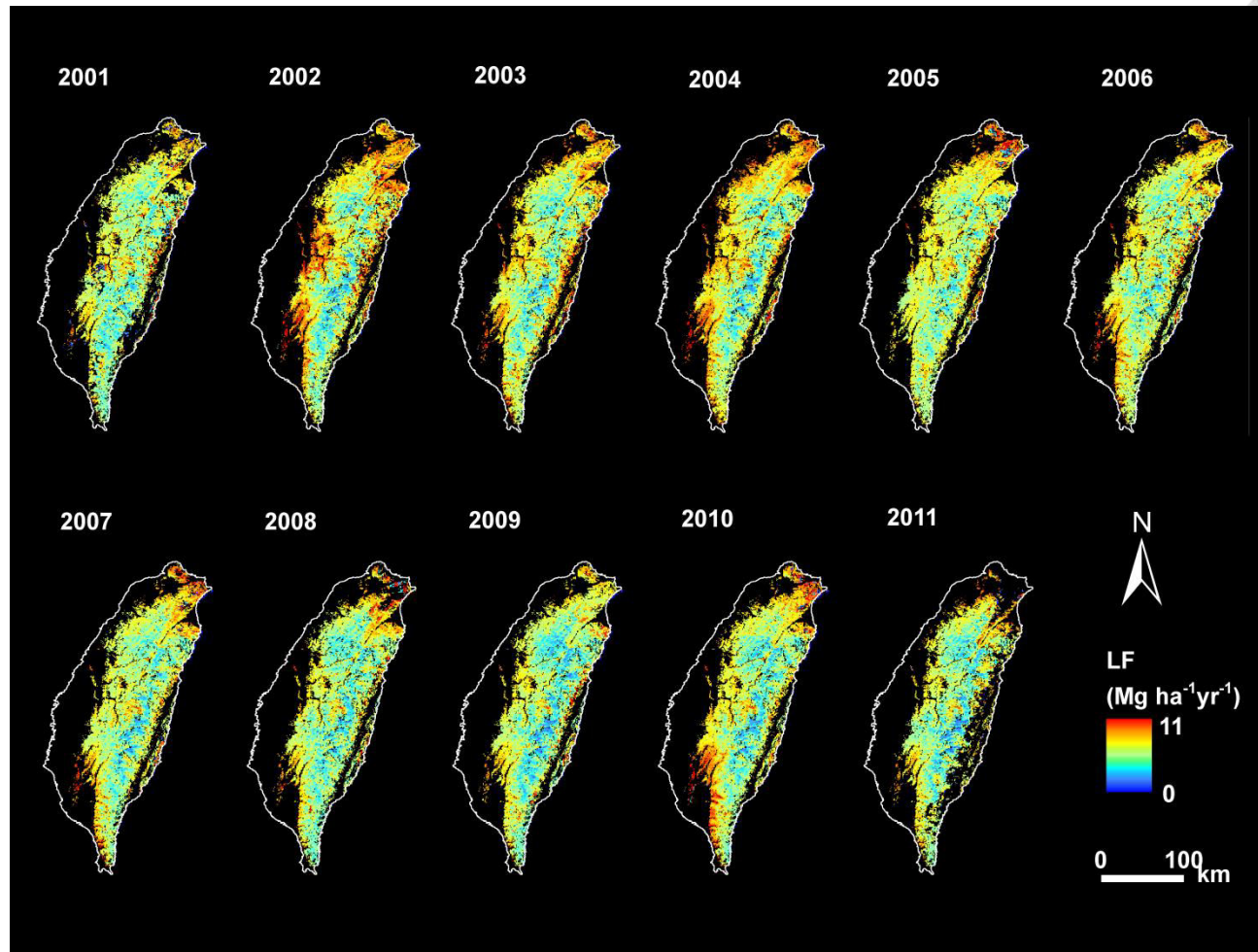


Figure 15. The temporal variations of annual litterfall during 2001–2011. The 11-year LST (Land Surface Temperature) and PV-CV (annual coefficient of variation of PV) were calculated as explanatory parameters to estimate the LF with a multiple regression model.

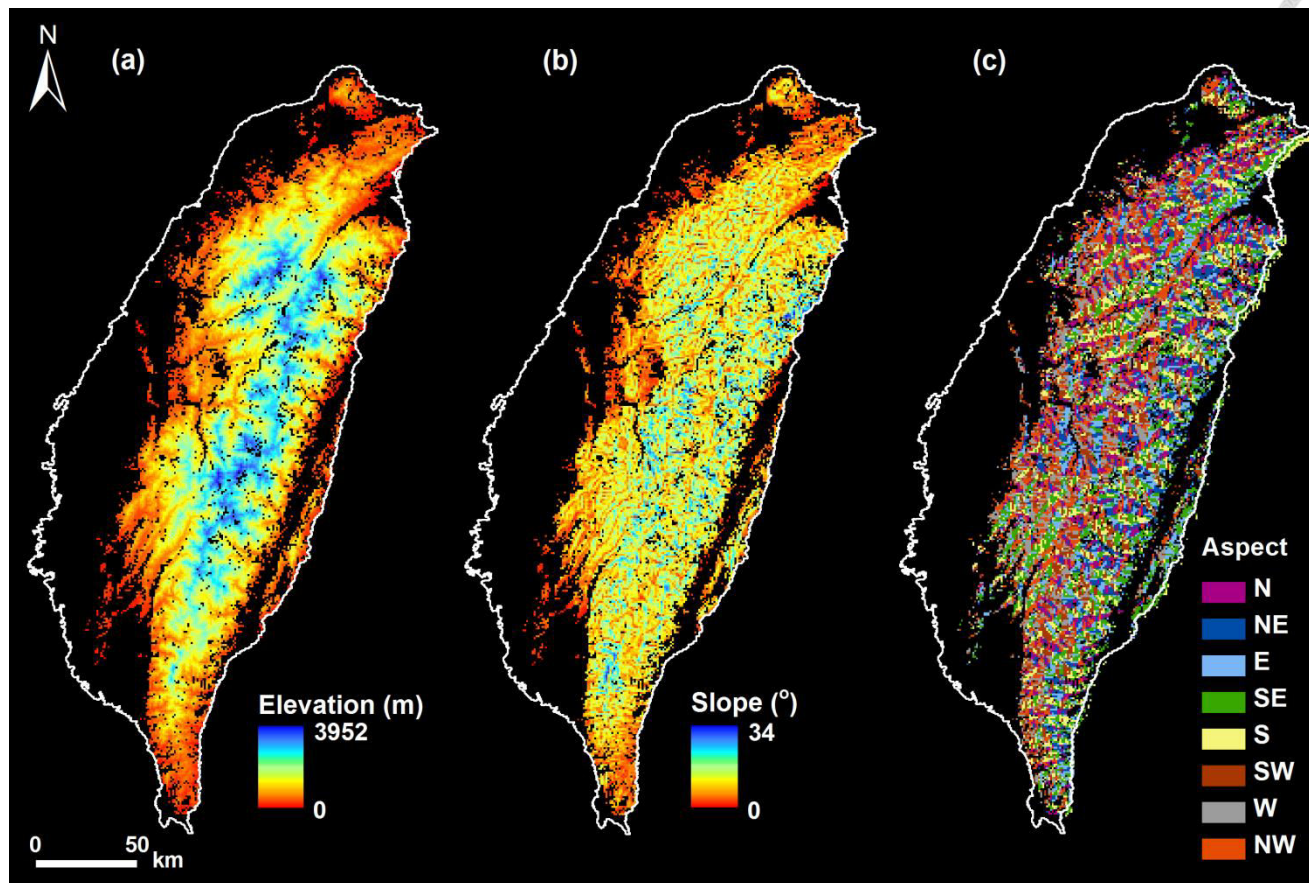


Figure 16. The topography ((a) elevation, (b) slope and (c) aspect) of Taiwan. The aspect classes are: north (N: 0–22.5° and 337.5–360°), northeast (NE: 22.5–67.5°), east (E: 67.5–112.5°), southeast (SE: 112.5–157.5°), south (S: 157.5–202.5°), southwest (SW: 202.5–247.5°), west (W: 247.5–292.5°) and northwest (NW: 292.5–337.5°).

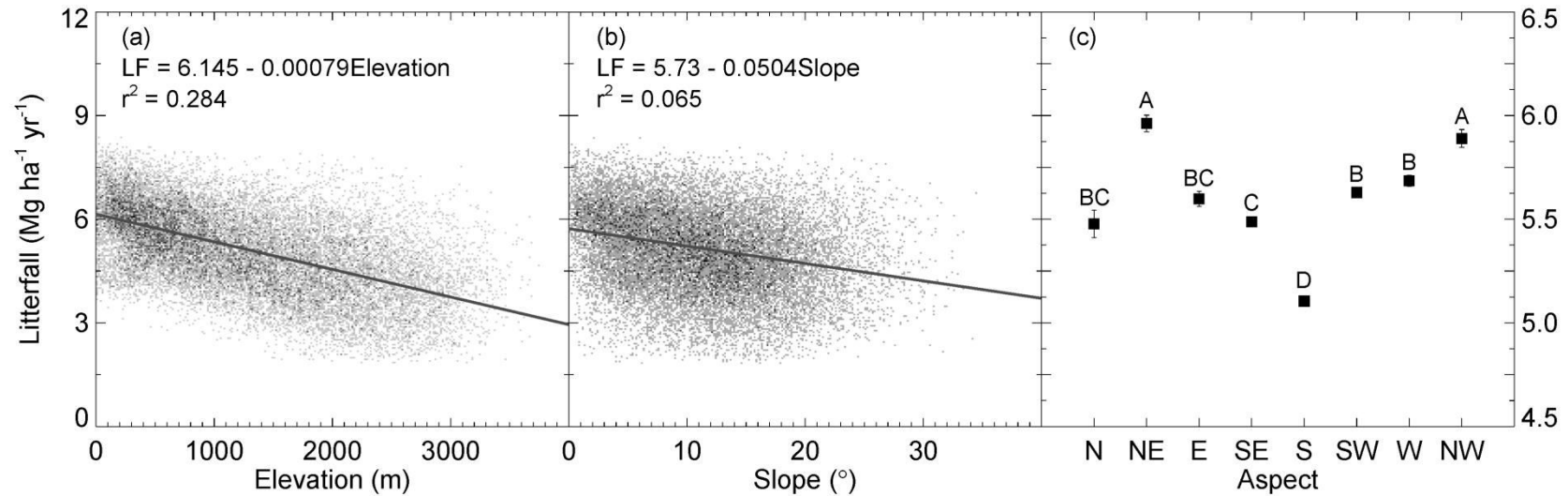


Figure 17. (a) The significant ($r^2 = 0.284$, $p < 0.05$) relationship between 11-year (2001–2011) modeled (Table 4) mean annual litterfall (LF) and elevation. (b) The insignificant ($r^2 = 0.065$, $p > 0.05$) correlation between mean LF and slope. (c) The mean LF and standard error (bars) of different aspect classes (north [N: 0–22.5° and 337.5–360°], northeast [NE: 22.5–67.5°], east [E: 67.5–112.5°], southeast [SE: 112.5–157.5°], south [S: 157.5–202.5°], southwest [SW: 202.5–247.5°], west [W: 247.5–292.5°], northwest [NW: 292.5–337.5°]) (One-way ANOVA F -test, $p < 0.05$). Different letters indicate significant differences between groups based upon a significant level (α) of 0.05 of the Tukey-Kramer multiple comparison.



4. Discussion

4.1 Regional litterfall estimation

A multiple regression model using MODIS-derived annual accumulated LST and dynamics of canopy closure (PV-CV) can be effective to delineate the data patterns. This is valuable because is extremely challenging to collect field litterfall data that is representative of a vast area. In addition, the high accessibility of MODIS data makes this protocol feasible for other regions. This study also reveals that the in-situ and remotely sensed precipitation variables are difficult to be a deterrent in this region (Table 4). According to the climate records during the observation period (2001–2011), the variation of monthly precipitation (dry vs. wet) was pronounced compared to the monthly temperature anomalies. Therefore, the vegetation phenology, including litterfall production, may not be able to adjust to the rapid change of rainfall patterns. This regional propensity could reflect the global trend because of the amplification of precipitation anomalies in recent decades (Facelli and Pickett 1991). This study also noted that our finding was similar to a field study showing that the dynamics of 18-year annual litterfall was unrelated to the pattern of annual precipitation in a temperate deciduous forest (Knutson 1997). By contrast, other studies indicated that inter-annual variation of litterfall may be associated with precipitation seasonality for certain vegetation type (Sánchez-Andrés et al. 2010; Williams-Linera et al. 1996). This inconsistency across bioclimates suggests different strategies for plants in response to the alteration of precipitation regimes, particularly water shortage, such as leaf shedding, decrease in leaf area index, branch die-off or dormancy (da Costa et al. 2014). The plant adjustments may or may not modify the storage of live carbon, which weakens the predictivity of precipitation for forest litterfall production.

4.2 Model validation

In this study, the annual mean (2001–2011) (\pm s.d.) litterfall production was $5.1 \pm 1.2 \text{ Mg ha}^{-1} \text{ yr}^{-1}$ in Taiwan's forests (Figure 14). A global scale synthesis study indicated that the mean annual litterfall was approximately $11 \text{ Mg ha}^{-1} \text{ yr}^{-1}$ in equatorial forests, $5.5 \text{ Mg ha}^{-1} \text{ yr}^{-1}$ in warm temperate forests, $3.5 \text{ Mg ha}^{-1} \text{ yr}^{-1}$ in cold temperate forests and $1 \text{ Mg ha}^{-1} \text{ yr}^{-1}$ in arctic-alpine forests (Bray and Gorham (1964)). There is a strong agreement between these two independent studies because Taiwan is located in tropical/subtropical regions with a warm and humid climate yielding a moderate amount of annual litterfall.

Our regional litterfall is also comparable to field data acquired from validated sites (Figure 13) with moderate (16.6%) underestimation. This study also used the model to evaluate the litterfall in other subtropical forests, and the results showed the model could estimate litterfall well at some sites but may underestimate litterfall at the other sites (Figure 13). The forests are formed by multiple layers of canopies, such as top-canopy, sub-canopy and understory, particularly in tropical and subtropical regions. The litterfall is the defoliation from top-canopy and sub-canopy. Although leaves from certain species are senescent during a specific time period, there remain multiple layers of photosynthetically active leaves present along the vertical profile, which is an inevitable limitation of transforming the 3-D forest structure into a 2-D satellite image (Chambers et al. 2007b). The systems would maintain relatively stable PV and subsequently lower PV-CV, which may not entirely reflect the seasonal pattern of litterfall. Therefore, the underestimation of litterfall in the model might be due to difficult to capture the defoliation from sub-canopy. Furthermore, typhoons can contribute large amounts of litterfall (Lin et al. 2003a; Xu et al. 2004b), but the change of canopy structure may be relatively subtle in 2-D satellite images because

the loss of greenness may be compensated for by the lower layers of canopies and/or understory shrubs. In addition, satellite measured phenological variation (e.g., induced by climate anomalies) might not entirely reflect forest metabolism (Triadiati et al. 2011; Zhou et al. 2014). These aforementioned complexities in canopy structures coupled with the limitations of passive optical remote sensing may constrain the effectiveness of PV-CV to portray the dynamics of forest litterfall. Another possible uncertainty may be that the field data (Table 3) were not sufficient to represent the smallest remote sensing sampling unit (100 ha). Moreover, the accuracy of these field measures was extremely difficult to assess. Field litterfall acquisition is very labor intensive, and it is extremely challenging to find an adequate amount of field data for a vast region. Therefore, data representativity and quality related issues might be unavoidable.

4.3 Temporal dynamics of litterfall

The abundance of annual litterfall in Taiwan's forests varied over the years (4.7–5.6 Mg ha⁻¹), which may be due to episodic and continuous climate fluctuations (Figure 9 and 15). Taiwan is frequently disturbed by typhoons (Figure 9), and the number of major tropical cyclones was higher (n = 165) than in the North Atlantic (91) from 1970–2007 (Lin et al. 2011). Typhoons with heavy precipitation and strong wind speeds result in a large amount of defoliation, accounting for 30–60% of the variation in the annual litterfall in Pacific Asia (Lin et al. 2003a; Xu et al. 2004b). The annual production of litterfall may be higher in one single year with frequent and strong (central wind velocity > 32.7 m s⁻¹) typhoons, such as 2004 (n = 4), 2005 (3) and 2008 (4) (Figure 9 and 15) compared to the average ± s.d. (n = 1.9 ± 1.3). Wang et al. (2013) found that typhoon-induced litterfall could contribute 60% (3.43 Mg C ha⁻¹ yr⁻¹) and

80% ($3.21 \text{ Mg C ha}^{-1} \text{ yr}^{-1}$) of annual litterfall in evergreen broadleaf and Chinese-fir forests from four typhoon events in 2008 in central Taiwan. Typhoon-induced litterfall is a potential way of releasing carbon into the atmosphere via litter decomposition and soil respiration, which is the major outlet of the terrestrial carbon cycle of this bioclimatic region (Chambers et al. 2007a; McNulty 2002). High return time of tropical cyclones ($1.9 \text{ typhoons yr}^{-1}$ [Figure 9]) makes variations of annual litterfall influenced by the amount and intensity of typhoons in one single year in this study.

Higher annual litterfall was observed in some years without severe effects of typhoons, particularly in 2002 and 2003 when drought occurred (Figure 9 and 15), which may be another critical factor affecting the annual production of litterfall. Chang et al. (2013) found that the lowest vegetation cover and NPP (23.3 Tg C) in 2002 during 2001-2010 may be due to the effect of long-lasting drought from ENSO events. The lowest vegetation cover and NPP observed in 2002 might imply there has higher defoliation in these periods. Some studies reported similar results showing a negative relationship between the annual litterfall and precipitation during drought events (Beard et al. 2005; PeñUelas et al. 2007). By contrast, Brando *et al.* (2008) demonstrated that the annual litterfall production was also decreased after severe drought. Overall, the litterfall was very responsive to anomalous events, and long-term monitoring of litterfall production may be critical for understanding the responses of different ecosystems to disturbances.

4.4 Spatial pattern of litterfall

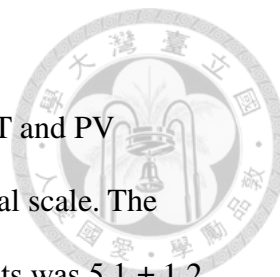
The topography can significantly influence the spatial variations of the microclimate, solar radiation and soil water movement, which critically affect vegetation (Aiba et al. 2004; Yasuhiro et al. 2004). A linear negative relationship was

observed between the elevation and litterfall (Figure 16(a) and 17(a)). In Taiwan, the type of vegetation varied with the elevation, from low elevation (0–2200 m a.s.l.) broadleaf rainforests to mid-altitude (2200–3000 m) coniferous forests and high-altitude alpine dwarf bamboo (3000–3952 m) (Chang et al. 2011). Brown and Lugo (1982) demonstrated a positive relationship between the forest biomass and litterfall, and the shift of biomes may result in the reduction of live carbon storage in highly elevated regions (Aplet and Vitousek 1994; Raich et al. 1997). This may explain the negative elevation-litterfall relationship. Similar trends were also found in many sites around the world (Bray and Gorham 1964; Reiners and Lang 1987).

No apparent relationship was observed between the slope and litterfall (Figure 16(b) and 17(b)), possibly due to a lack of relationship between the slope and biomass (Clark and Clark 2000; de Castilho et al. 2006) and productivity (Huang et al. 2012a). Additionally, the coarse spatial resolution (1 km) may not capture the variation of terrain incline. The pattern of litterfall to aspect was apparent (Figure 16(c)). The northeast and northwest-facing classes yielded the highest amount of litterfall, which were in contrast to the south-facing classes (Figure 17(c)). The aspect governs the intensity of the surface solar radiation resulting in the differences of bioclimate environments, which may significantly influence plant growth and biomass (Bennie et al. 2008; de Castilho et al. 2006; Huang et al. 2012a). In general, the lower solar radiation on north-facing aspects in the Northern Hemisphere would form a wetter and cooler microclimate and vice versa (Bennie et al. 2006; Haase 1970). This may be the key for the spatial pattern of litterfall production.

5. Conclusions

This study demonstrates the feasibility of utilizing MODIS LST and PV time-series data to scale up the field litterfall measures to the regional scale. The results show that the mean (\pm s.d.) annual litterfall of Taiwan's forests was 5.1 ± 1.2 Mg ha⁻¹ yr⁻¹ during the observation period (2001–2011). The temporal dynamics were pronounced ranging from 4.7 to 5.6 Mg ha⁻¹ yr⁻¹, which may be influenced by typhoons and consecutive years of drought. This study also investigated the effects of topography on litterfall, and found that the elevation and aspects governed the spatial arrangement of litterfall. A negative relationship was observed between the litterfall and elevation, which may be due to the change of vegetation types and their ability to sequester carbon. Northeast and northwest facing slopes yielded the highest amount of litterfall, which was in contrast to the south facing slopes. This was possibly due to the effects of microclimates in this tropical/subtropical region. Overall, this study demonstrated a systematic processing protocol for the broad scale litterfall assessment, which may facilitate large-scale assessment of carbon and nutrient fluxes and perturbations in forest ecosystems.



CHAPTER IV



Using a dynamic global vegetation Hybrid 4.2 model to simulate typhoon-induced leaf litter under different typhoon intensity and frequency in a subtropical forest

Using a dynamic global vegetation Hybrid 4.2 model to simulate typhoon-induced leaf litter under different typhoon intensity and frequency in a subtropical forest



Abstract

Typhoon is the major natural disturbance in Western North Pacific region, and can derive substantial leaf litter which is a critical return of carbon and nutrients to the soil. The changes of typhoon intensity or frequency under warmer sea surface temperature might affect forest defoliation and biogeochemistry by strong wind speed and precipitation. A wind build-in function with wind speed, temperature and precipitation was developed to incorporate into the dynamic global vegetation Hybrid 4.2 model to simulate leaf litter at the Fushan experimental forest in Taiwan. The simulations of typhoon intensity and frequency were modeled based on the fitted normal and Poisson distribution functions. The *in-situ* maximum daily wind speed was a critical variable to estimate *in-situ* typhoon-induced leaf litter ($r^2 = 0.13$, $p = 0.02$). Leaf litter was significantly different among typhoon intensity ($p < 0.05$) but not significant among typhoon frequency ($p > 0.05$). Substantial leaf litter occurred not only in typhoon season (summer and autumn) but also in spring from effects of plant physiology and phenology. The Hybrid modeled and observed leaf litter was significant correlated ($r^2 = 0.33$, $p < 0.001$) with moderate underestimation (15.6%). The leaf litter, leaf area index (LAI), total biomass, gross primary production (GPP) and net primary production (NPP) were higher in typhoon events than without typhoon events. The raises of typhoon intensity and frequency would increase leaf litter and soil respiration resulted in the decreases of LAI, biomass, GPP and NPP. Leaf litter is highly associated with the combination of climate factors and plant

physiology. The Hybrid model with wind built-in function might be potential way to simulate ecosystem processing under scenarios of typhoon intensity and frequency.

The high defoliation from more intense or frequent typhoon might influence regional carbon budget in the long-term time.



Keywords: Leaf litter, carbon cycle, biogeochemistry, typhoon, Hybrid, dynamic global vegetation model

1. Introduction

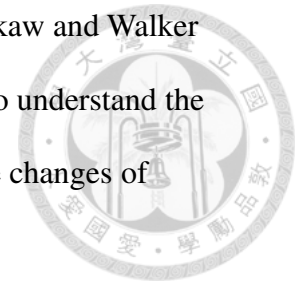
Rising sea surface temperature under global warming might lead to a change in the occurrence or intensity of tropical cyclones ('typhoons' or 'hurricanes', depending on the geographic region; this study uses 'typhoons') (Bender et al. 2010; Emanuel 2005; Knutson et al. 2010; Webster et al. 2005). A typhoon derives energy from the evaporated water over a relatively warm, large ocean surface and is a rapidly rotating storm system with a low-pressure center, heavy precipitation and strong winds (the minimum central wind velocity of typhoon is 33 m s^{-1} under the classification system of Saffir-Simpson Hurricane Scale) (Dent et al. 2006). Forest ecosystems might be affected by changes of frequency and intensity of amplified typhoons in the future. Assessing the potential impacts of extreme typhoon events on ecosystem structure and biogeochemical processes is critical, especially in frequently perturbed regions such as Taiwan (3.7 typhoons/year) (Lin et al. 2011).

Typhoons with heavy precipitation and strong wind speeds may trigger large amounts of litterfall, accounting for 30-60% of the annual litterfall (Lin et al. 2003a; Sato et al. 2010; Xu et al. 2004b). Substantial amounts of typhoon-induced leaves, branches, bark, twigs, fruits and other forms of dead organic material suddenly transferred from canopies into forest floor could have a major impact on forest

structure and function (Sato et al. 2010; Whigham et al. 1991). For instance, large production of litter would reduce leaf area index and increase canopy gap fraction which may lead to more light penetrating through defoliated canopies (Lin et al. 2003c). The higher understory light environment from gap formations can promote seedling growth and influence the regeneration and survival of species, which might have a large effect on the species composition, community dynamics and forest structures (Lin et al. 2011; Turton 2008; Zeng et al. 2009).

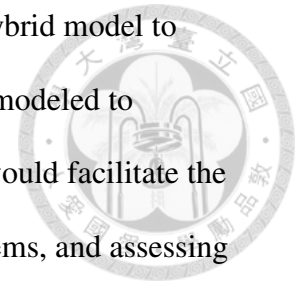
Leaf litter is the major nutrients return to the soil, and large amounts of typhoon-induced leaf litter will therefore not only influence forest structures but also affect forest biogeochemical processes such as carbon and nitrogen cycles (Lin et al. 2011). In general, plant tissues will remove a fraction of their nutrients prior to senescence, and retranslocated nutrients are available for reuse by the plant in the next growth cycle (Del Arco et al. 1991; Zalamea and González 2008). However, typhoon-induced leaves do not undergo retranslocation before they fall, and could contain more fresh leaves with 1.3-2.4 times the amounts of nitrogen and phosphorus nutrient inputs compared to normal litterfall with lower nutrients inputs (Lodge et al. 1991; Ostertag et al. 2003). The sudden increase in nutrient inputs from plant into forest floor might alter litter decomposition and soil nutrient patterns (Ostertag et al. 2003; Xu et al. 2004b). The large production of litter could also potentially release carbon to the atmosphere by increasing litter decomposition and soil respiration (Chambers et al. 2007a; Vargas and Allen 2008). Owing to the differences of species mortality and regeneration, typhoons may be an important factor in controlling forests long-term changes in species composition, which may affect forest biomass and nutrient accumulations (Turton 2008; Van Bloem et al. 2005; Zeng et al. 2009). Overall, substantial defoliation induced by typhoons may have a major impact on

forest structures, energy flows, and biogeochemical processes (Brokaw and Walker 1991; Lin et al. 2011; Zeng et al. 2009). Therefore, it is important to understand the interaction and response of forest carbon and nutrient cycling to the changes of typhoon intensity and frequency.



Simulation models are important in understanding how the components of a system operate and interact with each other. When the ecosystem is disturbed by typhoons, changes of biogeochemical cycles and ecological process might constrain the system's structure and function such as growth, succession, competition, carbon, nitrogen and water fluxes (Beard et al. 2005; Lin et al. 2011; Zeng et al. 2009). A simulation model tries to model the biogeochemical linkages and ecological process, and predict behavior and responses of the ecosystem under future climate scenarios. A dynamic global vegetation model, Hybrid v4.2 is process-based model to predict ecosystem structure (e.g. biomass and vegetation patterns) and fluxes of an ecosystem (e.g. NPP, nutrient cycles and soil carbon) (Friend and White 2000). The Hybrid model consists of a gap-modeling approach that takes the growth, reproduction, mortality, phenology and biogeochemistry into account (Friend et al. 1997; Friend et al. 1993; Friend and White 2000). However, the Hybrid or other process-based ecosystem models (ex. CASA and Biome-BGC) do not include the effects of typhoon disturbance on the model, which is critically important for frequently perturbed ecosystems. Although Ito (2010) tried to use the Vegetation Integrative Simulator for Trace gases (VISIT) model to estimate typhoon-induced defoliation, this study eventually used a Monte Carlo simulation to find the estimated defoliation by minimizing the root mean square error (RMSE) between modeled and observed data (e.g. LAI, GPP and RE). This method was therefore not based on a process-based function but on the stochastic simulation. Overall, a function with wind,

temperature, precipitation as variables was incorporated into the Hybrid model to simulate leaf litter flux, and typhoon intensity and frequency were modeled to evaluate the influences of typhoon on carbon cycling. The results would facilitate the understanding of the carbon cycles in frequently perturbed ecosystems, and assessing the potential ramifications of extreme typhoons.



2. Methods

2.1 Study site

This study was carried out at the Fushan experimental forest in northeastern Taiwan (24°34'N, 121°34'E). The Fushan experimental forest has an area of 10 km² and various topographies in elevation from 670m to 1400m. The climate is warm and humid, and the annual temperature is 18.2°C with a low monthly average temperature 12.0°C in January and a high monthly average temperature 24.6°C in July from 1988 to 2009. Annual mean precipitation was about 4096 mm with a mean relative humidity 93.7%, and the period of May to October accounts for approximately 66% of the annual precipitation generated from typhoon and East Asian rainy season (commonly called as plum rain). The Fushan experimental forest is a moist subtropical mixed evergreen forest and the dominant tree species are *Castanopsis carlesii* var. *sessilis* Nakai, *Machilus thunbergii* (Sieb. et Zucc.) Kostermans, *Engelhardtia roxburghiana* Wall., *Meliosma squamulata* Hance, *Litsea acuminata* (Blume) Kurata, *Diospyros morrisiana* Hance, *Helicia formosana* Hems, and *Pyrenaria shinkoensis* (Hayata) Keng. The mean Leaf Area Index (LAI) from 1994 to 2010 is 3.2 and the mean canopy height is 10.2 m. The topography varies in elevation from 670 to 1100 m with a mean slope of 54% (Lin et al. 2011). The bedrock in this site consists a metamorphosed sedimentary rock from the Oligocene and Miocene,

containing argillite and slate. The soil is very acidic (pH 3.8-5.0) with medium quantity of organic matter in sublayer (2-5%), low cation exchangeable capacity and base saturation percentage in the whole pedons (Owen et al. 2010).



2.2 Field data

The field climate data were acquired from Fushan meteorological station in Taiwan Forestry Research Institute at 634m above sea level. The daily maximum temperature, minimum temperature, precipitation, solar radiation, vapor pressure and wind speed from 1993 to 2013 were obtained as the input variables in the Hybrid model. To compare with international studies, typhoons were classified as mild (category 1), moderate (category 2) and severe (category 3 and above) typhoons based on the typhoon intensity classification from Saffir-Simpson Hurricane Wind Scale (<http://www.nhc.noaa.gov/aboutsshws.php>). The central wind velocity of mild typhoon is 119–153 km hr⁻¹, the central wind velocity of moderate typhoon is 154–177 km hr⁻¹ and the central wind velocity of severe typhoon is over 178 km hr⁻¹. If the study site was within the radius of a typhoon, it was regarded as a typhoon event in this study. The radius of a typhoon was different based on the typhoon intensity and characteristics, which were defined by Taiwan Central Weather Bureau (<http://rdc28.cwb.gov.tw/>). Twenty-one years field leaf litter data was used to calibrate (1993–2003) and validate (2004–2013) the model (K.C. Lin unpublished). Leaf litter were collected from ten litter traps with 0.25m² in size under canopies at 1m above ground to avoid microbe decomposition (Lin et al. 2003a). The traps were visited monthly, and the collected leaf litter was oven dried at 65 °C for 48–72 h to constant weight.

2.3 The Hybrid model

The Hybrid v4.2 model is a dynamic and process-based representation of ecosystem biogeochemistry and competition. The hybrid is mechanistic, driven by climate, and deals with dynamic vegetation growth processes. The characteristics of Hybrid are simulating carbon, water, nutrients cycles in soil-plant-atmosphere system to reflect components of complex interactions and feedbacks between vegetation, soil and atmosphere. Secondly, the driving force for the model is only climatic variables such as CO₂, nitrogen deposition, solar radiation and precipitation, which are the fundamental biological and physical-chemical processes. Thirdly, the Hybrid is based on a gap-modelling approach within a plot to simulate the growth of individual over time and competition for environment resources such as light, water and nitrogen. This approach can get the transitions of vegetation types (Friend et al. 1997; Friend and White 2000).

In the Hybrid v4.2 model, daily climate is the principal variable provided by a daily weather generator from monthly climate data (Friend 1998). The daily maximum and minimum air temperatures, daily precipitation, daily shortwave irradiance, and daily atmospheric water vapor pressure are regarded as climate input in the model. The individuals are seeded every year into 200 m² plots to grow, die and regenerate like a forest gap model on a daily time step. Each of the plots in a simulation is completely independent and mean of plots is mean ecosystem characteristic. The light, water, and nitrogen are assumed to be homogeneously, horizontally distributed in each plot. Photosynthesis, maintenance respiration, nitrogen uptake, transpiration, carbon and nitrogen litter production are simulated on a daily time step. The vegetation dynamics processes of allocation, mortality, regeneration are implemented each year. The soil is divided into three hydrological layers and soil water holding capacity is allowed to vary as a function of soil carbon

based on soil texture. Soil carbon and nitrogen dynamics determine the availability of mineral nitrogen to the plants, rates of decomposition and heterotrophic respiration, and amounts of soil carbon. The competition of individuals for environmental resources such as light, water, nitrogen within each plot is critical for vegetation succession and transition from one to the others under climate change or disturbed forces. The eight Generalised Plant Types (GPTs) are used in the Hybrid v4.2 model and classified as C₃ and C₄ herbaceous, evergreen broadleaf, cold and dry deciduous broadleaf, evergreen needleleaf, cold and dry deciduous needleleaf. A complete description of the Hybrid 4.2 model is given by previously studies (Friend et al. 1997; Friend et al. 1993; Friend and White 2000).

2.4 Model calibration

Temperature and precipitation are the major factors that control plant physiology and phenology, which affect inter-and intra-year dynamics of leaf emergence and defoliation (Chave et al. 2010; Wang et al. 2013; Wood et al. 2005). Compared to phenological variables, strong wind and heavy rain dominate the critical impacts of typhoons on the forest ecosystems by damaging leaves as well as changing the biomass (Brokaw and Walker 1991; Sato et al. 2010; Wang et al. 2013; Xu et al. 2004a). Based on the aforementioned, temperature, precipitation and wind speed were used as the variables to calibrate the leaf litter in Hybrid model. The leaf litter was calculated in phenology function using the following expression in the Hybrid model:

$$L_l = \frac{C_f}{i_c} + f_L \times \left(C_f - \frac{C_f}{i_c} \right) \quad (1)$$

where L_l is leaf litter carbon, C_f is total leaf carbon mass, i_c is the number of layers in crown, f_L is the leaf turnover rate. The first part is the carbon mass of the leaves in the lowest layer, and the second part is the turnover of the remaining leaves. The

variability of leaf litter was affected by the climatic parameters:

$$L_l = f(L_f, T, R, W) \quad (2)$$

The T is temperature (°C), R is daily precipitation (mm day⁻¹) and W is maximum daily wind speed (m s⁻¹). The differential of temperature was adopted to capture the growth season in the function (Figure 18). However, wind speed might be different along the canopy heights, and this study calculated wind speed at different heights based on a wind profile formula for each individual tree in the model:

$$u(z) = \frac{u_*}{K} \ln \left(\frac{z - d}{z_0} \right) \quad (3)$$

where $u(z)$ is wind speed at height z , u_* is friction velocity, z_0 is roughness length, K is von Karman's constant 0.4 and d is the zero-plane displacement height. The value of d is 0.65*tree height, while z is 0.1*tree height (Campbell and Norman 1998). To evaluate how wind speed affects defoliation, the daily maximum wind speed, variance and turbulence kinetic energy (TKE) from filed weather data were used to find the relationships between wind speed and litter:

$$Var(X) = \frac{1}{n} \sum_{i=1}^n (x_i - \mu)^2 \quad (4)$$

$$\frac{TKE}{m} = \frac{1}{2} (\overline{u'^2}) \quad (5)$$

where x_i is the sample value and μ is the mean in the eq. 4. The m is mean and u'^2 is the variance in the eq. 5. For the precipitation, the daily precipitation in typhoon events was analyzed (Figure 19). The daily precipitation in typhoon events was greater than the normal events, and the low and the high daily precipitation in typhoon and non-typhoon events was 150 mm day⁻¹, which was considered into the function.



In Hybrid model simulations, the plant will grow and compete within a plot, and the leaf area index, biomass and NPP etc. will reach a quasi-equilibrium after ~250 years (Friend et al. 1997). Therefore, this study used one year data to reach a quasi-equilibrium after 250 years simulation and used the half of observed data to calibrate (1993–2003) and validate (2004–2013) the model in the following simulation. In the Hybrid model, the input values of variables were used based on the observed data in the field or on the setting of the baseline model (Appendix A). After the simulation, this study accumulated the daily leaf litter into monthly leaf litter to validate with the observed data. The annual leaf area index, biomass, soil respiration, GPP and NPP were also calculated for the analysis.

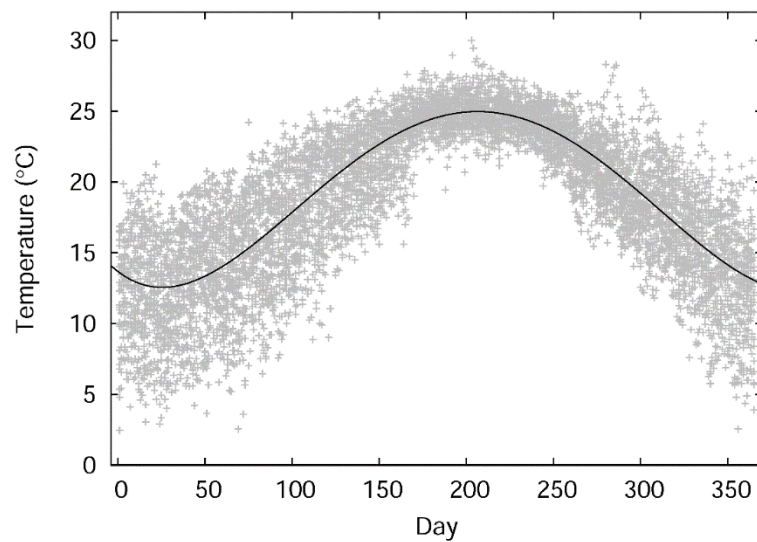


Figure 18. The daily mean temperature from 1993 to 2013 was fitted by a polynomial formula ($\text{Temperature} = 15.44 - 5.15\text{day} + 2.44\text{day}^2 - 0.28\text{day}^3 + 0.00959\text{day}^4$).

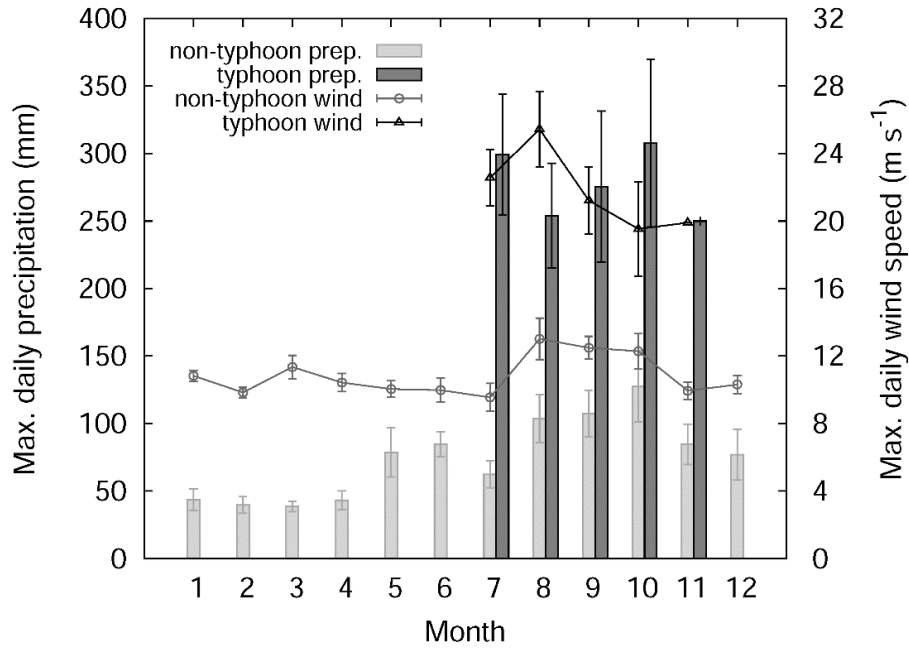


Figure 19. The patterns of monthly maximum daily precipitation and wind speed in typhoon and non-typhoon months.

2.5 Typhoon intensity and frequency simulations

To evaluate the effect of typhoon on the ecosystem, the climate dataset of typhoon events were replaced by mean of climate dataset to compare with the modeled results from historical climate dataset. The historical climate dataset with and without typhoons were regarded as input climatic variables to simulate the carbon cycle of forest ecosystem. For typhoon intensity simulation, the maximum daily wind speed was the variable regarded as the influence of typhoon intensity and frequency on litter in the model. The frequency distribution of wind speed displays the wind speed of various typhoon events, and follows a normal distribution ($p = 0.298$):

$$f(x | \mu, \sigma) = \frac{1}{\sigma\sqrt{2\pi}} e^{-\frac{(x-\mu)^2}{2\sigma^2}} \quad (6)$$

where μ is the mean of distribution and σ is variance. The frequency distribution of

typhoon events from 1993–2013 was fitted based on a formula of normal distribution and the mean of distribution was adjusted to model the changes of typhoon intensity. For typhoon intensity simulation, the mean of fitted normal distribution was adjusted from -10.0 to 10.0 with 0.2 interval, while the zero means the mean of distribution is the same with historical climate dataset. The modeled wind speeds at various intensities were placed into the same typhoon event dates to simulate how typhoon intensity affect litter and carbon cycling.

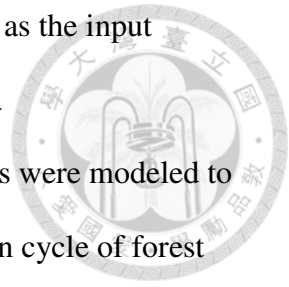
For typhoon frequency simulation, the occurrence of typhoon events per year was regarded as the effect of typhoon frequency on litter. The typhoon occurs independently of one another, and the frequency distribution follows discrete Poisson probability distribution ($p = 0.636$). The formula of Poisson probability mass function is:

$$f(x; \lambda) = \frac{\lambda^x e^{-\lambda}}{x!} \quad (7)$$

where x is observed number of events, λ is average number of events within a given region and e is Euler's number 2.71828. The frequency distribution of historical typhoon events were fitted to model the number of typhoon events occurring within a given region. The number of typhoon events were extracted from the fitted Poisson distribution with a lambda (λ) from -1.8 to 5.0, and the zero means the occurrence is the same with historical dataset. The intensity of wind speed was set as the historical mean of normal distribution. The modeled typhoon events were placed into the historical climate dataset in the typhoon season based on a Monte Carlo simulation to simulate how the changes of typhoon frequency per year influence the litter and ecosystem.

After simulating the scenarios of typhoon intensity and frequency, the climate

dataset with various typhoon intensity and frequency were regarded as the input variables into the Hybrid model. The model ran 250 years to reach a quasi-equilibrium first and the climate dataset with various scenarios were modeled to evaluate the effects of typhoon intensity and frequency on the carbon cycle of forest ecosystem. The daily leaf litter, annual leaf area index, total biomass, soil respiration, GPP and NPP were outputted for analysis.



3. Results

3.1 *Patterns of in-situ leaf litter and wind speed*

The monthly maximum, mean and variance of maximum daily wind speed and turbulence kinetic energy were used to correlate with field leaf litter data to find the suitable variable for simulation. The results showed that there were no significant relationships ($p = 0.556 - 0.874$) between turbulence kinetic energy and leaf litter whether in total or typhoon months data, while the relationships between maximum daily wind speed and litter were weak significant ($p < 0.001 - 0.605$) (Table 5). The field litter data were collected monthly, and the monthly maximum daily wind speed, monthly mean wind speed and monthly variance of wind speed were calculated to find the relationships with field monthly leaf data. For total months data, the monthly maximum daily wind speed had a significant but poor correlation with litter ($r^2 = 0.063$, $p < 0.001$) (Figure 20 (a)) compared to monthly mean wind speed ($r^2 = 0.057$, $p < 0.001$) and variance ($r^2 = 0.011$, $p = 0.053$). For the typhoon months data, the monthly maximum daily wind speed had a significant but weak relationship with litter ($r^2 = 0.125$, $p = 0.020$) (Figure 20 (a)) compared to monthly mean wind speed ($r^2 = 0.0$, $p = 0.605$) and variance ($r^2 = 0.084$, $p = 0.048$). Based on aforementioned analysis, the monthly maximum daily wind speed was used as variable of wind speed

in the following analysis. The relationships between maximum daily wind speed and leaf litter were significant on a linear, exponential, power, polynomial regression models ($r^2 = 0.07 - 0.16$, $p < 0.05$), and polynomial regression was used in the wind built-in function based on the model fitting results. For the multiple climate factors, the relationships between maximum daily wind speed, precipitation and temperature were not significant on a multiple regression model ($p = 0.055 - 0.125$).

For the seasonality of leaf litter, there were significant difference among spring, summer, autumn and winter seasons ($p < 0.001$) based on one-way ANOVA analysis, and the spring had the highest mean (\pm s.d.) litter production (0.0262 ± 0.00889 kgC m⁻²) (Table 6 and Figure 20 (b)). The maximum daily wind speed were also significantly different among four seasons ($p < 0.001$), and summer (14.6 ± 2.75 m s⁻¹) and autumn (13.8 ± 7.62 m s⁻¹), which are the major typhoon seasons, had higher wind speed than the spring (10.6 ± 5.98 m s⁻¹) and winter (10.3 ± 1.92 m s⁻¹) (Table 6 and Figure 20 (b)).

The difference of leaf litter was significant for typhoon intensities ($p = 0.016$), but not for typhoon frequency in typhoon occurrence per month ($p = 0.178$) and per year ($p = 0.073$) by one-way ANOVA analysis (Table 7). The highest mean of leaf litter (0.0333 ± 0.0206 kgC m⁻²) was produced in severe typhoons, while mild typhoons produced the lowest leaf litter (0.0169 ± 0.0069 kgC m⁻²) (Figure 20 (c)). For typhoon frequency, the mean litter production of two typhoon events per month (0.0300 ± 0.0086 kgC m⁻²) was higher than one event (0.0215 ± 0.0156 kgC m⁻²). The leaf litter was also higher in occurrence with more than three typhoon events per year ($0.214 - 0.259$ kgC m⁻² yr⁻¹) than in occurrence with less than three years ($0.173 - 0.192$ kgC m⁻² yr⁻¹). However, there was no clearly pattern between leaf litter and wind speed in different typhoon frequency (Figure 20 (d)).

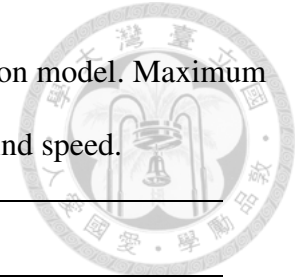


Table 5. The relationships between leaf litter (kgC m^{-2}) and wind speed for total and typhoon months by the linear regression model. Maximum daily wind speed (m s^{-1}) and turbulence kinetic energy were used to calculate monthly maximum, mean and variance of wind speed.

	Maximum daily wind speed				Turbulence kinetic energy			
	a	b	p-value	R^2_{adj} (%)	a	b	p-value	R^2_{adj} (%)
Total months								
Maximum value	0.011	0.0005	<0.001*	0.063	0.018	0.00006	0.647	0.0
Mean value	0.011	0.0011	0.053	0.011	0.019	-0.0010	0.874	0.0
Variance	0.016	0.0002	<0.001*	0.057				
Typhoon months								
Maximum value	0.004	0.0009	0.020*	0.125	0.019	0.0002	0.556	0.0
Mean value	0.016	0.0010	0.605	0.0	0.019	0.0036	0.857	0.0
Variance	0.016	0.0033	0.048*	0.084				

* p -value < 0.05

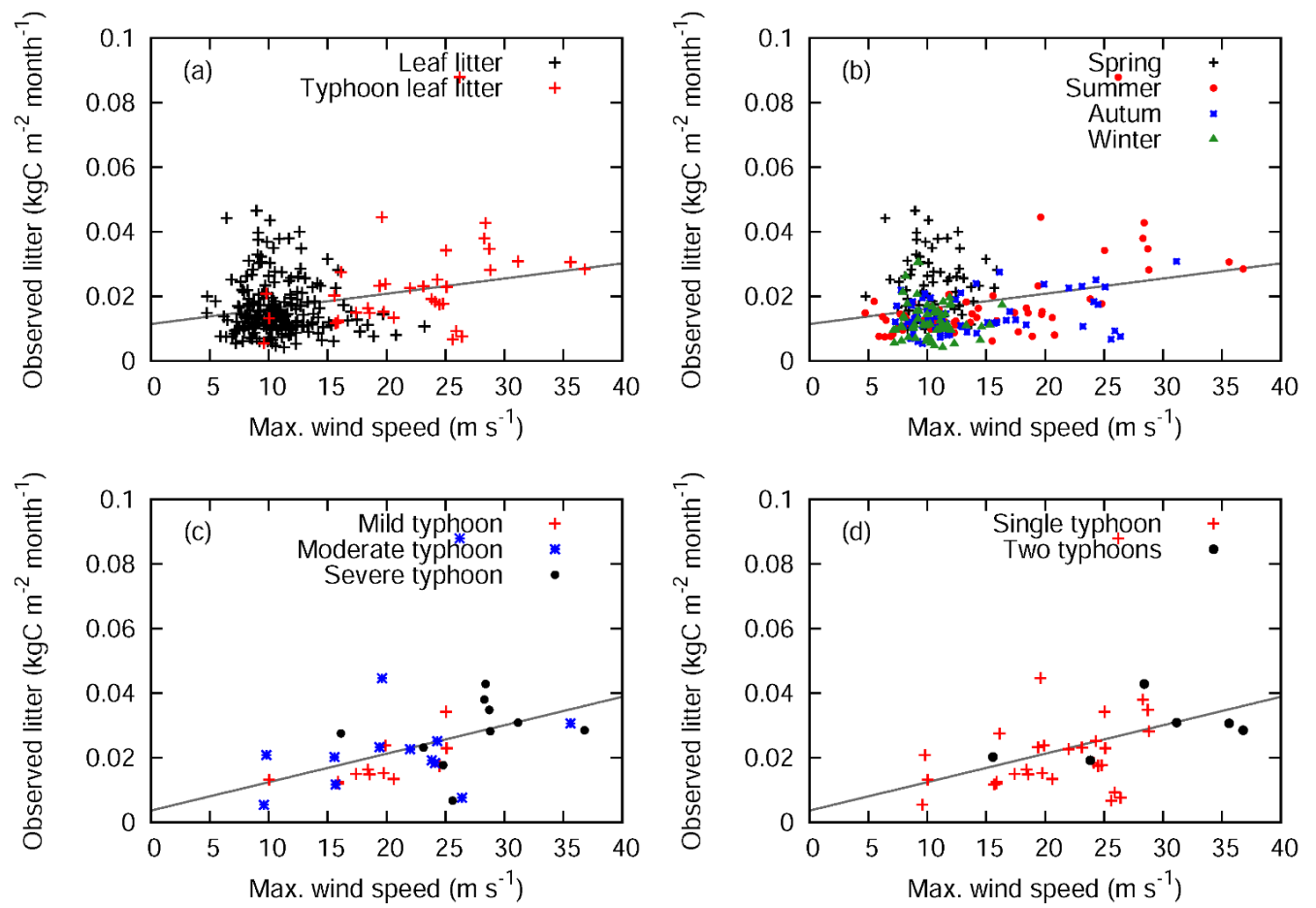


Figure 20. Plot of maximum wind speed and observed leaf litter. Wind speed represents maximum daily wind speed in a month, while observed leaf litter represents monthly litter. The relationships between wind speed and leaf litter for (a) typhoon and non-typhoon months, (b) spring, summer, autumn and winter seasons, (c) different typhoon intensities and (d) typhoon occurrence per month, respectively. The gray lines are linear regression.

Table 6. The statistics results of leaf litter productions and wind speeds among four seasons by one-way ANOVA analysis. Spring is from March to May, summer is from June to August, autumn is from September to November, and winter is from December to February.



	Leaf litter (kgC m ⁻²)			Maximum daily wind speed (m s ⁻¹)		
	Mean	S.D.	p-value	Mean	S.D.	p-value
Spring	0.026	0.009	<0.001*	10.61	5.98	<0.001*
Summer	0.017	0.001		14.63	2.75	
Autumn	0.014	0.006		13.81	7.62	
Winter	0.012	0.005		10.33	1.92	

* p -value < 0.05



Table 7. The statistics results of different typhoon intensities and frequency for leaf litter (kgC m^{-2}) by one-way ANOVA analysis. Typhoon intensity was classified as mild, moderate and severe typhoons, and typhoon frequency was classified as occurrence of typhoon per month and per year.

	Leaf litter ($\text{kgC m}^{-2} \text{ month}^{-1}$)			Leaf litter ($\text{kgC m}^{-2} \text{ month}^{-1}$)		Leaf litter ($\text{kgC m}^{-2} \text{ yr}^{-1}$)					
	Mild	Moderate	Severe	One	Two	Zero	One	Two	Three	Four	Five
<i>p</i> -value	0.016*			0.178		0.073					
Mean	0.017	0.021	0.033	0.022	0.030	0.176	0.192	0.173	0.249	0.214	0.259
S.D.	0.007	0.010	0.021	0.016	0.009	0.033	0.042	0.022	0.026	NA	0.087

* *p*-value < 0.05



3.2 Validation of the Hybrid model

The hybrid model with wind built-in function (a function of wind speed, temperature and precipitation (eq. 2)) was calibrated to validate leaf litter during 2004–2013. The predictivity between observed and modeled litter was significant ($r^2 = 0.33$, $p < 0.001$), while the modeled litter from the baseline Hybrid model (without wind built-in function) showed the pattern with observed litter was not clear (Figure 21). The Hybrid model with wind built-in function slightly underestimated the annual leaf litter ($0.173 \pm 0.049 \text{ kgC m}^{-2} \text{ yr}^{-1}$) compared to observed litter ($0.205 \pm 0.047 \text{ kgC m}^{-2} \text{ yr}^{-1}$), and the RMSE ($0.082 \text{ kgC m}^{-2} \text{ yr}^{-1}$) was moderate (Table 8). The modeled LAI (5.53 ± 1.13) in the wind built-in function model was in the range of observed LAI (3.54 – 7.04), and the modeled total biomass ($13.7 \pm 2.82 \text{ kgC m}^{-2}$) was 5.6% underestimation than the observed total biomass (14.5 kgC m^{-2}). Compared to the wind built-in function model, the baseline Hybrid model overestimated annual leaf litter ($0.266 \pm 0.069 \text{ kgC m}^{-2} \text{ yr}^{-1}$) and total biomass ($36.5 \pm 2.57 \text{ kgC m}^{-2}$) significantly.

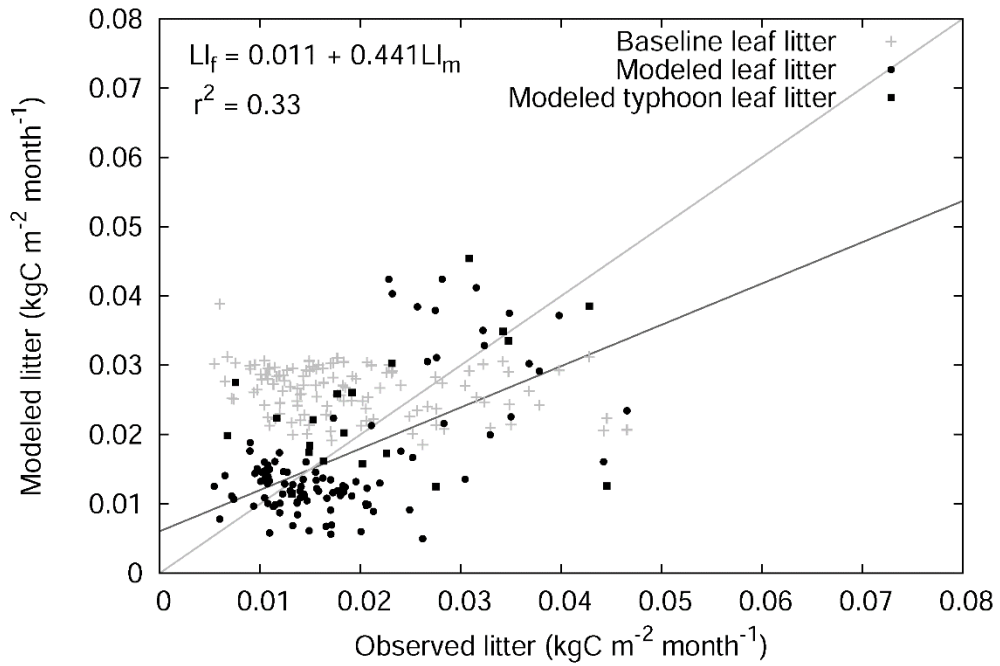


Figure 21. The plots of modeled against observed leaf litter for baseline Hybrid model and the Hybrid model with wind built-in function. The dark circle symbol represents non-typhoon impacted months, while the dark square symbol means typhoon months. The dark line represents linear regression and gray line represents 1:1 line.

Table 8. Validation of mean (\pm s.d.) of field observed and modeled data for leaf litter, LAI and total biomass. The first observed LAI was the direct measurement of foliage in the field, while the second one was indirect LAI measurement from LAI-2000 Plant Canopy Analyzer. The modeled data represent the Hybrid model with wind built-in function, while baseline modeled data represent the primitive Hybrid model.

	Leaf litter (kgC m ⁻² yr ⁻¹)	LAI	Biomass (kgC m ⁻²)
Observed	0.205 \pm 0.047	1.4 – 4.5	14.50
Modeled	0.173 \pm 0.049	5.53 \pm 1.13	13.7 \pm 2.82
Baseline modeled	0.266 \pm 0.069	5.20 \pm 1.18	36.5 \pm 2.57
References	(K.C. Lin unpublished)	(Lin et al. 2011)	(Lin et al. 2006)

3.3 The effects of typhoon and intensity and frequency simulations

The frequency distribution of daily wind speed in typhoon and non-typhoon events during 1993–2013 were calculated, and the mean of wind speed were 19.39 ± 6.02 and $5.72 \pm 2.13 \text{ m s}^{-1}$, respectively (Figure 22). The frequency distribution of wind speed in typhoon events was fitted by a normal distribution ($\mu = 19.39$, $\sigma = 5.99$), and the function was used to simulate the changes of typhoon intensity (Figure 23). The frequency of typhoon events per year was fitted by a Poisson distribution ($\lambda = 2.0$, $p = 0.636$), and the simulations of typhoon frequency were adjusted based on the distribution (Figure 24). However, the frequency distribution of typhoon events in typhoon season (July, August, September, October and November) did not follow the Poisson distribution ($p < 0.001$) (Figure 25).

The historical climate dataset with and without typhoon events were modeled to evaluate the effects of typhoon on the leaf litter, LAI, total biomass, soil respiration, gross primary production (GPP) and net primary production (NPP) (Figure 26). There had significant different between typhoon and non-typhoon historical dataset in LAI ($p = 0.023$), but not significant different in leaf litter ($p = 0.604$), total biomass ($p = 0.202$), soil respiration ($p = 0.149$), GPP ($p = 0.295$) and NPP ($p = 0.362$). In general, simulations of non-typhoon historical dataset had higher leaf litter ($0.179 \pm 0.027 \text{ kgC m}^{-2} \text{ yr}^{-1}$), LAI (6.23 ± 0.778), total biomass ($14.7 \pm 2.25 \text{ kgC m}^{-2}$), GPP ($2.51 \pm 0.768 \text{ kgC m}^{-2} \text{ yr}^{-1}$) and NPP ($1.15 \pm 0.494 \text{ kgC m}^{-2} \text{ yr}^{-1}$), but lower soil respiration ($6.14 \pm 0.231 \text{ kgC m}^{-2}$) than typhoon dataset ($0.173 \pm 0.049 \text{ kgC m}^{-2} \text{ yr}^{-1}$, 5.53 ± 1.13 , $13.7 \pm 2.82 \text{ kgC m}^{-2}$, $2.22 \pm 0.964 \text{ kgC m}^{-2} \text{ yr}^{-1}$, $0.997 \pm 0.609 \text{ kgC m}^{-2} \text{ yr}^{-1}$ and $6.28 \pm 0.376 \text{ kgC m}^{-2}$, respectively) (Figure 26).

For typhoon intensity simulation, the increases of intensity significantly raise leaf litter and soil respiration, but reduce LAI, total biomass, GPP and NPP ($p < 0.001$) (Figure 27). For typhoon frequency simulation, the increases of typhoon events per year significantly raise leaf litter and soil respiration, but reduce LAI and total biomass ($p < 0.05$) (Figure 28). However, increases of typhoon events per year did not significantly affect the trends of GPP and NPP ($p = 0.076$ and $p = 0.435$). The ratio of leaf litter to total biomass significantly increased with the typhoon intensity and frequency ($p < 0.001$) (Figure 29).

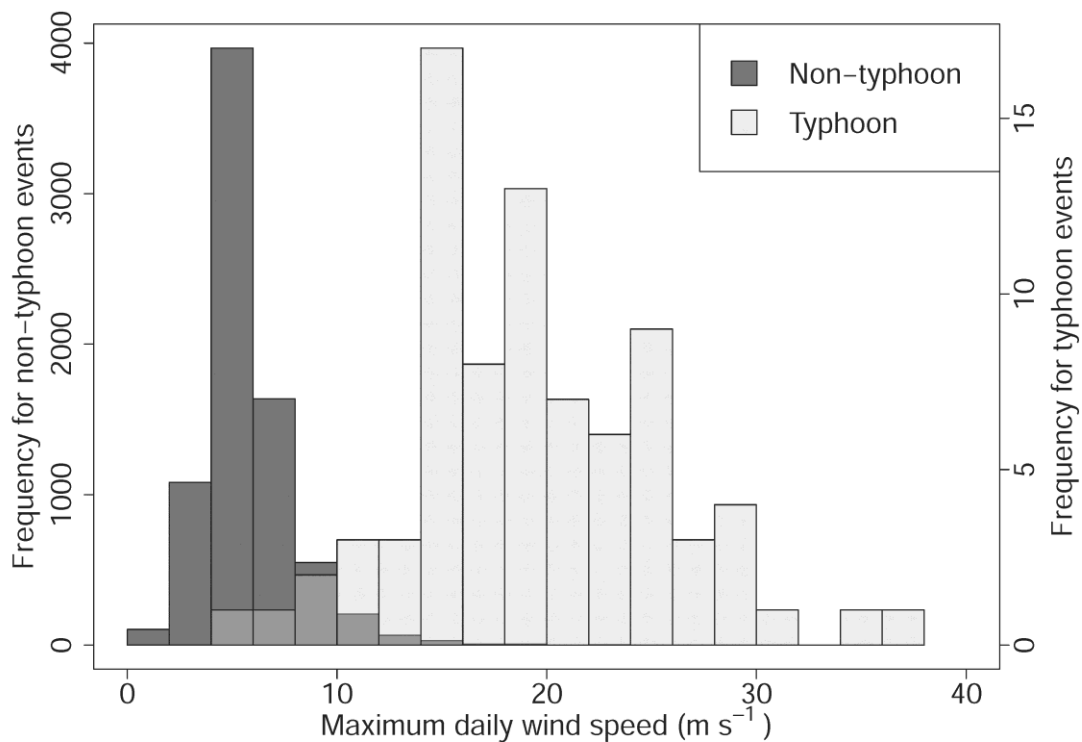


Figure 22. The frequency distribution of maximum daily wind speed in typhoon and non-typhoon events from 1993 to 2013.

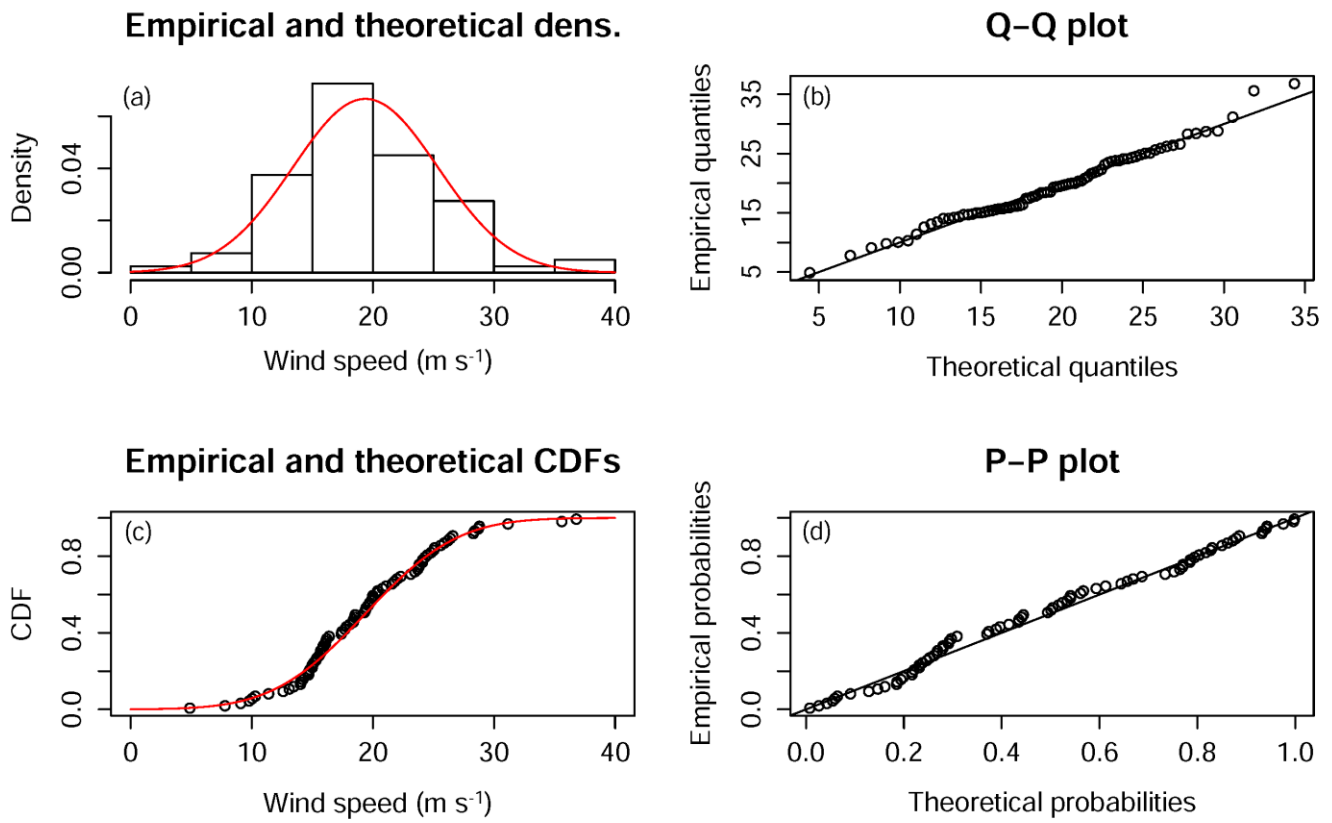


Figure 23. The frequency distribution of maximum daily wind speed in typhoon events was fitted by a normal distribution. (a) the fitted function of normal distribution ($\mu= 19.39, \sigma = 5.985$), (b) normal quantile-quantile plot, (c) patterns of empirical and theoretical CDFs, (d) normal probability plot.

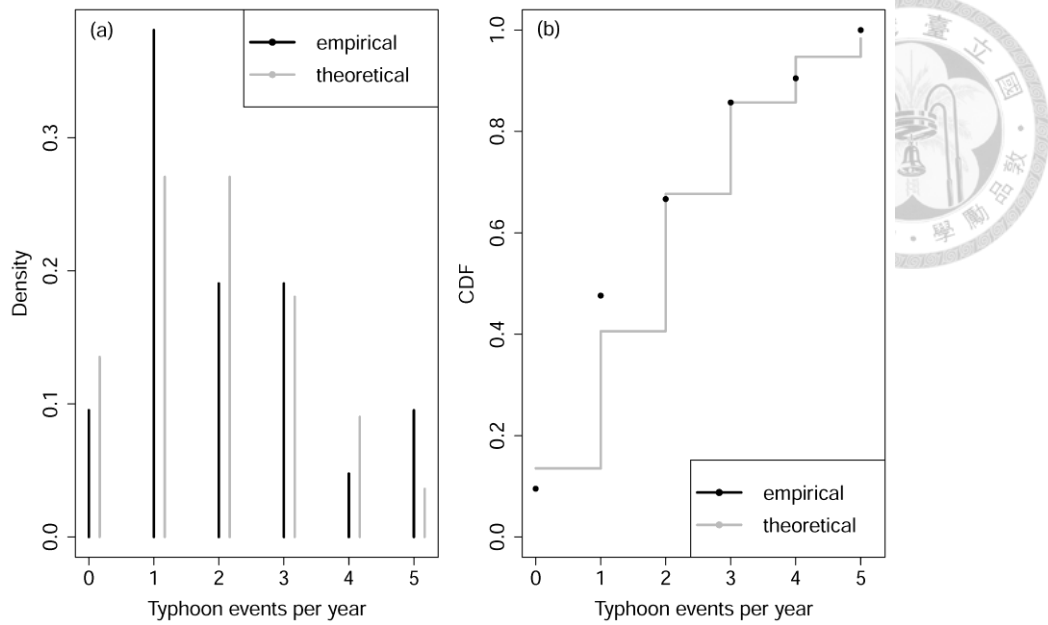


Figure 24. Frequency distribution of typhoon events per year. (a) The Poisson probability density function ($\lambda = 2.0, p = 0.636$) and (b) the Poisson cumulative distribution function.

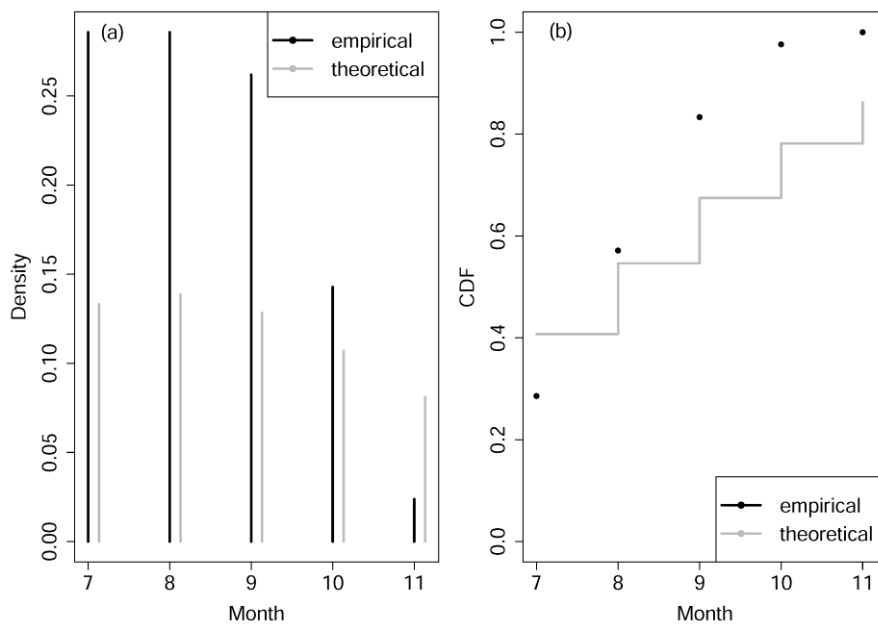


Figure 25. Frequency distribution of typhoon events per month in typhoon season. (a) The Poisson probability density function ($\lambda = 8.8$) and (b) the Poisson cumulative distribution function. The distribution did not follow Poisson distribution ($p < 0.001$).

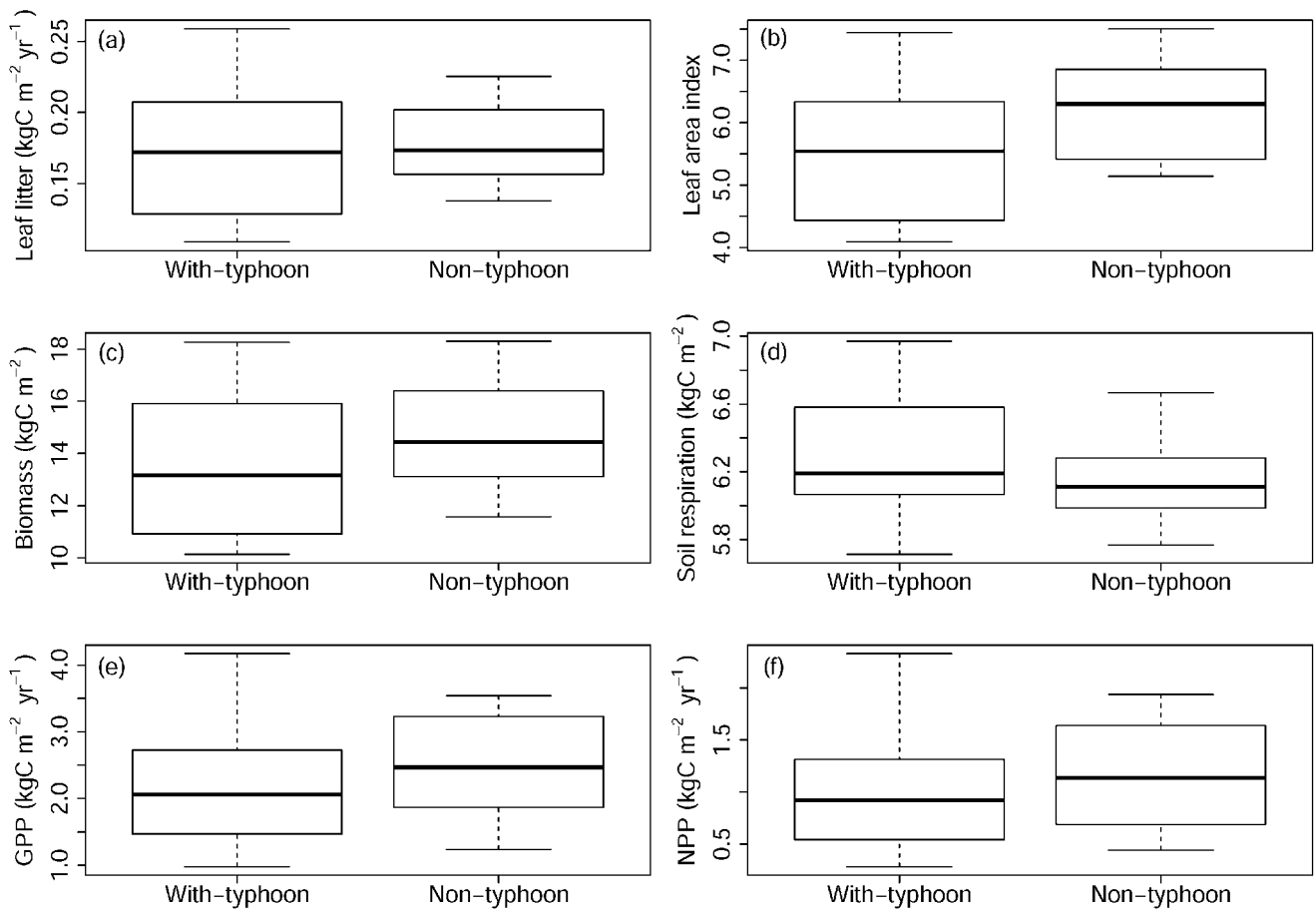


Figure 26. The historical climate dataset with typhoon and non-typhoon from 1993 to 2013 were modeled to evaluate the influences of typhoon on (a) leaf litter, (b) LAI, (c) total biomass, (d) soil respiration, (e) GPP and (f) NPP.

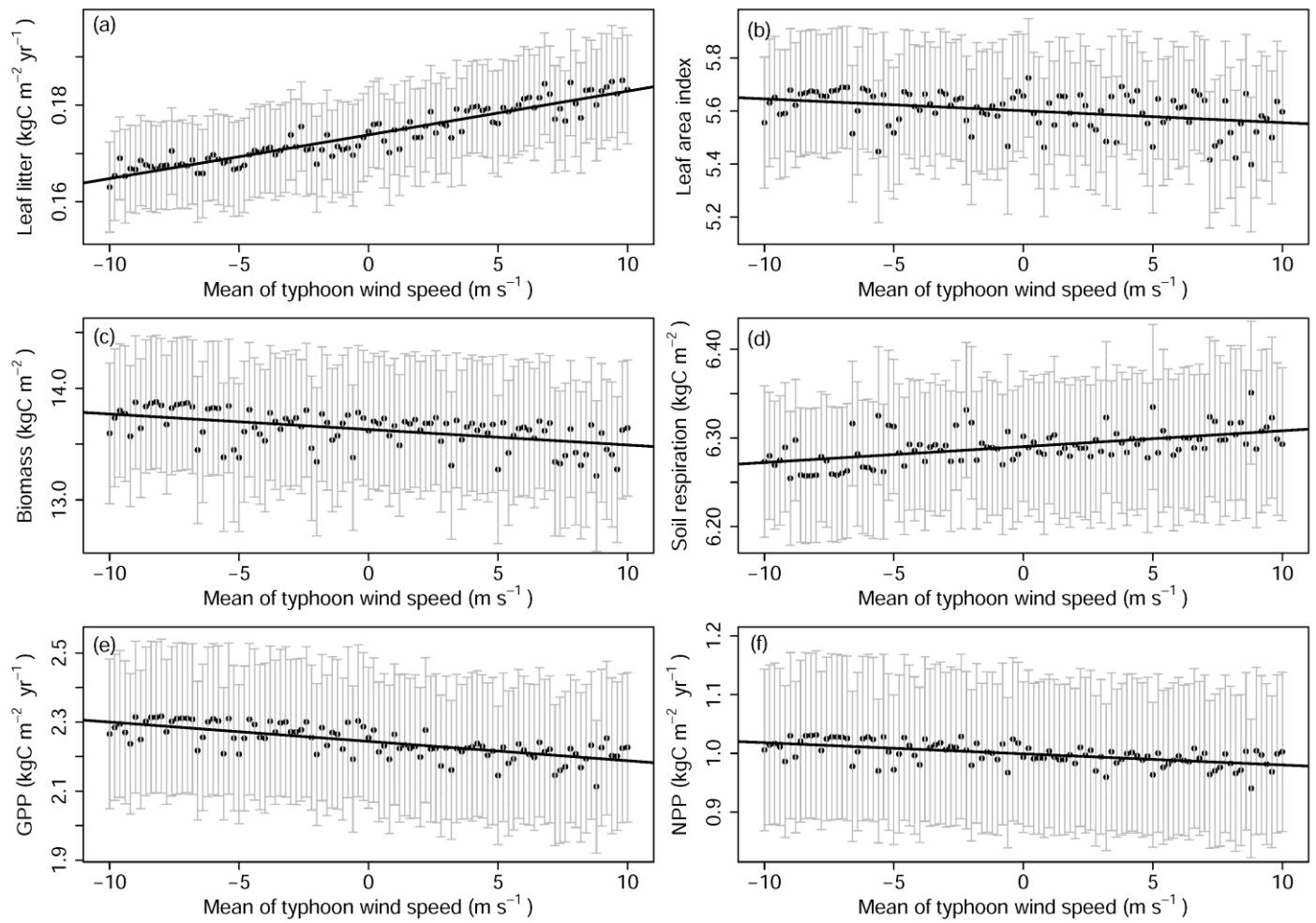


Figure 27. The increases of typhoon intensity on wind speed were modeled to evaluate the influences of intensity on (a) leaf litter, (b) LAI, (c) total biomass, (d) soil respiration, (e) GPP and (f) NPP. The zero represents the historical typhoon intensity with the mean wind speed at $19.39 \text{ (m s}^{-1}\text{)}$.

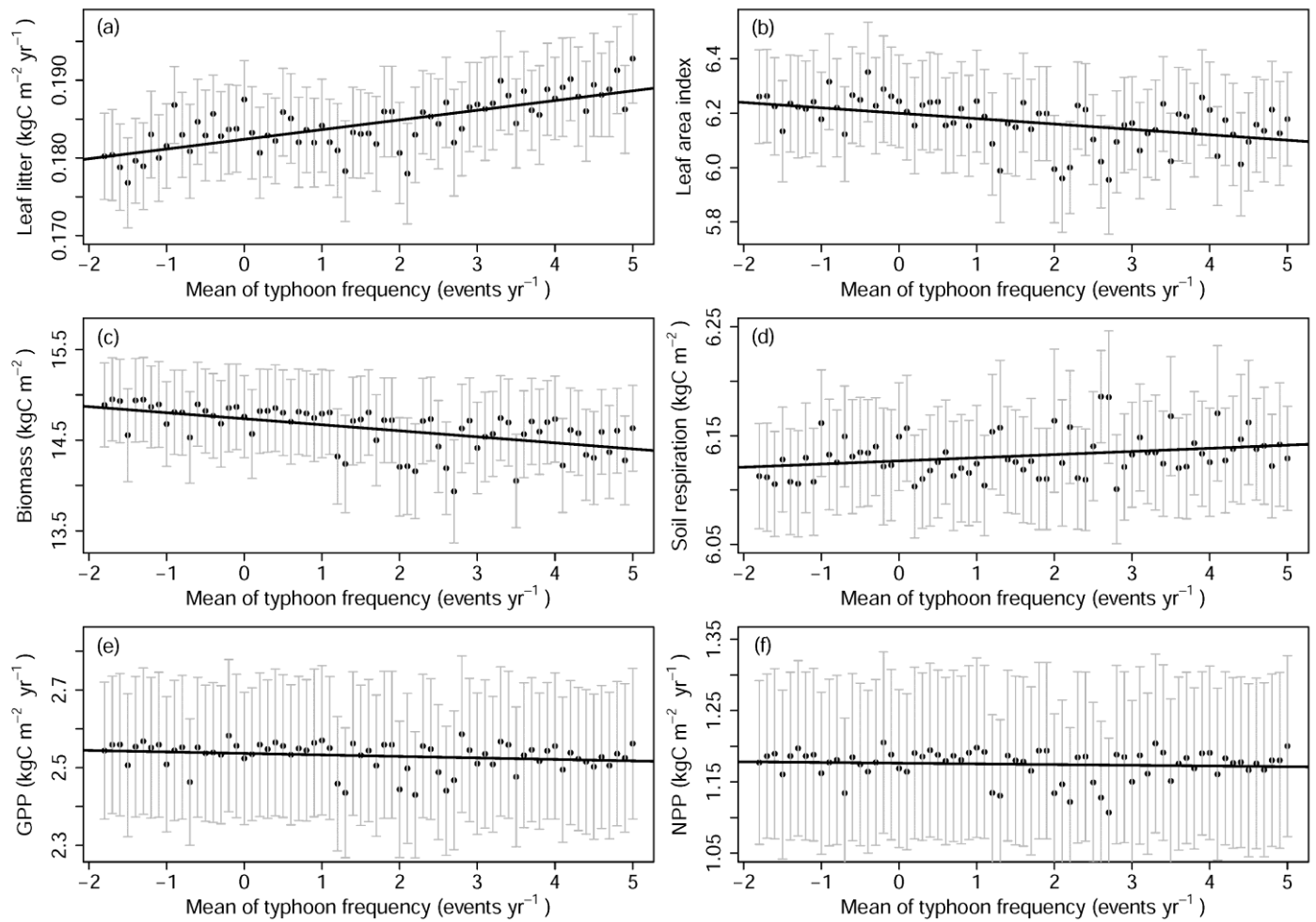


Figure 28. The increases of typhoon frequency per year were modeled to evaluate the influences of frequency on (a) leaf litter, (b) LAI, (c) total biomass, (d) soil respiration, (e) GPP and (f) NPP. The zero represents the historical typhoon frequency.

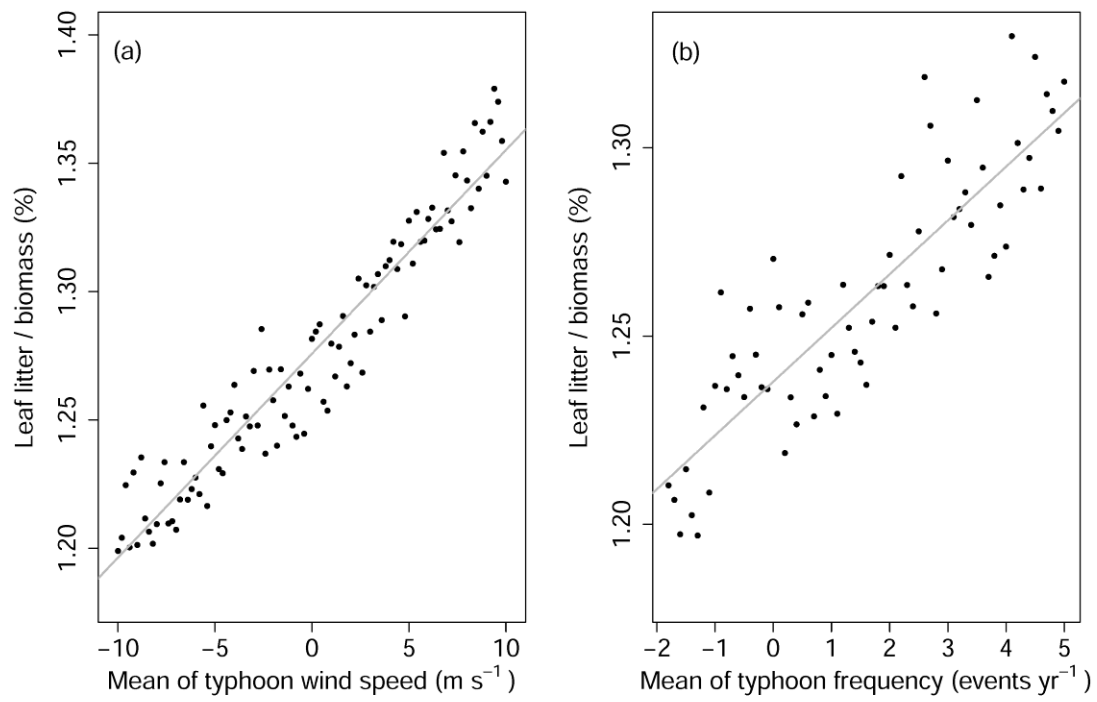



Figure 29. The changes of ratio of leaf litter to total biomass (%) in typhoon intensity and frequency simulations.

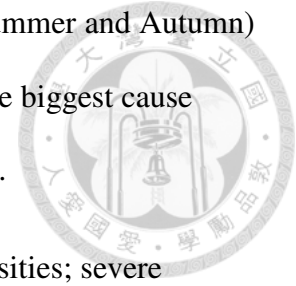
4. Discussion

4.1 *Patterns of in-situ leaf litter and wind speed*



The maximum daily wind speed could be a more suitable variable to estimate leaf litter compared to turbulence kinetic energy (Table 5). For the monthly wind speed variable, the monthly maximum daily wind speed could estimate leaf litter better than the monthly mean and variance of daily wind speed. Although it was statistically significant to predict leaf litter by maximum daily wind speed, the regression model might be weak to explain the pattern of leaf litter (Figure 20 (a)). The maximum daily wind speed could predict leaf litter in typhoon months better than in all months, and it showed that strong winds in typhoon season might contribute more to the litter (Figure 19). A higher production of litter produced in typhoon seasons in the field also showed that strong winds could be critical to deriving litter (Sato et al. 2010; Van Bloem et al. 2005; Wang et al. 2013). A study in Japan also showed that strong typhoon wind speeds in south and southwest slopes decreased canopy height in heavily damaged areas according to the Spaceborne light detection and ranging (LiDAR) estimates from Geoscience Laser Altimeter System (GLAS) (Hayashi et al. 2015). The weak relationship between wind speed and litter might be due to the fact that leaf litter is not only affected by wind speed but also related to plant physiology and phenology, which are affected by climatic variables such as temperature and precipitation (Lebret et al. 2001; Liu et al. 2004; Wang et al. 2013). The highest mean production of leaf litter was observed in the spring and the second-highest production occurred in the summer (Table 6 and Figure 20 (b)). Spring is the major season for leaf expansion which replaces old leaves resulting in the highest defoliation, while summer is the typhoon-dominated season, producing the most litter in this forest ecosystem (Lin 1997). Overall, wind speed might be the most

important factor to derive leaf litter during the typhoon seasons (Summer and Autumn) (Figure 19 and Figure 22), but increases of temperature might be the biggest cause during spring (Figure 18, Figure 20 (a) and (b)) (Chang et al. 2014).



The leaf litter was significantly different among typhoon intensities; severe typhoons derived the highest litter of all the typhoons (Table 7 and Figure 20 (c)). For typhoon frequency, leaf litter was not significantly different in number of typhoon per month and per year, but a greater frequency of typhoons in a month or year produces more litter (e.g. two events per month or more than three events per year) (Table 7 and Figure 20 (d)). The impact of typhoons on leaf litter was not only from intensity and frequency, but also from occurrence time and typhoon track (Wang et al. 2013). For instance, a severe typhoon might derive less litter if there was a typhoon one or two weeks ago, and the first typhoon in a year might produce substantial litter even if it is a mild or moderate typhoon (Sato et al. 2010; Wang et al. 2013). Besides, different typhoon tracks could make for high variability of wind speed and precipitation in local sites (Huang et al. 2012b; Wang et al. 2013).

4.2 Validations of the Hybrid model

The baseline Hybrid model without the wind built-in function overestimated leaf litter with low variability, but there was a significant relationship between modeled and observed litter in the Hybrid model with the wind built-in function (Figure 21). The mean of modeled leaf litter underestimated the observed litter by 15.6% (Table 8). The modeled LAI was reasonable in the range of observed LAI, and the modeled total biomass underestimated the observed total biomass by 5.6%. Defoliation was highly variable and difficult to predict as litter is dominated by a series of variables such as plant intrinsic circadian rhythm, temperature, precipitation,

wind and disturbance (Berg and Meentemeyer 2001; Staelens et al. 2003; Starr et al. 2005). Ito (2010) modeled typhoon-induced defoliation by fitting the low RMSE of LAI, GPP, RE and NEE with *in-situ* flux data, and validated with MODIS LAI at 1 km resolution. However, developing a wind built-in function into the process-based model might be useful to simulate and predict the changes of typhoon intensity and frequency in future climate scenarios.

4.3 The effects of typhoon on the ecosystem

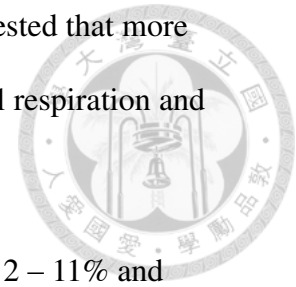
The mean of maximum daily wind speed in typhoon events was three times more than that of non-typhoon events in the historical climate dataset, and the frequency distribution showed that most of strong wind speeds occur in typhoon events (Figure 22). If the strong wind speeds from typhoon events were excluded in the historical climate dataset, there would be higher leaf litter (3.47%), LAI (12.7%), total biomass (7.46%), GPP (13.1%) and NPP (15.3%) but lower soil respiration (-2.23%) than that of the observed results with typhoon events in the ecosystem (Figure 26). The modeled results showed that the impact of strong winds by typhoon is a critical factor that dominates the carbon cycle in the frequently perturbed ecosystem. Ito (2010) also found that there was a significant correlation between maximum wind speed and leaf shedding during 10 typhoon events in 2004 in Japan. The LAI was reduced by 10 – 20%, and the photosynthetically active radiation (PAR) absorbed by understory plants increased more than 50% with higher GPP than normal years. The overall GPP was reduced but increased in net ecosystem exchange (NEE) during 10 typhoon events periods. The similar result was observed in the field of Mexico where soil respiration was 18% higher one year after typhoon disturbance (Vargas and Allen 2008). Wind could influence plant growth through affecting the photosynthesis mechanism by

convection exchanges, changing plant height by bending, and changing the shedding of light in the understory environment by defoliation (de Langre 2008). The substantial defoliation and reduced LAI from strong typhoon wind speed might restrict the tree growth to have a lower canopy height but higher canopy gaps in perturbed regions (Hayashi et al. 2015; Lin et al. 2003b; Lin et al. 2011). For the long-term effects, the frequent typhoons might alter the forest regeneration, community, structure and function, but the ecosystem might have resistance and resilience to the disturbance (Brokaw and Walker 1991; Lin et al. 2011). Overall, typhoons could play an important role in maintaining the regional balance of carbon budget through substantial defoliation and changes of soil respiration.

4.4 Typhoon intensity and frequency simulations

The leaf litter and soil respiration significantly increased with typhoon intensity, while the LAI, total biomass, GPP and NPP were significantly decreased with intensity (Figure 27). The leaf litter had 5.74% and -3.38% changes compared to the control data at the strongest and the weakest wind speed simulations, and was the major factor reflection of the effects of typhoon intensity on carbon cycle. The increased leaf litter would decrease LAI and biomass, resulting in the decreases of GPP and NPP, but producing more carbon loss from soil respiration. For the typhoon frequency simulation, the leaf litter and soil respiration significantly increased with typhoon frequency, while LAI and total biomass were significantly reduced with frequency (Figure 28). The changes of leaf litter were 4.14% and -1.52% compared to the control data at the highest and lowest frequency of typhoon (Figure 27). The increased typhoon-induced leaf litter would result in the increase of soil respiration but the decreases of LAI and total biomass. The stronger typhoon intensity and frequency

might increase the ratio of leaf litter to total biomass, and this suggested that more carbon and nutrients were returned into the forest floor to affect soil respiration and nutrient pool (Figure 29).



The more intense typhoons in 2100 with intensity increases of 2 – 11% and higher precipitation rate were simulated under warmer sea surface temperature and high CO₂ conditions from global climate models (Knutson and Tuleya 2004; Knutson et al. 2010). The numbers of strongest-typhoon categories (4 and 5) have increased in North Pacific, Indian and Southwest Pacific oceans over the 1970 – 2004 period (Webster et al. 2005). However, the trends of frequency of intense typhoon were still inconsistent under global climate models (Bender et al. 2010; Knutson et al. 2010; Webster et al. 2005). Based on typhoon predictions and the Hybrid simulations, if there are more intense typhoons under global warming, it might trigger substantial defoliation and decreased biomass, which could increase carbon loss to the atmosphere by litter decomposition and respiration in the future. Furthermore, typhoon intensity and precipitation could alter the tree growth rate according to a tree ring study in 1770 – 1970 (Altman et al. 2013), and the forest structure and biogeochemistry could have resistance and resilience to typhoon disturbance (Lin et al. 2011). Therefore, the changes of typhoon intensity and frequency under climate scenarios might alter the forest structure and ecosystem processing gradually in the long-term time.

CHAPTER V

Conclusions



Using cross-scale remote sensing and dynamic global vegetation model to monitor forest biomass, litterfall and carbon flux may be important in understanding the carbon cycle and ecosystem process. The findings in this dissertation suggest that topographical heterogeneity may cause the spatial variations of forest biomass by altering nutrients and bioclimate environments in the montane cloud forest. Topographical heterogeneity was also important to cause the spatial variations of annual litterfall on a regional scale by altering temperature, precipitation and vegetation type over Taiwan terrain. The temporal dynamics of the litterfall revealed that typhoons and consecutive drought events might affect the temporal variations of litterfall. Typhoon is an important natural disturbance in this frequently perturbed ecosystem, and a forest ecosystem with typhoons would produce higher leaf litter and soil respiration but decrease biomass and NPP than that of without typhoons. This implied typhoon disturbance may produce more carbon output but could be critical in maintaining the balance of regional carbon budget. The scenarios with increases of typhoon intensity and frequency might make the ecosystem have more carbon loss and alter the ecosystem structure and processing in the long-term time. Overall, the findings in this dissertation may facilitate local or regional-scale monitoring of biomass and litterfall in response to perturbations.

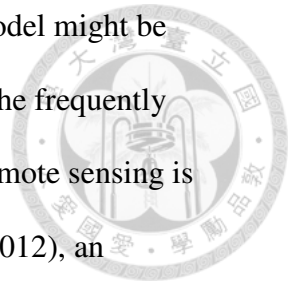
Litterfall or defoliation was highly variable and was challenging to estimate or simulate whatever in remote sensing or processes-based models. Although satellite images could be used to capture the patterns of annual litterfall, it is still challenging to estimate the monthly litterfall. The intra-annual variation of litterfall is related to

seasonal phenology with higher variability than inter-annual variation of litter. However, it might be difficult to get higher time-series images that temporal resolution is within a month, especially in tropical/subtropical regions with high cloud contamination. Although MODIS 8-day composites were used in this dissertation, high cloud contamination still make it hard to compose more than one cloudless image in a month in tropical/subtropical regions. Therefore, using satellite images to estimate high variability of monthly litterfall might be still challenging at the moment.

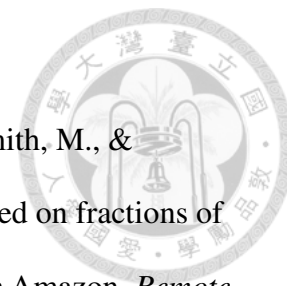
Furthermore, the high time-series MODIS 8-day composites are benefit to estimate the high temporal variability of litterfall, but the spatial resolution of the MODIS image is 500 m and 1 km. If the MODIS image could be integrated with the high spatial resolution sensor such as Landsat images (30 m spatial resolution), it might be able to capture the more detailed spatial patterns of litterfall. There have been some studies to develop fusion approaches to combine high temporal MODIS and spatial Landsat images (Feng et al. 2006; Hazaymeh and Hassan 2015; Roy et al. 2008), and it might be the potential approach to model the annual litterfall in high spatial resolution in the further study.

Using a process-based Hybrid model to simulate carbon cycle of forest ecosystem under typhoon disturbance might be able to understand the components and interactions of ecosystem. Although the empirical function was developed to imply the effect of typhoon on the leaf litter in this dissertation, it might be still a step for process-based model to simulate the typhoon-induced litter. However, the components of complex interactions and feedbacks between forest ecosystem and typhoons are still few and need more studies to understand the physical processing. If there is more physical processing studies about effects of typhoon on litter, it might be possible to develop a physical function to capture the typhoon-induced litter.

Integrating remote sensing and a dynamic global vegetation model might be useful to monitor the regional scale patterns of biogeochemistry in the frequently perturbed regions such as Western North Pacific Ocean. Whereas remote sensing is applied to capture spatial patterns of vegetation (Wang and Huang 2012), an ecosystem model is focused on biogeochemical processes and predicting the responses and feedbacks of ecosystems under future climate scenarios (Friend 2010; Hurtt et al. 2011). Integrating remotely sensed variables such as vegetation type, leaf area index, tree height and climate data with ecosystem process models could provide a regional assessment of carbon and nitrogen storage and fluxes (Turner et al. 2004). The role of remote sensing can be used as initialization and validation of models. For instance, absorbed photosynthetically active radiation (APAR) was derived from high resolution Landsat ETM+ and TM images with spectral mixture analysis to simulate effects of selective logging on carbon cycle by the CASA-3D model (Huang et al. 2008). The LAI derived from Terra Moderate Resolution Imaging Spectroradiometer (MODIS) was used to validate the typhoon-induced defoliation in VISIT model (Ito 2010). Impacts of typhoons often affect relatively wide regions, and might result in spatial heterogeneity of vegetation characteristics at different landscapes. Integrating large-scale remote sensing technique with a dynamic global vegetation model could be a potential method to understand vegetation transitions and biogeochemical distribution under effects of typhoons.



REFERENCES



- Adams, J., Sabol, D., Kapos, V., Almeida Filho, R., Roberts, D., Smith, M., & Gillespie, A. (1995). Classification of multispectral images based on fractions of endmembers: Application to land-cover change in the Brazilian Amazon. *Remote Sensing of Environment*, 52, 137-154
- Agam, N., Kustas, W.P., Anderson, M.C., Li, F., & Neale, C.M.U. (2007). A vegetation index based technique for spatial sharpening of thermal imagery. *Remote Sensing of Environment*, 107, 545-558
- Aguiar, A.V., & Tabarelli, M. (2010). Edge effects and seedling bank depletion: The role played by the early successional Palm *Attalea oleifera* (Arecaceae) in the Atlantic Forest. *Biotropica*, 42, 158-166
- Aiba, S.-i., Kitayama, K., & Takyu, M. (2004). Habitat associations with topography and canopy structure of tree species in a tropical montane forest on Mount Kinabalu, Borneo. *Plant Ecology*, 174, 147-161
- Altman, J., Doležal, J., Černý, T., & Song, J.-S. (2013). Forest response to increasing typhoon activity on the Korean peninsula: evidence from oak tree-rings. *Global Change Biology*, 19, 498-504
- Aplet, G.H., & Vitousek, P.M. (1994). An age-altitude matrix analysis of Hawaiian rain-forest succession. *Journal of Ecology*, 82, 137-147
- Asner, G., Archer, S., Hughes, R., Ansley, R., & Wessman, C. (2003). Net changes in regional woody vegetation cover and carbon storage in Texas drylands, 1937-1999. *Global Change Biology*, 9, 316-335
- Asner, G., & Lobell, D. (2000). A biogeophysical approach for automated SWIR unmixing of soils and vegetation. *Remote Sensing of Environment*, 74, 99-112
- Asner, G.P. (2009). Tropical forest carbon assessment: integrating satellite and

- airborne mapping approaches. *Environmental Research Letters*, 4, 034009
- Asner, G.P., Knapp, D.E., Cooper, A.N., Bustamante, M.C.C., & Olander, L.O. (2005). Ecosystem structure throughout the Brazilian Amazon from Landsat data and spectral unmixing. *Earth Interactions*, 9, 1-31
- Baker, W., & Dillon, G. (2000). Plant and vegetation responses to edges in the southern Rocky Mountains. *Forest fragmentation in the southern Rocky Mountains. University Press of Colorado, Boulder*, 221-245
- Bateson, C.A., Asner, G.P., & Wessman, C.A. (2000). Endmember bundles: a new approach to incorporating endmember variability into spectral mixture analysis. *Geoscience and Remote Sensing, IEEE Transactions on*, 38, 1083-1094
- Beard, K.H., Vogt, K.A., Vogt, D.J., Scatena, F.N., Covich, A.P., Sigurdardottir, R., Siccama, T.G., & Crowl, T.A. (2005). Structural and functional responses of a subtropical forest to 10 years of hurricanes and droughts. *Ecological Monographs*, 75, 345-361
- Bender, M.A., Knutson, T.R., Tuleya, R.E., Sirutis, J.J., Vecchi, G.A., Garner, S.T., & Held, I.M. (2010). Modeled impact of anthropogenic warming on the frequency of intense Atlantic hurricanes. *Science*, 327, 454-458
- Bennie, J., Hill, M.O., Baxter, R., & Huntley, B. (2006). Influence of slope and aspect on long-term vegetation change in British chalk grasslands. *Journal of Ecology*, 94, 355-368
- Bennie, J., Huntley, B., Wiltshire, A., Hill, M.O., & Baxter, R. (2008). Slope, aspect and climate: Spatially explicit and implicit models of topographic microclimate in chalk grassland. *Ecological Modelling*, 216, 47-59
- Berg, B., & Meentemeyer, V. (2001). Litter fall in some European coniferous forests as dependent on climate: a synthesis. *Canadian Journal of Forest Research*, 31,

Bonham, C. (1989). *Measurements for terrestrial vegetation*. Hoboken, New Jersey:

John Wiley & Sons, Inc.

Brando, P.M., Nepstad, D.C., Davidson, E.A., Trumbore, S.E., Ray, D., & Camargo, P.

(2008). Drought effects on litterfall, wood production and belowground carbon cycling in an Amazon forest: results of a throughfall reduction experiment.

Philosophical Transactions of the Royal Society B: Biological Sciences, 363, 1839-1848

Bray, J.R., & Gorham, E. (1964). Litter production in forests of the world. *Advances in Ecological Research*, 2, 101-157

Briggs, J.M., & Knapp, A.K. (1995). Interannual variability in primary production in Tallgrass Prairie: Climate, soil moisture, topographic position, and fire as determinants of aboveground biomass. *American Journal of Botany*, 82, 1024-1030

Brokaw, N.V.L., & Walker, L.R. (1991). Summary of the effects of caribbean hurricanes on vegetation. *Biotropica*, 23, 442-447

Brown, S., & Lugo, A.E. (1982). The storage and production of organic matter in tropical forests and their role in the global carbon cycle. *Biotropica*, 14, 161-187

Brown, S., Pearson, T., Slaymaker, D., Ambagis, S., Moore, N., Novelo, D., & Sabido, W. (2005). Creating a virtual tropical forest from three-dimensional aerial imagery to estimate carbon stocks. *Ecological Applications*, 15, 1083-1095

Brus, D.J., & DeGrujter, J.J. (1993). Design-based versus model-based estimates of spatial means: Theory and application in environmental soil science. *Environmetrics*, 4, 123-152

Campbell, G.S., & Norman, J.M. (1998). *Introduction to environmental biophysics*.



Springer Verlag



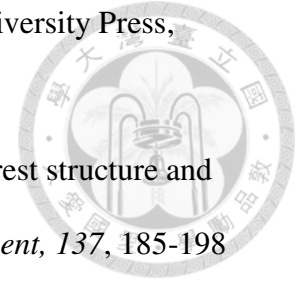
- Canty, M.J. (2006). *Image analysis, classification and change detection in remote sensing: with algorithms for ENVI/IDL*. CRC Press, Taylor & Francis Group
- Cavelier, J., & Goldstein, G. (1989). Mist and fog interception in elfin cloud forests in Colombia and Venezuela. *Journal of Tropical Ecology*, 5, 309-322
- Chambers, J., Fisher, J., Zeng, H., Chapman, E., Baker, D., & Hurtt, G. (2007a). Hurricane Katrina's carbon footprint on US Gulf Coast forests. *Science*, 318, 1107
- Chambers, J.Q., Asner, G.P., Morton, D.C., Anderson, L.O., Saatchi, S.S., Espírito-Santo, F.D.B., Palace, M., & Souza Jr, C. (2007b). Regional ecosystem structure and function: ecological insights from remote sensing of tropical forests. *Trends in Ecology & Evolution*, 22, 414-423
- Chang, C.-T., Lin, T.-C., Wang, S.-F., & Vadeboncoeur, M.A. (2011). Assessing growing season beginning and end dates and their relation to climate in Taiwan using satellite data. *International Journal of Remote Sensing*, 32, 5035-5058
- Chang, C.-t., Wang, H.-c., & Huang, C.-y. (2014). Retrieving multi-scale climatic variations from high dimensional time-series MODIS green vegetation cover in a tropical/subtropical mountainous island. *Journal of Mountain Science*, 11, 407-420
- Chang, C.L. (2005). Dynamic of litterfall and its nutrient contents at different Stands in Hui-Sun experimental forest. In, *Forestry: National Chung Hsing University*
- Chang, C.T., Wang, H.-C., & Huang, C.-y. (2013). Impacts of vegetation onset time on the net primary productivity in a mountainous island in Pacific Asia. *Environmental Research Letters*, 8, 045030
- Chang, S.-C., Tseng, K.-H., Hsia, Y.-J., Wang, C.-P., & Wu, J.-T. (2008). Soil

respiration in a subtropical montane cloud forest in Taiwan. *Agricultural and Forest Meteorology*, 148, 788-798



- Chapin III, F.S., Matson, P.A., & Vitousek, P.M. (2011). *Principles of terrestrial ecosystem ecology*. Springer
- Chave, J., Navarrete, D., Almeida, S., Alvarez, E., Aragão, L.E., Bonal, D., Châtelet, P., Silva-Espejo, J., Goret, J.-Y., & Hildebrand, P.v. (2010). Regional and seasonal patterns of litterfall in tropical South America. *Biogeosciences*, 7, 43-55
- Chen, X.F., Chen, J.M., An, S.Q., & Ju, W.M. (2007). Effects of topography on simulated net primary productivity at landscape scale. *Journal of Environmental Management*, 85, 585-596
- Chin, C.C. (2008). Study on the spatial and temporal change of litterfall in Nanjenshan lowland rain forest. In, *Forestry: National Pingtung University of Science and Technology*
- Chou, Y.J. (2003). Seasonal dynamics of litterfall, recycling amount of nutrients and decomposition rates in Hui-Sun experimental forest. In, *Forestry: National Chung Hsing University*
- Chu, H.C. (2005). Estimation of nutrient storage and fluxes of litterfall in a yellow cypress forest ecosystem. In, *Natural Resources and Environmental Studies: National Dong Hwa University*
- Ciais, P., C. Sabine, G. Bala, L. Bopp, V. Brovkin, J. Canadell, A. Chhabra, R. DeFries, J. Galloway, M. Heimann, C. Jones, C. Le Quéré, R.B. Myneni, S. Piao, & Thornton, P. (2013). Carbon and Other Biogeochemical Cycles. In: *Climate Change 2013: The Physical Science Basis. Contribution of Working Group I to the Fifth Assessment Report of the Intergovernmental Panel on Climate Change*. In T.F. Stocker, D. Qin, G.-K. Plattner, M. Tignor, S.K. Allen, J. Boschung, A.


Nauels, Y. Xia, V. Bex and P.M. Midgley (Ed.). Cambridge University Press,
Cambridge, United Kingdom and New York, NY, USA.



- Clark, D.B., & Clark, D.A. (2000). Landscape-scale variation in forest structure and biomass in a tropical rain forest. *Forest Ecology and Management*, 137, 185-198
- Couêteaux, M.-M., Bottner, P., & Berg, B. (1995). Litter decomposition, climate and litter quality. *Trends in Ecology & Evolution*, 10, 63-66
- da Costa, T.C.e.C., Viana, J.H.M., & Ribeiro, J.L. (2014). Semideciduous seasonal forest production of leaves and deciduousness in function of the water balance, LAI, and NDVI. *International Journal of Ecology*, 2014, 15
- Dale, V.H., Joyce, L.A., McNulty, S., Neilson, R.P., Ayres, M.P., Flannigan, M.D., Hanson, P.J., Irland, L.C., Lugo, A.E., Peterson, C.J., Simberloff, D., Swanson, F.J., Stocks, B.J., & Michael Wotton, B. (2001). Climate change and forest disturbances. *Bioscience*, 51, 723-734
- Davidson, E.A., & Janssens, I.A. (2006). Temperature sensitivity of soil carbon decomposition and feedbacks to climate change. *Nature*, 440, 165-173
- de Castilho, C.V., Magnusson, W.E., de Araújo, R.N.O., Luizão, R.C.C., Luizão, F.J., Lima, A.P., & Higuchi, N. (2006). Variation in aboveground tree live biomass in a central Amazonian Forest: Effects of soil and topography. *Forest Ecology and Management*, 234, 85-96
- de Langre, E. (2008). Effects of wind on plants. *Annual Review of Fluid Mechanics*, 40, 141-168
- DeFries, R. (2008). Terrestrial vegetation in the coupled human-earth system: Contributions of remote sensing. *Annual Review of Environment and Resources*, 33, 369-390
- Del Arco, J.M., Escudero, A., & Garrido, M.V. (1991). Effects of site characteristics

- on nitrogen retranslocation from senescing leaves. *Ecology*, 701-708
- Delta-T (2000). *HemiView Canopy Analysis Software: User's Manual. Version 2.0.* .
Delta-T Devices Ltd., Cambridge
- Dent, D., Bagchi, R., Robinson, D., Majalap-Lee, N., & Burslem, D.R.P. (2006).
Nutrient fluxes via litterfall and leaf litter decomposition vary across a gradient of
soil nutrient supply in a lowland tropical rain forest. *Plant and Soil*, 288, 197-215
- Emanuel, K. (2005). Increasing destructiveness of tropical cyclones over the past 30
years. *Nature*, 436, 686-688
- Facelli, J., & Pickett, S.A. (1991). Plant litter: Its dynamics and effects on plant
community structure. *The Botanical Review*, 57, 1-32
- FAO (2005). Global forest resources assessment. *Key Findings. FAO, Rome, Italy*, 3
- Feng, G., Masek, J., Schwaller, M., & Hall, F. (2006). On the blending of the Landsat
and MODIS surface reflectance: predicting daily Landsat surface reflectance.
Geoscience and Remote Sensing, IEEE Transactions on, 44, 2207-2218
- Field, C., Barros, V., Dokken, D., Mach, K., Mastrandrea, M., Bilir, T., Chatterjee, M.,
Ebi, K., Estrada, Y., & Genova, R. (2014). IPCC, 2014: Climate Change 2014:
Impacts, adaptation, and vulnerability. Part A: Global and sectoral aspects.
contribution of working group II to the Fifth Assessment Report of the
Intergovernmental Panel on Climate Change. In: Cambridge University Press,
Cambridge, United Kingdom and New York, NY, USA
- Foster, P. (2001). The potential negative impacts of global climate change on tropical
montane cloud forests. *Earth-Science Reviews*, 55, 73-106
- Friend, A., Stevens, A., Knox, R., & Cannell, M. (1997). A process-based, terrestrial
biosphere model of ecosystem dynamics (Hybrid v3. 0). *Ecological Modelling*,
95, 249-287

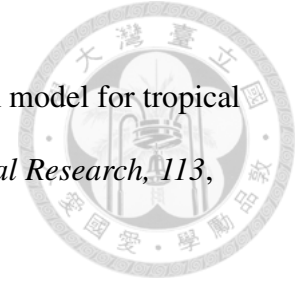


- 
- Friend, A.D. (1998). Parameterisation of a global daily weather generator for terrestrial ecosystem modelling. *Ecological Modelling*, 109, 121-140
- Friend, A.D. (2010). Terrestrial plant production and climate change. *Journal of Experimental Botany*, 61, 1293-1309
- Friend, A.D., Schugart, H.H., & Running, S.W. (1993). A physiology-based gap model of forest dynamics. *Ecology*, 74, 792-797
- Friend, A.D., & White, A. (2000). Evaluation and analysis of a dynamic terrestrial ecosystem model under preindustrial conditions at the global scale. *Global Biogeochemical Cycles*, 14, 1173-1190
- Frolking, S., Palace, M., Clark, D., Chambers, J., Shugart, H., & Hurtt, G. (2009). Forest disturbance and recovery: A general review in the context of spaceborne remote sensing of impacts on aboveground biomass and canopy structure. *Journal of Geophysical Research*, 114: G00E02
- Fuchs, H., Magdon, P., Kleinn, C., & Flessa, H. (2009). Estimating aboveground carbon in a catchment of the Siberian forest tundra: Combining satellite imagery and field inventory. *Remote Sensing of Environment*, 113, 518-531
- Gibbs, H.K., Brown, S., Niles, J.O., & Foley, J.A. (2007). Monitoring and estimating tropical forest carbon stocks: making REDD a reality. *Environmental Research Letters*, 2, 045023
- Haase, E.F. (1970). Environmental fluctuations on south-facing slopes in the Santa Catalina Mountains of Arizona. *Ecology*, 959-974
- Hamilton, L., Juvik, J., & Scatena, F. (1995). *Tropical montane cloud forests*. Springer-Verlag New York
- Hayashi, M., Saigusa, N., Oguma, H., Yamagata, Y., & Takao, G. (2015). Quantitative assessment of the impact of typhoon disturbance on a Japanese forest using

- satellite laser altimetry. *Remote Sensing of Environment*, 156, 216-225
- Hazaymeh, K., & Hassan, Q. (2015). Fusion of MODIS and Landsat-8 surface temperature images: a new approach. *PLoS ONE*, 10, e0117755
- Hirabuki, Y. (1991). Heterogeneous dispersal of tree litterfall corresponding with patchy canopy structure in a temperate mixed forest. *Vegetatio*, 94, 69-79
- Hook, P.B., & Burke, I.C. (2000). Biogeochemistry in a shortgrass landscape: control by topography, soil texture, and microclimate. *Ecology*, 81, 2686-2703
- Hsiao, Y.J. (2005). Dynamics of litterfall of secondary forest, Japanese cedar plantation and bamboo plantation in the Wulai Area. In, *Forestry and resource conservation* National Taiwan University
- Huang, C.-y., Asner, G.P., & Barger, N.N. (2012a). Modeling regional variation in net primary production of pinyon–juniper ecosystems. *Ecological Modelling*, 227, 82-92
- Huang, C., Asner, G.P., Martin, R., Barger, N., & Neff, J. (2009). Multiscale analysis of tree cover and aboveground carbon stocks in pinyon-juniper woodlands. *Ecological Applications*, 19, 668-681
- Huang, C., Chai, C., Chang, C., Huang, J., Hu, K., Lu, M., & Chung, Y. (2013). An integrated optical remote sensing system for environmental perturbation research. *IEEE JSTARS*
- Huang, C., Marsh, S.E., McClaran, M., & Archer, S. (2007). Postfire stand structure in a semi-arid savanna: Cross-scale challenges estimating biomass. *Ecological Applications*, 17, 1899-1910
- Huang, J.-C., Yu, C.-K., Lee, J.-Y., Cheng, L.-W., Lee, T.-Y., & Kao, S.-J. (2012b). Linking typhoon tracks and spatial rainfall patterns for improving flood lead time predictions over a mesoscale mountainous watershed. *Water Resources Research*,

48, W09540

Huang, M., Asner, G., Keller, M., & Berry, J. (2008). An ecosystem model for tropical forest disturbance and selective logging. *Journal of Geophysical Research*, *113*, G01002



Huete, A., Didan, K., Miura, T., Rodriguez, E.P., Gao, X., & Ferreira, L.G. (2002). Overview of the radiometric and biophysical performance of the MODIS vegetation indices. *Remote Sensing of Environment*, *83*, 195-213

Huete, A., Restrepo-Coupe, N., Ratana, P., Didan, K., Saleska, S., Ichii, K., Panuthai, S., & Gamo, M. (2008). Multiple site tower flux and remote sensing comparisons of tropical forest dynamics in Monsoon Asia. *Agricultural and Forest Meteorology*, *148*, 748-760

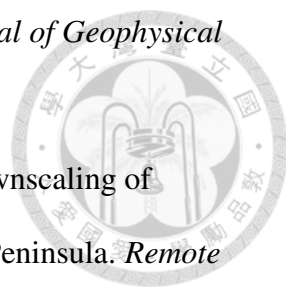
Huffman, G.J., Adler, R.F., Rudolf, B., Schneider, U., & Keehn, P.R. (1995). Global precipitation estimates based on a technique for combining satellite-based estimates, rain gauge analysis, and NWP model precipitation information. *Journal of Climate*, *8*, 1284-1295

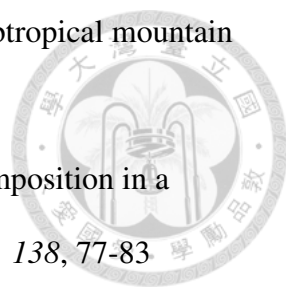
Hughes, R.F., & Denslow, J.S. (2005). Invasion by a N₂-fixing tree alters function and structure in wet lowland forests of Hawaii. *Ecological Applications*, *15*, 1615-1628

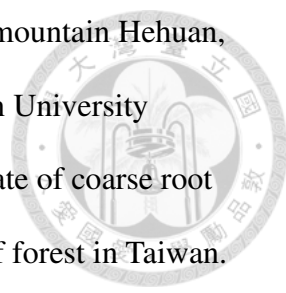
Hung, S.F. (2003). Study on the litterfall and forest soil nutrient dynamics of natural hardwoods in Nao-Liao river. In, *Forestry: National Chung Hsing University*


Hurtt, G., Chini, L.P., Froking, S., Betts, R., Feddema, J., Fischer, G., Fisk, J., Hibbard, K., Houghton, R., & Janetos, A. (2011). Harmonization of land-use scenarios for the period 1500–2100: 600 years of global gridded annual land-use transitions, wood harvest, and resulting secondary lands. *Climatic Change*, 1-45

Hurtt, G.C., Fisk, J., Thomas, R.Q., Dubayah, R., Moorcroft, P.R., & Shugart, H.H.

- 
- (2010). Linking models and data on vegetation structure. *Journal of Geophysical Research*, 115, G00E10
- Immerzeel, W.W., Rutten, M.M., & Droogers, P. (2009). Spatial downscaling of TRMM precipitation using vegetative response on the Iberian Peninsula. *Remote Sensing of Environment*, 113, 362-370
- Isaaks, E.H., & Srivastava, R.M. (1989). *Applied geostatistics*. New York, USA: Oxford University Press Inc.
- Ito, A. (2010). Evaluation of the impacts of defoliation by tropical cyclones on a Japanese forest's carbon budget using flux data and a process-based model. *Journal of Geophysical Research: Biogeosciences*, 115, G04013
- Jandl, R., Lindner, M., Vesterdal, L., Bauwens, B., Baritz, R., Hagedorn, F., Johnson, D., Minkinen, K., & Byrne, K. (2007). How strongly can forest management influence soil carbon sequestration? *Geoderma*, 137, 253-268
- Jenkins, J.C., Chojnacky, D.C., Heath, L.S., & Birdsey, R.A. (2003). National-scale biomass estimators for United States tree species. *Forest Science*, 49, 12-35
- Jensen, J.R. (2004). *Introductory digital image processing: a remote sensing perspective*. Upper Saddle River, New Jersey: Prentice Hall
- Jha, P., & Prasad Mohapatra, K. (2010). Leaf litterfall, fine root production and turnover in four major tree species of the semi-arid region of India. *Plant and Soil*, 326, 481-491
- Jia, S., Zhu, W., Lü, A., & Yan, T. (2011). A statistical spatial downscaling algorithm of TRMM precipitation based on NDVI and DEM in the Qaidam Basin of China. *Remote Sensing of Environment*, 115, 3069-3079
- Joffre, R., Rambal, S., & Romane, F. (1996). Local variations of ecosystem functions in Mediterranean evergreen oak woodland. *Annals of Forest Science*, 53, 561-570

- 
- Klemm, O., Chang, S.C., & Hsia, Y.J. (2006). Energy fluxes at a subtropical mountain cloud forest. *Forest Ecology and Management*, 224, 5-10
- Knutson, R.M. (1997). An 18-year study of litterfall and litter decomposition in a Northeast Iowa deciduous forest. *American Midland Naturalist*, 138, 77-83
- Knutson, T., & Tuleya, R. (2004). Impact of CO₂-induced warming on simulated hurricane intensity and precipitation: Sensitivity to the choice of climate model and convective parameterization. *Journal of Climate*, 17, 3477-3495
- Knutson, T.R., McBride, J.L., Chan, J., Emanuel, K., Holland, G., Landsea, C., Held, I., Kossin, J.P., Srivastava, A.K., & Sugi, M. (2010). Tropical cyclones and climate change. *Nature Geoscience*, 3, 157-163
- Kuo, C.H. (2012). Estimation of litterfall and soil organic carbon storage under three habitat types in Nanjenshan lowland rain forest. In, *Forestry: National Pingtung University of Science and Technology*
- Lebret, M., Nys, C., & Forgeard, F. (2001). Litter production in an Atlantic beech (*Fagus sylvatica* L.) time sequence. *Annals of Forest Science*, 58, 755-768
- Lee, C.L. (2006). A research of litterfall in warm-temperate evergreen broad-leaved forest in Chungtzekuan area. In, *Science Education: National University of Tainan*
- Leff, J.W., Wieder, W.R., Taylor, P.G., Townsend, A.R., Nemergut, D.R., Grandy, A.S., & Cleveland, C.C. (2012). Experimental litterfall manipulation drives large and rapid changes in soil carbon cycling in a wet tropical forest. *Global Change Biology*, 18, 2969-2979
- Liao, J.H. (2006). The relationships between litterfall and soil dynamics on Kenting uplifted coral reef nature reserve forest ecosystem. In, *Environmental Science and Engineering National Pingtung University of Science and Technology*

- 
- Lin, C.H. (2012). Litterfall dynamics of *Abies Kawakamii* stand at mountain Hehuan, Taiwan In, *Forestry and resource conservation* National Taiwan University
- Lin, K.-C., Duh, C.-T., Huang, C.-M., & Wang, C.-P. (2006). Estimate of coarse root biomass and nutrient contents of trees in a subtropical broadleaf forest in Taiwan. *Taiwan Journal of Forest Science*, 21, 155-166
- Lin, K., Hamburg, S., Tang, S., Hsia, Y., & Lin, T. (2003a). Typhoon effects on litterfall in a subtropical forest. *Canadian Journal of Forest Research*, 33, 2184-2192
- Lin, K.C. (1997). Dynamics of litterfall and the litter layer in the Fushan forest of northeastern Taiwan. *Taiwan Journal of Forest Research*, 12, 135-144
- Lin, T.-C., Hamburg, S.P., Hsia, Y.-J., Lin, T.-T., King, H.-B., Wang, L.-J., & Lin, K.-C. (2003b). Influence of typhoon disturbances on the understory light regime and stand dynamics of a subtropical rain forest in northeastern Taiwan. *Journal of Forest Research*, 8, 139-145
- Lin, T., Hamburg, S., Hsia, Y., Lin, T., King, H., Wang, L., & Lin, K. (2003c). Influence of typhoon disturbances on the understory light regime and stand dynamics of a subtropical rain forest in northeastern Taiwan. *Journal of Forest Research*, 8, 139-145
- Lin, T.C., Hamburg, S., Lin, K.C., Wang, L.J., Chang, C.T., Hsia, Y.J., Vadeboncoeur, M., Mabry McMullen, C., & Liu, C.P. (2011). Typhoon disturbance and forest dynamics: Lessons from a Northwest Pacific subtropical forest. *Ecosystems*, 14, 127-143
- Liu, C., Westman, C.J., Berg, B., Kutsch, W., Wang, G.Z., Man, R., & Ilvesniemi, H. (2004). Variation in litterfall-climate relationships between coniferous and broadleaf forests in Eurasia. *Global Ecology and Biogeography*, 13, 105-114

- 
- Lodge, D.J., Scatena, F.N., Asbury, C.E., & Sanchez, M.J. (1991). Fine litterfall and related nutrient inputs resulting from hurricane Hugo in subtropical wet and lower montane rain forests of Puerto Rico. *Biotropica*, 23, 336-342
- Lodhiyal, L.S., & Lodhiyal, N. (1997). Variation in biomass and net primary productivity in short rotation high density central Himalayan poplar plantations. *Forest Ecology and Management*, 98, 167-179
- Lonsdale, W.M. (1988). Predicting the amount of litterfall in forests of the world. *Annals of Botany*, 61, 319-324
- Lovett, G.M., Christenson, L.M., Groffman, P.M., Jones, C.G., Hart, J.E., & Mitchell, M.J. (2002). Insect defoliation and nitrogen cycling in forests. *Bioscience*, 52, 335-341
- Lu, S.W. (2010). Nutrient accumulation and litterfall return of natural hardwood among different elevation in central Taiwan. In, *Forestry*: National Chung-Hsing University
- Malcolm, J.R. (1994). Edge effects in central Amazonian forest fragments. *Ecology*, 75, 2438-2445
- Matala, J., Kellomäki, S., & Nuutinen, T. (2008). Litterfall in relation to volume growth of trees: Analysis based on literature. *Scandinavian Journal of Forest Research*, 23, 194-202
- McNulty, S.G. (2002). Hurricane impacts on US forest carbon sequestration. *Environmental Pollution*, 116, S17-S24
- Mildenberger, K., Beiderwieden, E., Hsia, Y.J., & Klemm, O. (2009). CO₂ and water vapor fluxes above a subtropical mountain cloud forest: The effect of light conditions and fog. *Agricultural and Forest Meteorology*, 149, 1730-1736
- Montagnini, F. (2000). Accumulation in above-ground biomass and soil storage of

mineral nutrients in pure and mixed plantations in a humid tropical lowland.

Forest Ecology and Management, 134, 257-270



Murcia, C. (1995). Edge effects in fragmented forests: implications for conservation.

Trends in Ecology & Evolution, 10, 58-62

Ormsby, T., Napoleon, E., Burke, R., Groessl, C., & Bowden, L. (2009). Getting to

know ArcGIS desktop. Updated for ArcGIS 9.3. basics of ArcView, ArcEditor,

ArcInfo. In: ESRI Press, Redmond, CA, USA

Ostertag, R., Marín-Spiotta, E., Silver, W., & Schulten, J. (2008). Litterfall and

decomposition in relation to soil carbon pools along a secondary forest

chronosequence in Puerto Rico. *Ecosystems*, 11, 701-714

Ostertag, R., Scatena, F.N., & Silver, W.L. (2003). Forest floor decomposition

following hurricane litter inputs in several Puerto Rican forests. *Ecosystems*, 6,

261-273

Owen, J.S., King, H.B., Wang, M.K., & Sun, H.L. (2010). Net nitrogen mineralization

and nitrification rates in forest soil in northeastern Taiwan. *Soil Science and Plant*

Nutrition, 56, 177-185

Ozdemir, I. (2008). Estimating stem volume by tree crown area and tree shadow area

extracted from pan-sharpened Quickbird imagery in open Crimean juniper forests.

International Journal of Remote Sensing, 29, 5643-5655

PeÑUelas, J., Prieto, P., Beier, C., Cesaraccio, C., De Angelis, P., De Dato, G.,

Emmett, B.A., Estiarte, M., Garadnai, J., Gorissen, A., LÁNg, E.K., KrÖEl-Dulay,

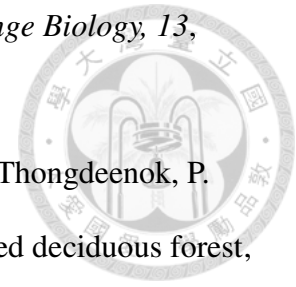
G., Llorens, L., Pellizzaro, G., Riis-Nielsen, T., Schmidt, I.K., Sirca, C., Sowerby,

A., Spano, D., & Tietema, A. (2007). Response of plant species richness and

primary productivity in shrublands along a north–south gradient in Europe to

seven years of experimental warming and drought: reductions in primary

productivity in the heat and drought year of 2003. *Global Change Biology*, 13, 2563-2581



Podong, C., Poolsiri, R., Katzensteiner, K., Pengthamkeerati, P., & Thongdeenok, P. (2013). Species diversity and litter dynamics in secondary mixed deciduous forest, Thung Salaeng Lung National Park, Northern, Thailand. In, *Folia Forestalia Polonica, Seria A - Forestry* (p. 196)

Pounds, J., Fogden, M., & Campbell, J. (1999). Biological response to climate change on a tropical mountain. *Nature*, 398, 611-615

Raich, J.W., Russell, A.E., & Vitousek, P.M. (1997). Primary productivity and ecosystem development along an elevational gradient on Mauna Loa, Hawai'i. *Ecology*, 78, 707-721

Ramsey, F.L., & Schafer, N.W. (1997). The statistical sleuth: A course in methods of data analysis. In: Duxbury Press, Belmont, California, USA

Reed, R.A., Johnson-Barnard, J., & Baker, W.L. (1996). Contribution of roads to forest fragmentation in the Rocky Mountains. *Conservation Biology*, 10, 1098-1106

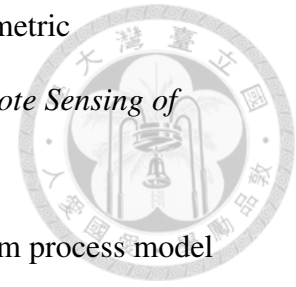
Reiners, W.A., & Lang, G.E. (1987). Changes in litterfall along a gradient in altitude. *Journal of Ecology*, 75, 629-638

Rich, P.M. (1990). Characterizing plant canopies with hemispherical photographs. *Remote Sensing Reviews*, 5, 13-29

Rothe, A. (1997). Influence of tree species composition on rooting patterns, hydrology, elemental turnover, and growth in a mixed spruce-beech stand in Southern Germany (Hoeglwald). [In German with English summary]. *Forstliche Forschungsberichte Muenchen*, 163, 1-179

Roy, D.P., Ju, J., Lewis, P., Schaaf, C., Gao, F., Hansen, M., & Lindquist, E. (2008).

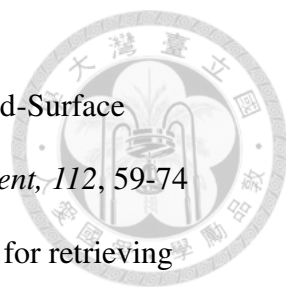
Multi-temporal MODIS–Landsat data fusion for relative radiometric normalization, gap filling, and prediction of Landsat data. *Remote Sensing of Environment*, 112, 3112-3130



- Running, S., & Hunt, E. (1993). Generalization of a forest ecosystem process model for other biomes, BIOME-BGC, and an application for global-scale models. *Scaling physiological processes: leaf to globe* (pp. 141-158): Academic Press
- Sánchez-Andrés, R., Sánchez-Carrillo, S., Alatorre, L., Cirujano, S., & Álvarez-Cobelas, M. (2010). Litterfall dynamics and nutrient decomposition of arid mangroves in the Gulf of California: Their role sustaining ecosystem heterotrophy. *Estuarine, Coastal and Shelf Science*, 89, 191-199
- Sato, T., Kominami, Y., Saito, S., Niiyama, K., Tanouchi, H., Nagamatsu, D., & Nomiya, H. (2010). Temporal dynamics and resilience of fine litterfall in relation to typhoon disturbances over 14 years in an old-growth lucidophyllous forest in southwestern Japan. *Plant Ecology*, 208, 187-198
- Sayer, E.J., Powers, J.S., & Tanner, E.V.J. (2007). Increased litterfall in tropical forests boosts the transfer of soil CO₂ to the atmosphere. *PLoS ONE*, 2, e1299
- Specht, A., & West, P. (2003). Estimation of biomass and sequestered carbon on farm forest plantations in northern New South Wales, Australia. *Biomass and Bioenergy*, 25, 363-379
- Staelens, J., Nachtergale, L., & Luysaert, S. (2004). Predicting the spatial distribution of leaf litterfall in a Mixed deciduous forest. *Forest Science*, 50, 836-847
- Staelens, J., Nachtergale, L., Luysaert, S., & Lust, N. (2003). A model of wind-influenced leaf litterfall in a mixed hardwood forest. *Canadian Journal of Forest Research*, 33, 201-209
- Starr, M., Saarsalmi, A., Hokkanen, T., Merilä, P., & Helmisaari, H.-S. (2005). Models

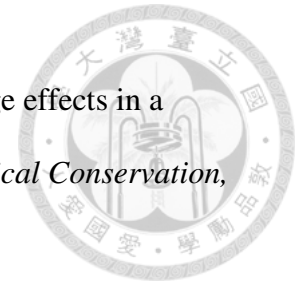
- of litterfall production for Scots pine (*Pinus sylvestris* L.) in Finland using stand, site and climate factors. *Forest Ecology and Management*, 205, 215-225
- Tan, Y., Huai, J., Tang, Z., & Xi, W. (2010). An improved hierarchical segmentation method for remote sensing images. *Journal of the Indian Society of Remote Sensing*, 38, 686-695
- Taskinsu-Meydan, S., Evrendilek, F., Berberoglu, S., & Donmez, C. (2010). Modeling above-ground litterfall in eastern Mediterranean conifer forests using fractional tree cover, and remotely sensed and ground data. *Applied Vegetation Science*, 13, 485-497
- Triadiati, S., Tjitrosemito, E., Guhardja, E., Sudarsono, H., Qayim, I., & Leuschner, C. (2011). Litterfall production and leaf-litter decomposition at natural forest and cacao agroforestry in Central Sulawesi, Indonesia. *Asian Journal of Biological Sciences*, 4, 221-234
- Turner, D.P., Ollinger, S.V., & Kimball, J.S. (2004). Integrating remote sensing and ecosystem process models for landscape- to regional-scale analysis of the carbon cycle. *Bioscience*, 54, 573-584
- Turton, S.M. (2008). Landscape-scale impacts of Cyclone Larry on the forests of northeast Australia, including comparisons with previous cyclones impacting the region between 1858 and 2006. *Austral Ecology*, 33, 409-416
- Van Bloem, S.J., Murphy, P.G., Lugo, A.E., Ostertag, R., Costa, M.R., Bernard, I.R., Colón, S.M., & Mora, M.C. (2005). The influence of hurricane winds on Caribbean dry forest structure and nutrient pools. *Biotropica*, 37, 571-583
- Vargas, R., & Allen, M.F. (2008). Diel patterns of soil respiration in a tropical forest after hurricane Wilma. *Journal of Geophysical Research*, 113, G03021
- Vitousek, P.M. (1984). Litterfall, nutrient cycling, and nutrient limitation in tropical

forests. *Ecology*, 65, 285-298

- 
- Wan, Z. (2008). New refinements and validation of the MODIS Land-Surface Temperature/Emissivity products. *Remote Sensing of Environment*, 112, 59-74
- Wan, Z., & Dozier, J. (1996). A generalized split-window algorithm for retrieving land-surface temperature from space. *Geoscience and Remote Sensing, IEEE Transactions on*, 34, 892-905
- Wang, H.-C., & Huang, C.-Y. (2012). Investigating the spatial heterogeneity of a subtropical montane cloud forest plantation with a QuickBird image. *International Journal of Remote Sensing*, 33, 7868-7885
- Wang, H.-C., Wang, S.-F., Lin, K.-C., Lee Shaner, P.-J., & Lin, T.-C. (2013). Litterfall and element fluxes in a natural hardwood forest and a Chinese-fir plantation experiencing frequent typhoon disturbance in central Taiwan. *Biotropica*, 45, 541-548
- Wang, J.L. (2011). Litterfall dynamics in a Yellow Cypress forest at the Chi-Lan mountain site. In, *Natural Resources and Environmental Studies*: National Dong Hwa University
- Wang, L., Sousa, W.P., & Gong, P. (2004). Integration of object-based and pixel-based classification for mapping mangroves with IKONOS imagery. *International Journal of Remote Sensing*, 25, 5655-5668
- Webster, P.J., Holland, G.J., Curry, J.A., & Chang, H.-R. (2005). Changes in tropical cyclone number, duration, and intensity in a warming Environment. *Science*, 309, 1844-1846
- Weng, C.Y. (2009). The dynamics of leaf litter and phenological patterns in the forest dynamics plot at upstream basin of Nantzuhsienhsi in middle elevation of Taiwan In, *Ecology*: Providence University

- Whigham, D.F., Olmsted, I., Cano, E.C., & Harmon, M.E. (1991). The impact of hurricane Gilbert on trees, litterfall, and woody Debris in a dry tropical forest in the Northeastern Yucatan Peninsula. *Biotropica*, 23, 434-441
- Williams-Linera, G. (1990). Vegetation structure and environmental conditions of forest edges in Panama. *Journal of Ecology*, 78, 356-373
- Williams-Linera, G., Tolome, J., Forest, C., Litterfall, & Forest, L.M. (1996). Litterfall, temperate and tropical dominant trees, and climate in a Mexican lower montane forest. *Biotropica*, 28, 649-656
- Wood, T.E., Lawrence, D., & Clark, D.A. (2005). Variation in leaf litter nutrients of a Costa Rican rain forest is related to precipitation. *Biogeochemistry*, 73, 417-437
- Xu, X., Hirata, E., Enoki, T., & Tokashiki, Y. (2004a). Leaf litter decomposition and nutrient dynamics in a subtropical forest after typhoon disturbance. *Plant Ecology*, 173, 161-170
- Xu, X., Hirata, E., & Shibata, H. (2004b). Effect of typhoon disturbance on fine litterfall and related nutrient input in a subtropical forest on Okinawa Island, Japan. *Basic and Applied Ecology*, 5, 271-282
- Yamane, T. (1967). *Elementary sampling theory*. Prentice-Hall Englewood Cliffs, NJ
- Yang, S.H. (2007). Dynamics in litterfall and nitrogen and phosphorus concentrations of leaf fall in the natural hardwood forests of Chitou. In, *Forestry and resource conservation* National Taiwan University
- Yasuhiro, K., Hirofumi, M., & Kihachiro, K. (2004). Effects of topographic heterogeneity on tree species richness and stand dynamics in a subtropical forest in Okinawa Island, southern Japan. *Journal of Ecology*, 92, 230-240
- Yeh, C.-F. (2004). Estimation of biomass and fog deposition of a yellow cypress forest. In, *Institute of Natural Resources* (p. 93). Hualien City, Taiwan: National

Dong Hwa University



- Young, A., & Mitchell, N. (1994). Microclimate and vegetation edge effects in a fragmented podocarp-broadleaf forest in New Zealand. *Biological Conservation*, 67, 63-72
- Zalamea, M., & González, G. (2008). Leaf fall phenology in a subtropical wet forest in Puerto Rico: from species to community patterns. *Biotropica*, 40, 295-304
- Zeng, H., Chambers, J.Q., Negrón-Juárez, R.I., Hurtt, G.C., Baker, D.B., & Powell, M.D. (2009). Impacts of tropical cyclones on U.S. forest tree mortality and carbon flux from 1851 to 2000. *Proceedings of the National Academy of Sciences*, 106, 7888-7892
- Zhang, X., Friedl, M.A., Schaaf, C.B., Strahler, A.H., Hodges, J.C.F., Gao, F., Reed, B.C., & Huete, A. (2003). Monitoring vegetation phenology using MODIS. *Remote Sensing of Environment*, 84, 471-475
- Zheng, D., Rademacher, J., Chen, J., Crow, T., Bresee, M., Le Moine, J., & Ryu, S.-R. (2004). Estimating aboveground biomass using Landsat 7 ETM+ data across a managed landscape in northern Wisconsin, USA. *Remote Sensing of Environment*, 93, 402-411
- Zhou, L., Shalom, A.-D., Wu, P., Li, S., Jia, Y., & Ma, X. (2014). Litterfall production and nutrient return in different-aged Chinese fir (*Cunninghamia lanceolata*) plantations in south China. *Journal of Forestry Research*, 1-10

Appendix A: The values of input variables



Variable	Value	Unit
PAR extinction coefficient	0.650	
Shortwave extinction coefficient	0.48	
PAR reflection coefficient	0.05	
Shortwave reflection coefficient	0.2	
Turnover rate of foliage	0.9579	Proportion yr ⁻¹
Turnover rate of wood	0.0091	Proportion yr ⁻¹
Turnover rate of fine roots	2.0	Proportion yr ⁻¹
Specific leaf area	18.13	m ² kg C ⁻¹
Ratio of DBH to bark thickness	0.033	m m ⁻¹
Ratio between leaf area and sapwood area	4167	m ² m ⁻²
Allometry a parameter for dbh (m) to height	28.51	
Allometry b parameter for dbh (m) to height	0.4667	
Proportion of woody biomass below ground	0.26	
Biomass ratio between fine roots and foliage	0.5	kg C
Foliage nitrogen retranslocation coefficient	0.5	
Fine root nitrogen retranslocation coefficient	1.0	
Mean wood and bark specific gravity	305	kg C m ⁻³
Tree form factor	0.6	
Ratio between C:N ratios of foliage and sapwood	0.224	
Ratio between C:N ratios of foliage and fine roots	0.876	
Proportion of sapwood alive	0.17	
Maximum proportion of live sapwood used as C storage	0.67	

Variable	Value	Unit
N uptake parameter	0.036	$\text{m}^2 \text{kg C}^{-1} \text{d}^{-1}$
Maximum leaf conductance to CO_2	1672	m s^{-1}
Cuticular conductance to CO_2	0.0000481	m s^{-1}
Proportion of foliage nitrogen bound in Rubisco	0.67	
Proportion of foliage nitrogen bound in chlorophyll	9.13	
Leaf characteristic dimension	0.04	m
Factor to calculate effect of WFPS on N uptake	2.0	
Factor to calculate $K_c \text{CO}_2$ of Rubisco	3.0669999	
Factor to allow for growth respiration	0.75	
Factor for calculating minimum wood mass increment	0.1	